Aus der Fachrichtung Biophysik
Theoretische Medizin und Biowissenschaften
der Medizinischen Fakultät
der Universität des Saarlandes, Homburg /Saar

$\alpha_2\delta3$ is the preferred auxiliary $\alpha_2\delta$ subunit of $Ca_v2.1$ channels in spiral ganglion

neurons and is required for development of auditory nerve fiber synapses

Dissertation
Zur Erlangung des Grades eines Doktors der Naturwissenschaften
der Medizinischen Fakultät
der Universität des Saarlandes

2019

vorgelegt von
Friederike Lene Brigitte Stephani
geb. am 23.04.1988 in Würzburg

Table of content

Abbreviations

A	$\alpha_2\delta1$	$Cav_{\alpha2\delta1}$-auxiliary subunit of voltage gated Ca^{2+} channel
	$\alpha_2\delta2$	$Cav_{\alpha2\delta2}$-auxiliary subunit of voltage gated Ca^{2+} channel
	$\alpha_2\delta3$	$Cav_{\alpha2\delta3}$-auxiliary subunit of voltage gated Ca^{2+} channel
	$\alpha_2\delta4$	$Cav_{\alpha2\delta4}$-auxiliary subunit of voltage gated Ca^{2+} channel
	ABR	auditory brainstem response
	AC	auditory cortex
	Aga	ω-agatoxin IVA
	ANF	auditory nerve fiber
	AMPA	α-amino-3-hydroxy-5-methyl-4-isoxazolepropionic acid
	AVCN	anteroventral cochlear nucleus
B	BDNF	brain derived neurotrophic factor
	BM	basilar membrane
	BP	blocking buffer
C	*Cacna2d2*	calcium channel, voltage-dependent, alpha 2 / delta subunit 2
	Cacna2d3	calcium channel, voltage-dependent, alpha 2 / delta subunit 3
	Cb	cerebellum
	CC	current clamp
	CNC	cochlear nuclear complex
	CNS	central nervous system
	Cono	ω-conotoxin MVIIa / GVIa
D	DC / DCN	dorsal cochlear nucleus
	DIC	differential interference contrast
	DIV	days in vitro
	DPOAE	distortion product of otoacoustic emission
G	GluR	glutamate receptor
	GM 130	golgi matrix protein of 130 kD
	GPI	glycosylphosphatidylinositol
	GrC	granule cell layer
H	HVA	high voltage-activated
I	I_{Ca}	Ca^{2+} current
	I-solution	internal solution
	I/V	current / voltage
	IC	inferior colliculus
	IHC	inner hair cell
	IRES	internal ribosome entry site
K	KO	knockout
L	LAMP2	lysosome-associated membrane protein 2
	LJP	liquid junction potential
	LL	lateral lemniscus
	LOC	lateral olivocochlear
	LSM	Laser scanning microscope
	LSO	lateral superior olivary nucleus
	LVA	low voltage-activated

1

M	MET	mechanoelectrical transducer channel
	MG	medial geniculate nucleus
	ML	molecular layer
	MNTB	medial nucleus of the trapezoid body
	MOC	medial olivocochlear
	mRNA	messenger RNA
	MSO	medial superior olive
N	NA	numerical aperture
	Nimo	nimodipine
	NMDA	N-methyl-D-aspartate
	NMJ	neuromuscular junction
	NMRI	Naval Medical Research Institute
	NT3	neurotrophic factor 3
O	OHC	outer hair cell
	OoC	organ of Corti
P	P	postnatal day
	PAB	primary antibody
	PFA	paraformaldehyde
	PM	plasma membrane
	PNGase F	peptide-n-glycosidase f
	PNS	peripheral nervous system
	PP	permeabilization buffer
	PSD	post-synaptic density protein
	PVCN	posterior ventral cochlear nucleus
R	RP	reaction buffer
S	SAB	secondary antibody
	SBC	spherical bushy cell
	S.D.	standard deviation
	SG	spiral ganglion
	SOC	superior olivary complex
	SNX	ω-theraphotoxin-Hg1a, SNX-482
T	tg	transgene
	TM	tectorial membrane
	Tuj1	neuronal class iii beta-tubulin
V	VC	voltage clamp
	VCA	ventral cochlar nucleus anterior
	VCP	ventral cochlar nucleus posterior
	VCN	ventral cochlear nucleus
	VGCC	voltage-gated Ca^{2+} channels
	VGLUT1	vesicular glutamate transporter 1
W	WP	washing buffer
	wt	wildtype

List of figures

List of tables

Abstract

Voltage-gated calcium channels (VGCCs) are composed of a pore-forming α_1 subunit and the auxiliary β and $\alpha_2\delta$ subunits. The largely extracellular $\alpha_2\delta$ proteins $\alpha_2\delta1$-4 modulate the Ca^{2+} current properties but the reasons for their partial redundancy/specificity are unknown. VGCCs are expressed in a huge variety of tissues, including the auditory system. Acoustically evoked signal processing is carried out in an ultrafast and timely precise way and requires fully functional and developed connections. The cochlea converts mechanical into electrical signals, and transmits these signals via spiral ganglion (SG) neurons to the auditory brainstem. SG neurons are indispensable for a proper hearing function and their loss cannot be compensated by any hearing aid or cochlea implant. The presynaptic Ca^{2+} channel complex of the mature inner hair cell (IHC) is formed by $Ca_v1.3$, β_2 and $\alpha_2\delta2$ (Fell et al., 2016). Recently, $\alpha_2\delta$ subunits have become of interest due to their multiple roles in pain processing, synapse formation and use as therapeutic targets for different drugs.

In this work, the role of the $\alpha_2\delta3$ subunit of VGCCs was analyzed with respect to (i) its contribution to the I_{Ca} in neonatal and mature SG neurons and (ii) the development of the endbulb of Held synapse.

Lack of $\alpha_2\delta3$ reduced $Ca_v2.1$ currents, the dominating Ca^{2+} channel in cultured SG neurons of mice aged 3-weeks, by 60 %. Furthermore, we found malformed and smaller endbulbs of Held in mice aged 3-weeks. Surprisingly, at P5, when P/Q-type ($Ca_v2.1$) channels in SG neurons were not yet expressed, $\alpha_2\delta3$ was nevertheless required for a normal endbulb of Held synapse development. This indicates a specific function of $\alpha_2\delta3$ in synapse development, which was independent of the presence of the P/Q-type Ca^{2+} current.

The endbulb of Held synapse has been studied not only in the $\alpha_2\delta3$ knockout mouse but also in $\alpha_2\delta2$ null mutants, to determine how the deletion of $\alpha_2\delta2$ affects the development. Analysis of the endbulb of Held synapse showed a decreased VGLUT1-labeled area as well as a decreased number of boutons per bushy cell compared to the wildtype, indicating that also $\alpha_2\delta2$ is required for proper endbulb of Held formation at P20.

In contrast to IHCs, SG neurons express at least 6 pore-forming subunits and all three neuronal $\alpha_2\delta$ subunits ($\alpha_2\delta1$-3). Taken together, we could show that (i) only $Ca_v2.1$ channels mediating P/Q currents were strongly reduced in SG neurons isolated from $\alpha_2\delta3^{-/-}$ mice at P20, (ii) $\alpha_2\delta3$ has a function for synaptic development independent of $Ca_v2.1$ channels and (iii) also deletion of $\alpha_2\delta2$ affects the development and maturation of the endbulb of Held synapse at P20.

Zusammenfassung

Spannungsgesteuerte Kalziumkanäle (VGCCs) bestehen aus einer porenbildenden α_1-Untereinheit und den akzessorischen β und $\alpha_2\delta$-Untereinheiten. Die weitgehend extrazellulären $\alpha_2\delta$ Proteine $\alpha_2\delta$1-4 modulieren die Eigenschaften von Ca^{2+}-Kanälen, aber die Gründe für ihre partielle Redundanz bzw. Spezifität sind unbekannt. VGCCs werden in einer Vielzahl von Geweben, einschließlich der Cochlea, exprimiert. Die Cochlea ist für die Schalltransduktion und die Übertragung der Informationen zum auditorischen Hirnstamm verantwortlich.

Die Aufgabe der Spiralganglien (SG) Neurone ist die Übertragung von Schallinformationen von den Haarzellen der Cochlea zu Neuronen im auditorischem Hirnstamm. SG-Neurone, sind unerlässlich für die Hörfunktion, denn ihr Verlust kann nicht durch ein Hörgerät oder ein Cochlea-Implantat ersetzt werden.

Der Ca^{2+}-Kanal-Komplex der ausgereiften Präsynapsen der IHC wird von $Ca_v1.3$, β_2 und $\alpha_2\delta$2 gebildet (Fell et al. 2016). Besonders die $\alpha_2\delta$-Untereinheiten sind aufgrund ihrer vielfältigen Funktionen bei der Schmerzverarbeitung, Synapsenbildung und als therapeutische Angriffspunkte für verschiedene Medikamente interessant geworden. In dieser Arbeit wurde die Rolle der $\alpha_2\delta$3-Untereinheit von VGCCs im Hinblick auf ihren Beitrag zum Ca^{2+}-Strom von neonatalen und reifen SG-Neuronen und die Entwicklung der Endbulb of Held-Synapse an $\alpha_2\delta$3-defizienten Mäusen analysiert.

Das Fehlen der $\alpha_2\delta$3-Untereinheit reduzierte die $Ca_v2.1$-Ströme, welche die dominierenden Ca^{2+}-Ströme von reifen kultivierten SG-Neuronen von 3 Wochen alten Mäusen sind, um 60%. Zudem zeigten $\alpha_2\delta$3-defiziente Mäuse im Alter von drei Wochen deformierte und kleinere Endbulb of Held-Synapsen. Überraschenderweise wurde bereits an P5, wenn P/Q ($Ca_v2.1$)-Kanäle in SG-Neuronen noch nicht exprimiert werden, $\alpha_2\delta$3 für eine normale Bildung von Endbulb of Held-Synapsen benötigt. Dies weist auf eine spezifische Funktion von $\alpha_2\delta$3 für die Synapsentwicklung hin, die unabhängig vom P/Q-Ca^{2+}-Strom ist.

Die Endbulb of Held-Synapse wurde auch in einer funktionellen $\alpha_2\delta$2-null-Mutante untersucht, da diese Mäuse verzerrte auditorische Hirnstammantworten in Welle I zeigten. Ziel war es herauszufinden, wie sich die Deletion von $\alpha_2\delta$2 auf die Synapsentwicklung auswirkt. Die Analyse der Endbulb of Held-Synapse zeigte eine verringerte VGLUT1-markierte Fläche der Axonterminale sowie eine geringere Anzahl von Boutons pro Bushy-Zelle im Vergleich zum Wildtyp. Im Gegensatz zu IHCs exprimieren SG-Neurone mindestens 6 porenbildende α_1-Untereinheiten und alle drei neuronalen $\alpha_2\delta$-Untereinheiten $\alpha_2\delta$1, 2 und 3.

In dieser Arbeit konnten wir zeigen, dass (i) nur $Ca_v2.1$ Kanäle durch das Fehlen der $\alpha_2\delta3$ in adulten Mäusen betroffen sind, (ii) $\alpha_2\delta3$ eine Funktion in der synpatischen Entwicklung hat, welche unabhängig von $Ca_v2.1$ Kanälen ist und (iii) auch das Fehlen von $\alpha_2\delta2$ einen Effekt auf die Entwicklung der „Endbulb of Held" synapse in adulten Mäusen hat.

1.   Introduction

Acoustically evoked signal processing is carried out in an ultrafast and timely precise way and requires fully functional and developed connections, which are already established in the embryonic period (Pierce 1967). Intrinsic programs determine the differentiation of these neural circuits, while initial wiring of sensory circuits is based on axon guidance molecules (Fekete & Campero 2007; Huberman et al., 2009). Their refinement toward mature functional characteristics is driven by intrinsically generated electrical activity (Defourny et al., 2011).

In mice and most other rodents, the auditory system is immature at birth. Sound processing starts/begins/is initiated around postnatal day 12 (P12) (Curzon et al., 2009) offering optimal conditions to study the auditory system in mice before and after the onset of hearing.

1.1   The ear

The ear is a sensory organ responsible for the detection and processing of sound and can be categorized into three parts referred to as external, middle and inner ear (**Fig. 1**). A change in sound pressure activates the auditory system, limited by a specific frequency range. In humans, this range is between 20 Hz and 20 kHz and in mice between 2 kHz and 100 kHz. Airborne sound is absorbed and collected by the auricle part of the external ear and impinges on the tympanic membrane, setting the auditory ossicles of the middle ear into motion. The orientation of the ossicles enables the precise transmission of the sound vibrations from the external and middle ear to the inner ear, where the vestibular organ and the cochlea, the actual hearing organ is located. As shown in Figure 1, the bony cochlea appears as coil-shaped structure and is directly attached to the vestibular organ, which contributes to the sense of balance and spatial orientation by detecting linear and rotational accelerations (Dabdoub et al., 2016; Malmierca and Mechán, 2004).
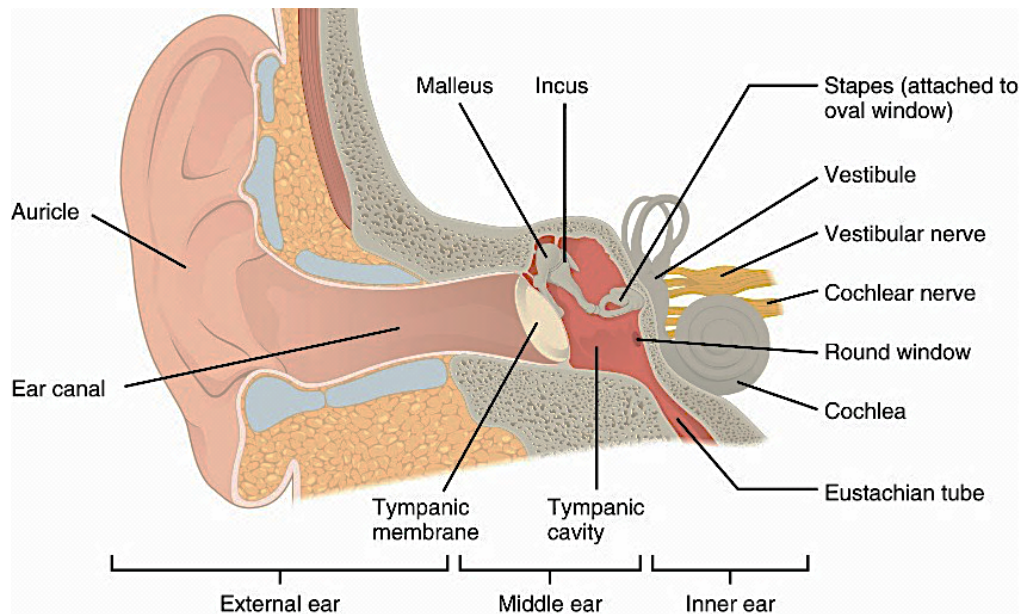
Figure 1. Structure of the human ear
The ear can be divided into three compartments - external, middle and inner ear; here the structure for the human ear is shown. Sound that enters the ear via the auricle travels along the ear canal and hits onto the tympanic membrane causing vibrations. These vibrations set the three ossicles malleus, incus and stapes into movement, which transmit the vibrations along to the cochlea, where the mechanical signal is converted to an electrical signal. The vestibular organ, attached to the cochlea functions in the sense of balance. Picture from: https://texasdeafed.org/topics/how-we-hear

Compared to the external and middle ear, which are air-filled, the inner ear is a fluid-filled organ. The cochlea is responsible for the transmission of sound as a pressure signal is converted to an electrical signal along the auditory pathway.

1.1.1   The cochlea

The cochlea has a coil-shaped form and is located in the temporal bone of the mammalian skull. The size of the cochlea can vary between species and has in mammals between 1.5 - 4 turns, compared to birds and reptiles, where the cochlea appears as a flat or sickle shaped epithelium (Malmierca and Mechán, 2004; Mann and Kelly, 2011). The cochlea is connected to the middle ear via the auditory ossicles that are set into motion by sound pressure waves, hitting onto the tympanic membrane. From these three ossicles the stapes is directly attached to the membrane of the oval window where it conveys oscillations and creates pressure fluctuations in the three fluid-filled internal cochlea compartments (**Fig. 2**).
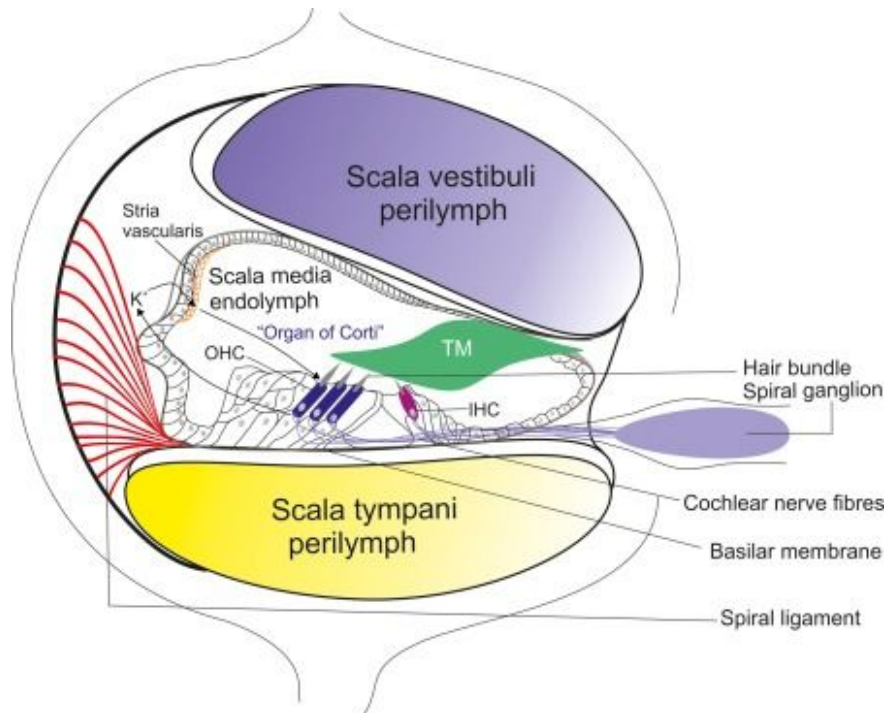
Figure 2. Compartments within the cochlea
In contrast to the air-filled middle and external ear, the cochlea is a fluid-filled organ, containing peri- and endolymph in different compartments. Perilymph, which is high in Na^+ (140 mM) and low in K^+ (4 mM) is found in the scala vestibuli and tympani, which surrounds the scala media. The scala media is separated from both by two membranes on each side and contains endolymph, which is high in K^+ (120 mM) and low in Na^+ (1 mM). The organ of Corti, the sensory epithelium is located on the basilar membrane within the scala media and spirals around the modiolus.
Picture from: http://3.aspire-atlantis.de/tion/cochlea-diagram-scala-media.html

In principle, the function of the cochlea is the detection of sound, transduction of electrical signals and transmission to the cochlear nuclear complex (CNC). Therefore the cochlea represents the first station within the auditory pathway.

From the three compartments (scala vestibule, scala media and scala tympani), the scala vestibuli is connected to the oval window, where as the scala tympani is connected to the round window. Both scalae meet only at the most apical part of the cochlea called helicotrema. The scala tympani and vestibuli are filled with perilymph, a fluid with a similar ion composition as the extracellular fluid, characterized by a high Na^+ and a low K^+ ion composition. The scala media, which is located between both scalae is seperated from the scala vestibuli by the Reissner's membrane and from the the scala tympani via the BM. In contrast to the scala vestibuli and tympani, the scala media contains endolymph, which contains a high K^+ and a low Na^+ concentration. Both, the high K^+ concentration and the positive potential of the endolymph (approx. +80 mV) generate a driving force for K^+ ions into hair cells if mechanotransducer channels open at the apex of hair cells as consequence of tip-link displacement due to vibrations caused by incoming sound (Kurbel et al., 2017). The

composition and potential of the endolymph are maintained by K^+ recycling and by active secretion of K^+ ions from cells of the stria vascularis. The stria vascularis represents a 3-layer epithelium with a dense network of capillaries and is involved in the regeneration of the ionic composition of the endolymph and thereby forms a physical seal between the bony and membranous labyrinth (Dallos et al., 1996; Malmierca and Mechán, 2004).

1.1.1.1 Structure and development of the organ of Corti

The OoC is the sensory epithelium laying on the BM and contains several types of supporting cells, and two types of sensory cells: inner (IHC) and outer hair cells (OHC) (Malmierca and Merchán, 2004) (Fig. 3). The sensory neurons also referred to as spiral ganglion (SG) neurons form the *nervus cochlearis*, which projects to the CNC. In the OoC, mechanical vibrations, which lead to a deflection of the stereocilia on hair cells, are converted into electrical signals, which are transmitted by SG neurons to the CNC and from there further on. The OoC is located on the BM and covered by the tectorial membrane (TM) (**Fig. 3**). The BM is an acellular structure made up by collagen fibers and tightly packed proteoglycans with tonotopically varying stiffness and width. The TM, an acellular viscoelastic connective tissue, covers sensory and supporting cells, which is present along the tonotopic axis of the cochlea (Gavara et al., 2011). The viscosity of the TM is maintained by collagen, which is one of the major components (collagen type II, V, IX and XI). Other components are al α-tectorin, β-tectorin and otogelin.
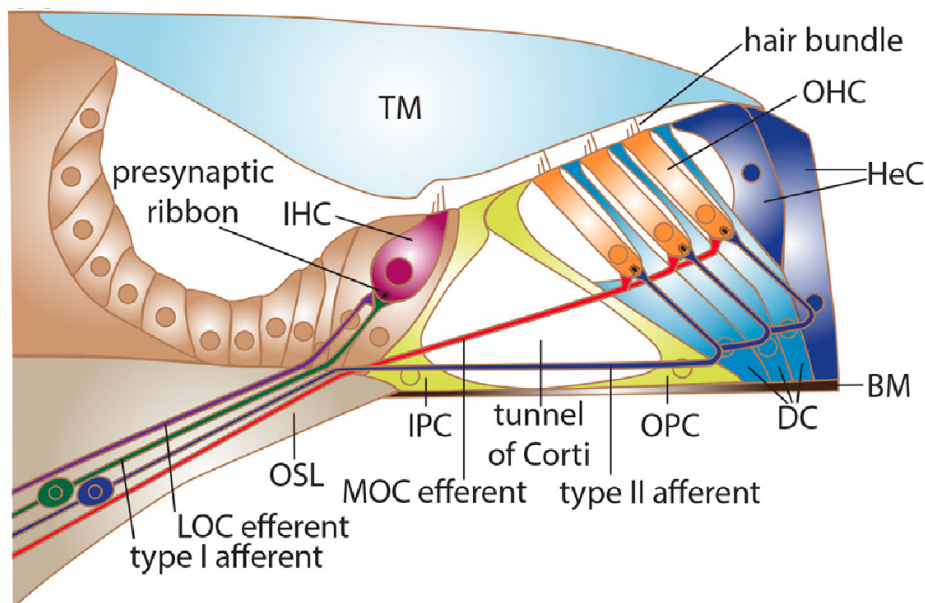
Figure 3. Scheme of the mature organ of Corti
Two different types of sensory hair cells as well as SG neurons and numerous types of supporting cells are found within the OoC. In the OoC, 3 rows of OHCs can be found, which receive afferent innervation from type

II SG neurons and efferent innervation from MOC fibers. Deiters cells separate OHCs from each other. IHCs, which are present in a single row, receive afferent input from type I SG neurons and LOC provide efferent input and contact the non-myelinated part of the type I SG neuron. Phalangeal cells separate IHCs from each other. The TM covers the sensory hair cells, which contact only the tallest stereocilia of the OHCs. Rows of stereocilia of IHC and OHC are connected with tip links and movement of the BM and TM cause a deflection of the stereocilia towards the tallest. Picture from: Zhang and Coate (2016)
Abbreviations: BM: basilar membrane, DC: Deiters cell, HeC: Hensen cells, IHC: inner hair cell, IPC: inner phalangeal cell, LOC: lateral olivocochlear, MOC: medial olivocochlear OHC: outer hair cell, OPC: outer phalangeal cell, OSL: outer spiral ligament, TM: tectorial membrane.

Relative movement as consequence of motion of the ossicles, causes deflection of the hair cell stereocilia and the mechanosensitive channels, which results in the inflow of K^+ and Ca^{2+} ions (Fettiplace, 2009; Gavara et al., 2001; Kazmierczak & Müller, 2012; Li et al., 2011). This causes a depolarization of the IHC, which activates voltage-gated Ca^{2+} channels (VGCCs) (Fuchs and Evans, 1990). The activation of VGCCs mediates Ca^{2+} influx, which triggers the exocytosis of synaptic vesicles (Glowatzki and Fuchs, 2000).

OHCs are activated similar to IHCs by K^+ influx at the tip of the stereocilia. The activation starts with a reverse transduction process, which enhances the cochlear sensitivity and frequency selectivity (Dallos et al., 2008; Yi and David, 2014). OHCs receive afferent innervation by type II SG neurons and efferent innervation by MOC fibers and due to their electromotile ability they are able to undergo rapid changes in somatic length when voltage changes go across their membrane (Zheng et al., 2002). This process occurs in a range of microseconds and does not depend on ATP, Ca^{2+} or contractile filaments (Dallos, 2008) and increases the cochlear sensitivity by around 40-50 dB, which further improves frequency discrimination (Zheng et al., 2002). While OHCs are referred to as motor-cells, IHCs are referred to as the true sensory cells because only IHCs are responsible for the transduction of sound stimuli, by transmitter release, which is converted into neuronal signals and passed on to the CNC and further on from there.

Characteristic for the IHCs is the presence of pre-synaptic ribbons located at the basal pole of the hair cell. The IHC ribbon synapse responds to changes in the membrane potential (Nouvian et al., 2006) caused by the influx of K^+ ions through transducer channels. The inner hair cell ribbon is a protein complex, which resembles ribbons found in photoreceptor and bipolar cells of the retina. Characteristic markers of the ribbon synapse are RIBEYE, Bassoon and Picolo (Wichmann, 2015). The neural pole of the IHC receives between 90 – 95 % of the total afferent fiber contacts, while OHC receive only 5 – 10 % (Malmierca and Mechán, 2004).

The transmission and processing of sound is a highly precise and ultrafast process that requires fully functional connections and optimal innervation of the cochlea by the sensory

neurons. In the mouse, the sensory organ develops as early as embryonic day E10.5 (Mann and Kelley, 2011). Development of the sensory epithelium includes axon growth towards the target cells, formation of synaptic contacts and in a final step, retraction of false connections to provide an optimal innervation pattern in the mature stage. SG neurons develop in parallel with the sensory hair cells (Dabdoub et al., 2016). In the first stage of the development, cells depend on the secretion of chemotropic agents by the sensory epithelium, on membrane proteins and non-diffusible extracellular matrix molecules, which support the neurons in path finding and provide guidance. These factors can support axon outgrowth but can also lead to the retraction of certain axons. Two important growth factors for the development and guidance of sensory neurons in the cochlea are neurotrophin 3 (NT3) and brain derived neurotrophic factors (BDNF). NT3 is expressed around embryonic day E12.5 and shortly after BDNF is expressed, too (Defourny et al., 2011; Green et al., 2012; Mann and Kelley, 2011). Both are needed for the growth of SG neuron afferents towards the OoC. Around E16.5, type II neurons exclusively project to OHCs, while type I neurons project to inner as well as outer hair cells. *In-vivo* experiments showed that both growth factors are indispensable for the proper development of SG neuron either in the organ itself but also in culture. NT3 as well as BDNF are tonotopically expressed as neurotrophin gradients in the cochlea, with NT3 being found in the apical to medial part and BDNF in the basal to medial part of the cochlea. The receptors for the growth factors (TrkB and TrkC) are found on all SG neurons following no tonotopic distribution. Clinical administration of NT3 after excitotoxic trauma showed *in vitro* that it supports regeneration of type I SG neuron / IHC cell synapse (Wang and Green, 2011). In the 2nd stage of development, the axon terminals undergo refinement and terminate at the sensory hair cells for optimal innervation. During this stage, a transient connection of type I neurons to OHCs is observed. This transient connection is retracted in the final stage in which the synapses connect to their target hair cells. As a consequence of axon retraction, OHCs are exclusively innervated by type II neurons and show a low number of synapses (1-3 per OHC) (Defourny et al., 2011). This retraction of type I peripheral dendrites occurs between postnatal day 1 and 4. At the mature IHC ribbon synapse, afferent type I SG neurons make a precise one to one IHC ribbon connection; thereby one IHC receives input from about 10 – 20 afferent type I SG neurons. This occurs between the 1st and 2nd week of development, presumably around the onset on hearing (Safieddine et al., 2012).

1.1.1.2   Spiral ganglion neurons

SG neurons are peripheral sensory neurons that provide afferent innervation of the OoC (Rusznák and Szucs, 2009). They are the first neurons in the auditory pathway that generate action potentials to transmit auditory information to the brain. SG neurons are indispensable for hearing and their loss cannot be compensated by any hearing aid and results in deafness. They represent a heterogeneous cell population, which can be divided into 2 categories, namely type I and type II SG neurons, which differ in morphology, physiological and molecular specializations (Kawase and Liberman, 1992; Reijntjes and Pyott, 2016).
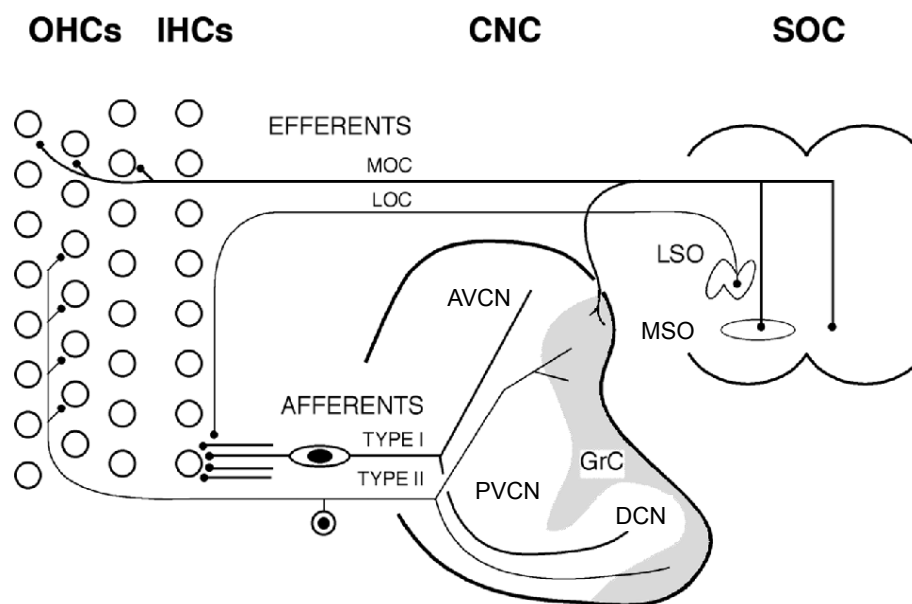
Figure 4. Afferent and efferent innervation of the organ of Corti
The OoC receives afferent innervation by type I and type II neurons, which transmit sensory information to the AVCN and DCN in the CNC. The afferent innervation of OHCs is accomplished by type II SG neurons, while the efferent innervation is provided by MOC fibers originating from the MSO. IHCs receive afferent innervation by type I SG neurons. Peripheral dendrites of type I SG neurons rather than IHCs receive efferent innervation from LOC fibers originating from the LSO. The afferent fibers of type I and type II neurons bundle and form together with afferent fibers form the vestibular organ the 8th cranial nerve that projects to the CNC. From here type I SG neurons project to the AVCN and DCN and type II SG neurons project to the granular cell layer. At the AVCN auditory nerve fiber terminals project onto bushy cells and form the endbulb of Held synapse. From: Malmierca and Merchán (2004).
Abbreviations: OHC: outer hair cells, IHC: inner hair cells, CNC: cochlear nuclear complex, SOC: superior olivary complex, MOC: medial olivocochlear system, MSO: medial superior olive, LOC: lateral olivocohlear, AVCN: anterior ventral cochlear nucleus, PVCN: posterior ventral cochlear nucleus, DCN: dorsal cochlear nucleus, GrC: granular cell layer, LSO: lateral superior olive, MSO: medial superior olive

Type I and type II SG neurons differ in their targets for synaptic input and in a number of markers used to distinguish between both groups. Afferent type I neurons make a precise one to one connection with IHC ribbon synapses at the basal pole of the IHC. On average, the peripheral dendrites of 10 – 20 afferent type I SG neurons fiber contact one IHC. In mice, the

soma as well as the neurites of type I SG neurons are myelinated, except a small part close to the IHC where LOC efferent fibers contact type I afferents. Based on the spontaneous discharge rate, afferent type I SG neurons can be subdivided into 3 groups, called high, medium and low spontaneous discharge rate neurons (Kawase and Liberman, 1992). Furthermore, SG neurons represent a highly heterogeneous cell population characterized by expression of different ion channel profiles, transcription factors, neurotransmitter receptors and adhesion molecules (Shrestha et al., 2018). Using specific single cell RNA sequencing analysis, 3 different classes of afferent type I SG neurons have been identified so far, showing that each cell type has specific functions regarding the processing of auditory information (Shrestha et al., 2018; Sun et al., 2018).

Type II SG neurons are non-myelinated and provide afferent innervation of several OHCs. They are tonotopically organized within the cochlea, meaning that at the base, the high frequency region, type II SG neurons mainly innervate the outer row of OHC, while at the apex, the low frequency part, type II SG neurons contact all 3 rows of OHCs. Even though, type II SG neurons mainly innervate the outer row of OHC, at the apex, the low frequency part, type II SG neurons contact all 3 rows of OHCs. Afferent type II SG neurons specifically express peripherin, which enables specific differentiation between type II and type I SG neurons. In contrast, type I SG neurons, which make a precise one to one connection to IHC ribbons, type II SG neurons contact several OHCs. On average one type II SG neuron contacts 15 – 20 OHCs (Carricondo and Romero-Gómez, 2018). Type I as well as type II SG neurons appear as bipolar cells. Their morphology can change after enzymatic digestion, such that cells appear as unipolar and multipolar lemon-like shaped cells (Rusznák and Szucs, 2009). SG neurons transmit all aspects of acoustic stimuli such as level, frequency pattern, and duration and thus are indispensable for a proper hearing function. Genetic and environmental factors such as medication, noise and ageing cause partial loss of SG neurons, which may result in frequency-specific hearing loss and in inability to hear in noisy environments. The afferent axons of both, type I and type II SG neurons form the acoustic portion of the 8th nerve, forming the connection between sensory hair cells in the cochlea and bushy cells located in the cochlear nuclear complex on the ipsilateral site. From the cochlea, SG neurons project to 2nd order neurons in the hindbrain. The fibers bifurcate to form 2 branches, one contacting the DCN while the other contact the VCN on the ipsilateral site.

1.2   The central auditory system

A fundamental organization within the auditory system is tonotopy, which is characterized by the arrangement of nearby frequencies throughout the auditory system. The cochlea before the onset of hearing, codes for mid-to-low sound frequencies (Lippe and Rubel, 1983), while shortly after the onset of hearing, the basal part of the cochlea becomes sensitive for high frequencies and the apex for lower frequencies (Kandler et al., 2009).

IHCs and OHCs have specific functions to process incoming sound signals. It has been shown by different groups that OHCs act as amplifier elements and enhance low-level sound, while IHCs are the main detectors of acoustic stimuli (Malmierca and Merchán, 2004). The 8th nerve is formed by ANFs of the SG neurons located in the Rosenthal's canal, which convey information and project to the first station of the central auditory pathway the CNC. Via this nerve, who's branches project to various neurons in the CNC, the auditory information are transferred to the central auditory system. Figure 5 gives an overview about the different stations of the auditory pathway.
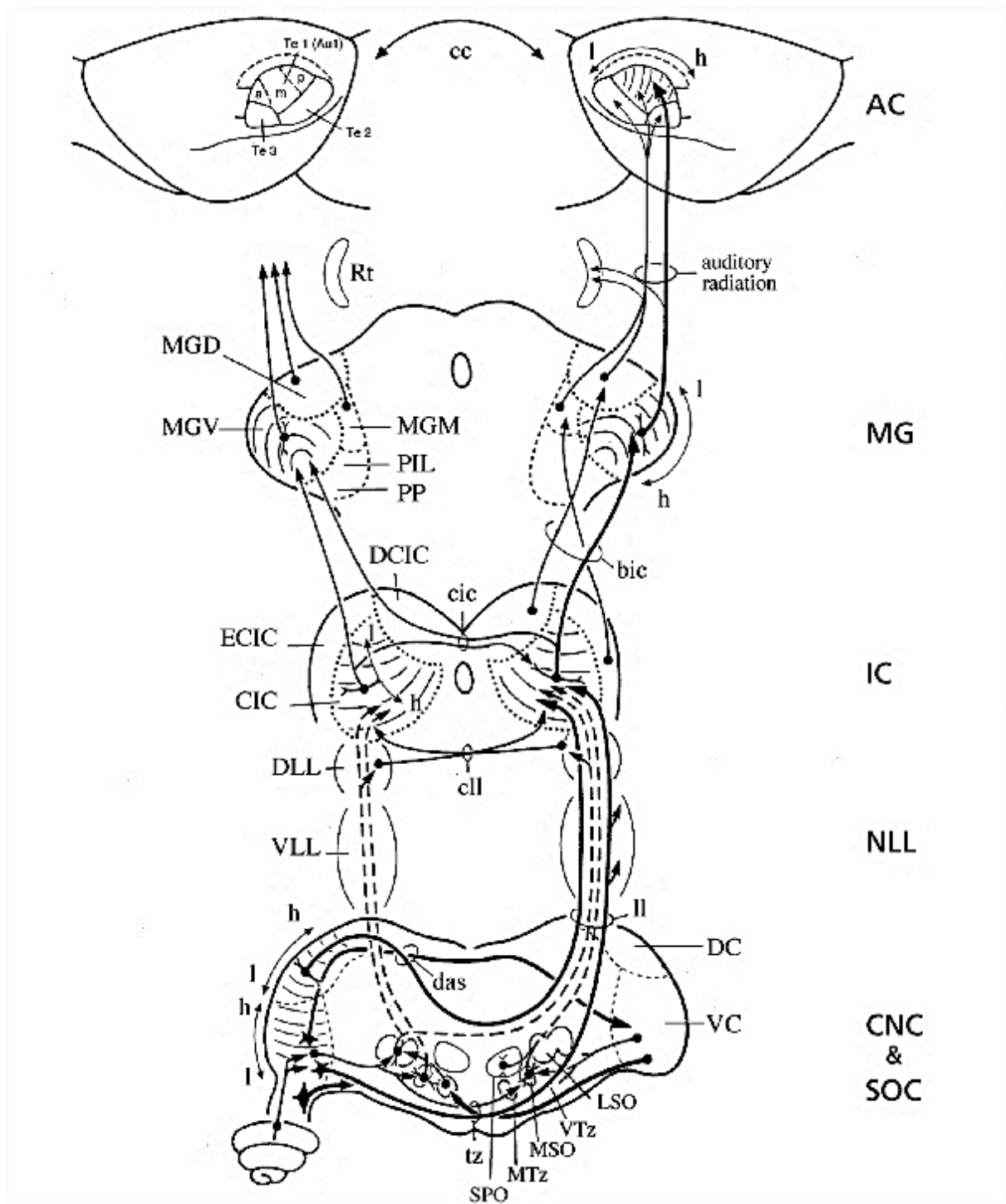
Figure 5. Simplified sketch of the auditory pathway
The auditory pathway starts at the cochlea, the peripheral hearing organ, that perceives incoming sound and transmits the signal along the auditory nerve to the CNC, the first station of the central auditory pathway. ANF axons branch and terminate on neurons of the ventral and dorsal cochlear nucleus. From the target neurons some axons cross the midline and project to neurons on the contralateral site, while others remain on the ipsilateral site. From the cochlear nucleus, the auditory signal is transmitted along the superior olivary nucleus, is further processed in the lateral lemniscus until it reaches the inferior colliculus. From there, it is processed in the auditory midbrain (medial geniculate body) and finally reaches the auditory cortex. From Malmierca and Merchán (2004).
Abbreviations: SOC: superior olivary complex; CNC: cochlear nuclear complex; NLL: nuclei of the lateral lemniscus; IC: inferior colliculus; MG: medial geniculate body; AC: auditory cortex.

The CNC serves arch to all other afferent processing units and can be divided into 3 parts called dorsal cochlear nucleus (DCN), posterior ventral dorsal cochlear nucleus (PVCN) and the anterior ventral cochlear nucleus (AVCN). Auditory nerve fiber bundles reach the CNC, where they branch and contact neurons in the AVCN, DCN and the PVCN. In the CNC a cluster of different neuronal cell types, having different electrophysiological properties and morphological patterns can be found.

The DCN contains a laminar cell structure including the molecular (ML), fusiform cell (FCL) and the deep (DL) layers. Characteristic cell types at the DCN are Golgi, ML-stellate, cartwheel, tuberculo-ventral, unipolar brush, giant and fusiform cells, which are arranged in mono- or multiple layers (Oertel, 1999). The VCN can be subdivided into AVCN and PVCN (Malmierca and Mechán, 2004). Characteristic for the VCN are octopus, bushy (globular and spherical) and stellate (T- and D-) cells. Stellate cells are contacted by a large number of small bouton-like endings (Cao and Oertel, 2010), while spherical- and globular bushy cells are contacted by large axosomatic terminals, called endbulbs of Held (chapter 1.2.1).

The superior olivary complex (SOC) is located in the caudal pons dorsal to the pontine gray and consists of three main nuclei: the medial superior olivary nucleus (MSO), the lateral superior olivary nucleus (LSO) and the medial nucleus of the trapezoid body (MNTB). These nuclei are most important for the ascending auditory pathway, even though several smaller nuclei are located around these three. The SOC is the first nucleus in the auditory pathway that receives information from both ears. CNC projections reach the SOC and can be divided into two groups. The ventral stream is associated with binaural sound localization whereas the dorsal stream is needed for sound identification. The ventral stream connects to the SOCs on both sides of the brain. Projections from the ipsilateral side directly project to the LSO, while those projecting to the contralateral side first pass the MNTB until they project to the LSO. At the LSO the intensities of the stimuli are compared. The MSO is characterized by bipolar neurons and receives ipsilateral and contralateral innervation from both VCNs without an intervening synapse. The dorsal stream functions in sound identification, which is identified by the inferior colliculus on the opposite side. The MNTB receives input from the ipsilateral PVCN and globular cells of the AVCN via the specialized calyx of Held. Cells of the MNTB are inhibitory interneurons (Malmierca and Mechán, 2004; Roberts et al., 2014). Fibers from the CNC connect contralateral and ipsilateral to the inferior colliculus (Sento and Ryugo, 1989; Yu and Goodrich, 2014). From the CNC the signal travels along the auditory pathway and is processed by different stations including the lateral lemniscus (LL) complex, the

inferior colliculus (IC) in the midbrain, the medial geniculate nucleus (MG) in the thalamus and winds up in the auditory cortex.

1.2.1   The endbulb of Held synapse

In general a synapse represents a structure that allows the transmission of an electrical signal to pass from one neuron to another. The endbulb of Held synapse is formed by one or more axosomatic terminals of ANF endings, that project onto bushy cells in the AVCN and represents one of the largest synapses in the brain. The principal neurons of the AVCN are bushy and stellate cells, both receiving input from the central projection of SG neurons (Limb and Ryugo, 2000; Wang and Manis, 2005). Bushy cells receive electrically encoded information form the axosomatic endings of SG neurons and convey this timing information to the MSO. One bushy cell gets contact from up to 5 – 8 endbulb terminals (Limb and Ryugo, 2000). From the AVCN, bushy cells project to the SOC where they play important roles in the processing of interaural time differences. Figure 6 shows the development of the endbulb of Held synapse from postnatal day 1 onwards.
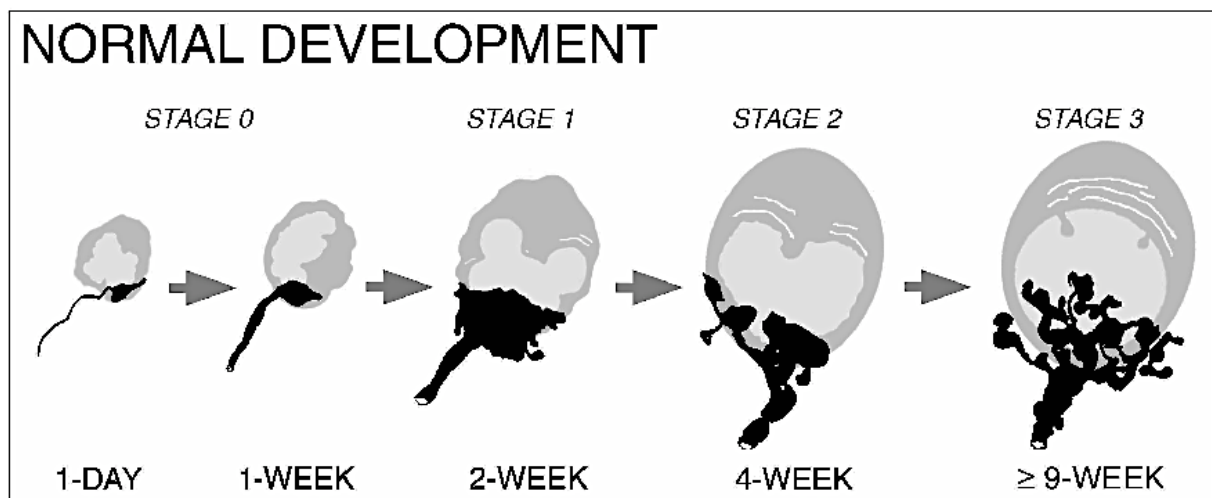
Figure 6. Development of the endbulb of Held synapse
Auditory nerve fiber terminals make axosomatic contact to spherical bushy cells (SBC, gray) and form the endbulb of Held synapse (black). The normal development is depicted above, starting at day 1 with a small swelling, that grows in size and shape until postnatal week 2. At the 2nd postnatal week, the swelling has become 10 – 15 times larger and displays a more distinct morphology characterized by random branches and filipodial-like extensions. During the following weeks the endbulb becomes a more complex structure with a extensive branching showing a tree-like morphology at the SBC soma with a highly fenestrated and branched structure. The synapse is fully matured at around 9 weeks. Picture from Limb and Ryugo, 2000

The morphological changes go in hand with physiological changes that facilitate effective signaling from SG neurons to SBCs in the mature animal. Mice start to hear around postnatal day 12, which is characterized by synchronous transmitter release that leads to strong post-

synaptic depolarization activating $K_v1.x$ and SK channels in SBCs. Activation of the $K_v1.x$ channels prevents asynchronous release and thereby increases temporal precision. In the mature endbulb synapse, P/Q-type channels at the presynaptic endbulb terminal mediate more than 90 % of the Ca^{2+} current (Lin et al., 2011; Yu and Goodrich, 2014). The endbulb of Held synapse is an excitatory synapse and provides coordinated release of glutamate from multiple presynaptic active zones. Transmission of electrical signals depends on neurotransmitter release. At the endbulb of Held synapse, this is managed by glutamate. When glutamate is released from the presynaptic terminals, it activates ionotropic α-amino-3-hydroxy-5-methyl-4-isoxazolepropionic acid (AMPA) and N-Methyl-D-aspartate (NMDA) receptors, which cause excitatory responses on the postsynaptic cell (Trussell et al., 2012). AMPA receptors are tetramers of independent subunits named GluR1-4, where GluR3 and 4 are mainly found in mature endbulb of Held synapse, while GluR2 dominates at neonatal ages. Their expression dramatically decreases during maturation. The different GluR types differ in their gating speed and partially in their Ca^{2+} permeability. The change in receptor composition that contributes to neurotransmitter release represents an important step in maturation. Changes in the synaptic transmission lead to increased synaptic efficacy, improved fidelity and temporal precision (Kandler et al., 2009; Parks. 2000). NMDA receptors open in response to depolarization via the AMPA receptors. The exact role of these receptors at the endbulb of Held synapse is not known. NMDA receptors are expressed during development but expression is down-regulated during the weaning period. Low levels of NMDA receptors remain at the mature endbulb of Held synapse, where they function in the promotion of firing probability and improvement of temporal precision. The major glutamate receptors are the GluR3 and GluR4 subunits, which enables fast synaptic transmission (Malmierca and Merchán, 2004; Nusser, 2000). During maturation of the synapse, synaptic efficacy increases and fidelity as well as temporal precision improves (Limb and Ryugo, 2000).

1.3 Voltage-gated Ca^{2+} channels

Voltage-gated Ca^{2+} channels (VGCCs) open in response to changes in the membrane potential and allow the subsequent influx of Ca^{2+} ions. They are composed of a pore-forming α_1-subunit and the auxiliary subunits ß and $\alpha_2\delta$ (Catteral et al., 2005; Dolphin, 2012; Zamponi et al., 2015). Chapter 1.4 will focus in more detail on the function of the auxiliary subunits. The formed Ca^{2+} channel complex consists of one α_1-subunit, which builds the channel pore. The α_1-subunit is a transmembrane spanning protein made up by approx. 212 amino acids. 4 homologous domains (I, II, III and IV), each made up by six segments (S1 - S6) build the α_1-subunit (**Fig. 7**). The 4th segment of each domain represents the voltage sensor and contains 5 - 6 positively charged arginins and lysines. With this sensor, the channel has the ability to detect and respond to voltage changes in the membrane potential (Lacinová, 2005).
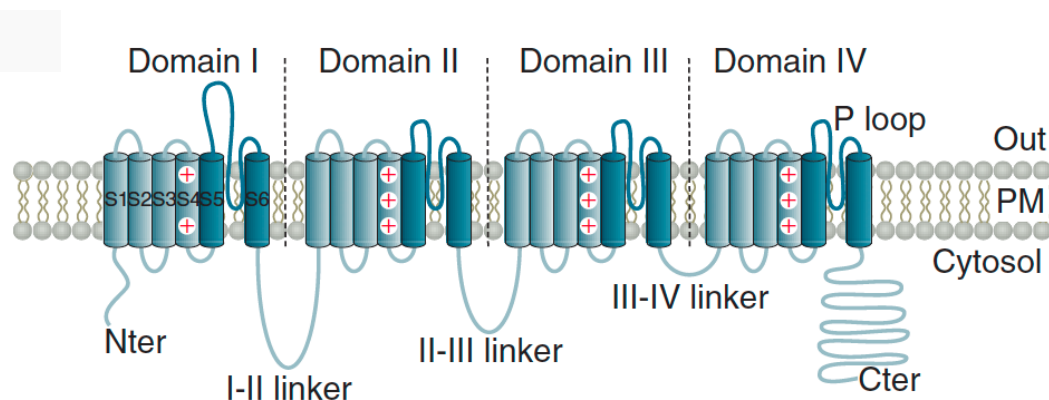
Figure 7. Topology of the α_1-subunit of voltage-gated Ca^{2+} channels
The α_1-subunit is a transmembrane spanning protein and forms the channel pore of VGCCs. Four domains (I - IV), which are connected with each other via intracellular and extracellular loops make up the alpha1 subunit. Each domain consists of 6 segments (S1-6). The loop between S5 and S6 named P-loop forms the channel pore. Segment 4 acts as voltage sensor, which responds to changes in the membrane potential (red + symbols). LVA Ca^{2+} channels consist of only the α_1 subunit as shown above, while HVA Ca^{2+} channels can be modified by the 2 auxiliary subunits ß and $\alpha_2\delta$. Picture from Weiss and Zamponi (2017)

The channel pore is formed by the intracellular loop between segments 5 - 6 and determines the ion conductance and the selectivity of the channel. Changes in the amino acid sequence of the pore loops in domain I, III and IV showed that a channel previously selective for Na$^+$ can convert and become selective for Ca^{2+} (Catterall et al., 2005). Alternative splicing occurs frequently and represents an important process that is necessary for neuronal development (Lipscombe et al., 2013). Especially in the nervous system a large number of VGCC splice variants can be found. Sites for alternative splicing are most often hypervariable regions which include the C-terminal region and the segment II - III intracellular linker (Lipscombe et

al., 2013). Alternative splicing of VGCCs is associated with different diseases referred to channelopathies described in chapter 1.3.3.

In the cell Ca^{2+} is indispensable for a number of more general events including proliferation, protein synthesis, Ca^{2+} dependent gene transcription and differentiation (Bourinet and Zamponi, 2016; Dolphin 2013). Yet, Ca^{2+} is also irreplaceable for more specific events such as muscle contraction, neurotransmitter release, electrical excitability and synaptic plasticity (Barbado et al., 2009).

In vertebrates, 10 genes encode for the α_1-subunit. They can be grouped into low voltage activated (LVA) or high voltage activated (HVA) Ca^{2+} channels, depending on the voltage range in which the channel activates. Three Ca^{2+} channel families have been identified, where Ca_v1 and Ca_v2 belong to the family of HVA and Ca_v3 belongs to the LVA Ca^{2+} channels. The abbreviation Ca_v includes two characteristic features of these channels. "Ca" represents the type of ion, the channel is selective for, whereas the subscript "v" indicates that the channel opens in response to changes in the membrane potential. Table 1 gives an overview about the different types of Ca^{2+} channels as well as their tissue localization (Ertel et al., 2000; Simms and Zamponi, 2014).

Table 1. Voltage-gated Ca^{2+} channel types and their tissue localization.
(Ertel et al., 2000; Simms and Zamponi, 2014)

Ca^{2+} channel	Ca^{2+} current type	Gene	Previous name	Primary localization
$Ca_v1.1$		*Cacna1s*	α_{1S}	Skeletal muscle
$Ca_v1.2$	L	*Cacna1c*	α_{1C}	Cardiac muscle Endocrine cells Neurons
$Ca_v1.3$		*Cacna1d*	α_{1D}	Endocrine cells Neurons
$Ca_v1.4$		*Cacna1f*	α_{1F}	Retina
$Ca_v2.1$	P/Q	*Cacna1a*	α_{1A}	Nerve terminals Dendrites
$Ca_v2.2$	N	*Cacna1b*	α_{1B}	Nerve terminals Dendrites
$Ca_v2.3$	R	*Cacna1e*	α_{1E}	Cell bodies Dendrites Nerve terminals
$Ca_v3.1$		*Cacna1g*	α_{1G}	Cardiac muscle Skeletal muscle Neurons
$Ca_v3.2$	T	*Cacna1h*	α_{1H}	Cardiac muscle Neurons
$Ca_v3.3$		*Cacna1i*	α_{1I}	Neurons

1.3.1 Low voltage activated Ca^{2+} channels

LVA Ca^{2+} channels activate close to the resting membrane potential and only small changes in the membrane potential are necessary to activate these channels. LVA channels exist as monomeric complexes harboring only the α_1-subunit, which is not associated with any $\alpha_2\delta$ or ß subunit.

However expression systems in which the α_1-subunit of T-type channels was co-expressed with different $\alpha_2\delta$ subunits showed an increase in the current density. In native tissues this channel complex formation was not reported so far (Zamponi et al., 2015). Within the VGGCC nomenclature, LVA channels include the Ca_v3 family and the T-type Ca^{2+} channels. T-type channels comprise three types of Ca^{2+} channels, $Ca_v3.1$ (*Cacna1g*), $Ca_v3.2$ (*Cacna1h*) and $Ca_v3.3$ (*Cacna1i*).

Characteristic for these channels is the very negative range of activation, rapid inactivation and slow deactivation (Santi et al., 2002). T-type channels are expressed in a huge variety of tissues and can be found for example in the central nervous system (CNS), heart, smooth muscle, kidney and many endocrine organs. They are involved in a variety of cellular processes including: pacemaker activity, hormone secretion, cell growth, proliferation and fertilization (Santi et al., 2002). In neurons, T-type channels play an important role in the production of spontaneous low-threshold action potentials and intracellular calcium oscillations (Chevalier et al., 2006).

Specific channel antagonists are not known for these channels, however mibefradil or bivalent ions like zinc, nickel and cadmium are often described as T-type channel blockers. In mice and humans, Ca_v3 channelopathies are linked to different seizure disorders, autism and hyperaldosteronism. Due to the huge range of functions of these channels, they are potential drug targets and are important for clinical research (François et al., 2014; Senatore et al., 2012).

1.3.2 High voltage activated Ca^{2+} channels

HVA Ca^{2+} channels the Ca_v1 family with the L-type and the Ca_v2 family including the P/Q-type, N-type and R-type Ca^{2+} channels. In contrast to the LVA Ca^{2+} channels, HVA Ca^{2+} channels require a high amount of voltage for activation. They are multimeric Ca^{2+} channel complexes associated with one ß and one $\alpha_2\delta$ subunit (Catterall, 2000; Kadurin et al., 2016; Zamponi 2005) (**Fig. 8**).

In the 1980s, L-type channels were first described by their high sensitivity to organic L-type Ca^{2+} channel blockers like for example dihydropyridines (DHPs). The channels were abbreviated as L-type due to their long lasting inward current during depolarization. Expression of L-type channels was confirmed for the brain, heart, smooth and skeletal muscle (Zamponi et al., 2015).

Four different isoforms of L-type channels are known that are all transcribed by four different genes, the *Cacna1s* gene codes for the $Ca_v1.1$ channel, *Cacna1c* for the $Ca_v1.2$ channel, *Cacna1d* for the $Ca_v1.3$ channel and *Cacna1f* code for the $Ca_v1.4$ channel. From the four identified L-type Ca^{2+} channel types, only $Ca_v1.2$ and $Ca_v1.3$ can be found in the auditory system and the brain. $Ca_v1.1$ is frequently expressed in muscles, while $Ca_v1.4$ expression is restricted to the retina. In humans, genetic diseases have been described for all four L-type channels. Especially $Ca_v1.2$ and $Ca_v1.3$ are essential for normal brain function and connectivity. Both types share a high similarity but can be differentiated based on the gating kinetics, voltage sensitivity, pharmacology and spatial distribution. For example $Ca_v1.3$ activate at lower voltage / membrane potentials as compared to $Ca_v1.2$ channels. Furthermore $Ca_v1.3$ channels are less sensitive to the block by DHPs (Roca-Lapirot et al., 2017). However each Ca^{2+} channel type is associated with specific proteins to form unique and specific signaling complexes at neuronal membranes (Kabir et al., 2017).

Even though all 4 genes show different expression sites, they are all sensitive to DHPs and can be blocked using nimodipine, a potent Ca^{2+} channel blocker. Although the exact mode of action still needs to be elucidate, it is known that nimodipine acts by stabilizing the channel in its inactivated state, thereby preventing Ca^{2+} ion flux (Striessnig et al., 2014; Zamponi et al., 2015). DHPs are thought to act as channel activators or inhibitors rather than other channel toxins, which occlude the channel pore (e.g. ω-conotoxin). DHPs shift the channel to an open or closed state. Clinically used L-type Ca^{2+} channel antagonists are beside many others nimodipine or nifedipine, while BayK 8644 act as L-type Ca^{2+} channel agonists and is used for research purposes.

P/Q-type calcium channels are one of three members of the Ca_v2 family. The channel is encoded by the *Cacna1a* gene and comprises two types of Ca^{2+} currents, P- and Q-type currents. P-currents were first found in Purkinje cells of the cerebellum, while Q-currents were found in cerebellar granule cells (Nimmrich and Gross, 2012; Tsunemi et al., 2002).

The main expression site of P/Q-type channels is the central nervous system, mainly presynaptic terminals and somatodendritic locations in the brain and the spinal cord, where the channel assists in the release of neurotransmitter release (Dolphin, 2016; Zamponi, 2016). Lower expression levels are found in the heart and pituitary; yet the channels are absent in skeletal muscles, stomach and kidney.

P/Q-currents are transcribed from the same gene, however P- and Q- channels display different biophysical properties and show different sensitivity to ω-agatoxin IVA. P-type currents are blocked by ω-agatoxin IVA with an IC_{50} of 1.2 nM while for the block of Q-type currents an IC_{50} of 89 nM is necessary, indicating that Q-type currents are less sensitive to ω-agatoxin IVA (Randall and Tsien, 1995). Several studies showed that during the development, Ca^{2+} channel composition changes. A developmental switch in the expression of N- and P/Q-type channels was already reported, with N-type channels being mainly present in neonatal or immature ages, while P/Q-type currents dominate in mature ages (Rosato Siri and Uchitel, 1999).

Jun et al. (1999) found in humans, that mutations in the *Cacna1a* gene causes familial hemiplegic migraine (FHM) and episodic ataxia type-2 (EA-2). Generation of a P/Q-type null mouse showed no difference between wildtype and knockout mice until postnatal day 10. From postnatal day 10 onwards the null mice were smaller compared to their wildtype siblings, showed a loss of balance while walking and started to roll onto their backs. They die around 4 weeks of age (Jun et al., 1999). Analysis of these mutant mice revealed that the cerebellum is smaller and has a reduced size compared to the cerebellum of their wildtype siblings. Immunolabeling using anti-calbindin showed Purkinje cell axons with swellings at the focal adhesion sites, which was not detected in the wildtype.

The *Cacna1a* gene undergoes excessive splicing resulting in many different isoforms of the channel, all having different neuronal distribution patterns, biophysical properties and different sensitivity towards ω-agatoxin IVA.

ω-agatoxin is small peptide isolated from the american funnel web spider *Agelenopsis aperta*. The toxin is the most potent and specific blocker of the P/Q-type Ca^{2+} channels and contains several fractions, which act differently and can be divided into 3 groups: α-agatoxin, μ-agatoxins and ω-agatoxins (Bourinet and Zamponi, 2016). All 3 agatoxin forms show different blocking results: α-agatoxin result in a postsynaptic block of transmitter-activated receptor channels, μ-agatoxins act mainly on sodium channels and ω-agatoxins are presynaptic antagonists of VGCCs. From these three groups, ω-agatoxins show the strongest effect and can be further categorized in the subgroups I, II, III and IV. Type I ω-agatoxins are

potent blockers of insect presynaptic calcium channels. Type II ω-agatoxins target different bindings sites compared to type I. The 3rd type of ω-agatoxins represents the largest class of ω-agatoxins with a molecular weight of 8.5 kDa, which seems to be the most non-specific, since it blocks all neuronal HVA calcium channels (L-, P/Q-, N- and R-type) with different affinities. Type IV ω-agatoxins target specifically mammalian VGCCs.

From the three identified ω-agatoxin type IV isoforms, ω-agatoxin IVA has the highest sensitivity in blocking P/Q-type Ca^{2+} channels. All ω-agatoxin type IV isoforms block the channel by binding to the voltage sensor thereby changing the gating properties of the channel. The toxin can be removed by strong depolarizations (Pingros et al., 2011), however washout of the toxin is incomplete. Several studies showed that ω-agatoxin IVA has the potential to block $Ca_v2.2$ and $Ca_v2.3$ channels to a certain extent (Williams et al., 1994).

N-type Ca^{2+} channels are encoded by the *Cacna1b* gene and are the second member of the Ca_v2 family. N-type channels are widely distributed in neuronal tissue and beside P/Q type channels are the main VGCCs in the nervous system and are often found at synapses where they control neurotransmitter release. N-type channels are often expressed in immature neurons, controlling neurotransmitter release including glutamate, γ-aminobutyric acid, acetylcholine, dopamine and norepinephrine (Ino et al., 2001; Turner et al., 2011). Furthermore, N-type channels are important for synaptic transmission of pain signals in dorsal root ganglions.

Mice lacking the N-type channel have a much milder overall phenotype compared to $Ca_v2.1$ null mice. These mice are hyposensitive to inflammatory and neuropathic pain (Weiss et al., 2014). Mutations in humans are not known because similar to mice, the phenotype is very mild and might often be undetected (Simms and Zamponi, 2014). ω-conotoxins, potent N-type channel blockers are produced by different cone snails, which use their venom to target the neuromuscular system of their prey (fish, worms and snails). To date 6200 different toxins have been identified from more than 100 species. The toxins can be categorized into 3 main groups according to: a) the gene superfamily, b) the pattern of cysteine distribution and c) their molecular targets (Bulaj et al., 2003; Olivera et al., 1987; Schroeder and Lewis, 2006). The toxins block the channel by binding to the channel pore. All toxins target the N-type Ca^{2+} channel ($Ca_v2.2$) whereas some toxins target in addition also P/Q-type channels ($Ca_v2.1$) (ω-conotoxin-CVID and -MVIIC) (Ramírez et al., 2017). The venom produced by *Conus geographus* contains the 4 isoforms ω-conotoxins GVIA, GVIB, GVIC and GVIIA. From

these ω-conotoxins GVIA has been studied more intensively on an electrophysiologically basis.

The cone snail *Conus magnus* produces the ω-conotoxins MVIIA, MVIIB, MVIIC and MVIID. Their main target is the $Ca_v2.2$ channel, however ω-conotoxins MVIIC also blocks $Ca_v2.1$ channels. This shows that a small change in the amino acid composition of these peptides is sufficient to change the target of the toxin. Especially ω-conotoxins MVIIA has aroused interest as it can be synthesized while retaining its native conformation. In 2004, Prialt®, a drug generated on the basis of ω-conotoxins MVIIA has been introduced to the market and is used for the treatment of chronic pain, when previous treatment with analgesics, intrathecal morphine therapy was ineffective (Bourinet and Zamponi, 2016).

R-type currents were first described by Randall and Tsien (1995) as a fraction of currents that remained in cultured cerebellar granule cells after blocking L-type, P/Q-type and N-type currents (Randall and Tsien, 1995). Based on the resistance to known Ca^{2+} channel blockers, these channels were termed "residual" in short R-type channels. Until now, R-type channels encoded by *Cacna1e* are the least well-characterized VGCCs with respect to their physiological properties, pharmacology and clinical relevance (Ertel et al., 2000).

Newcomb et al. described the first potent R-type Ca^{2+} channel blocker SNX-482, a small peptide toxin produced by *Hysterocrates gigas,* a giant African spider (Newcomb et al., 2000). SNX-482 targets the voltage sensor of the calcium channel, thus leading to a voltage shift and a change in the gating properties of the channel (Bourinet and Zamponi, 2016; Pringos et al., 2011). SNX-482 has been shown to effectively block VGCCs in neurons of rat neurohypophyseal nerve terminals at weak nanomolar concentrations. However, R-type currents in several types of rat central neurons are not affected by SNX-482, even at concentrations of 200-500 nM (Newcomb et al., 1998). Tottene et al. found different responses to the application of SNX-482 in the cerebellar granule cells G2 and G3. Using an antisense oligonucleotide strategy they could show that the α_{1E} gene encodes SNX-482 sensitive and SNX-482 resistant R-type currents (Tottene et al., 2000).

R-type channels are widely distributed in the CNS and PNS as well as in the endocrine, reproductive, cardiovascular and gastrointestinal system. Several splice variants of the *Cacna1e* gene are known and channel properties can be further increased by the combination with various auxiliary subunits. $Ca_v2.3$ null mice have a mild phenotype including hyposensitivity to pain, altered fear behavior and resistance to chemically induced seizures. However, mutations in humans have not been reported so far (Simms and Zamponi, 2014).

1.3.3   Channelopathies of voltage-gated Ca^{2+} channels

Channelopathies are defined as defects in ion channels, which can occur due to mutations of ion channel coding genes or as acquired defects in the ion channels (intoxication). Ion channel defects affect potassium, sodium and calcium signaling and can lead to a variety of diseases including epilepsy, migraine, deafness, blindness, hypertension and many more (Kim, 2014). The huge variety in VGCCs arises from processes such as alternative splicing, posttranslational modifications, interaction with auxiliary subunits and splice variants.

Most VGCC channelopathies affect the nervous system or skeletal muscle. Mutations of calcium channels in neurons are often associated with epilepsy, ataxia, migraine, deafness and peripheral pain syndrome (Cain and Snutch, 2013).

Mutations in the *Cacna1c* gene (Ca$_v$1.2 channel) were previously associated with different neuropsychiatric disorders including: bipolar disorder and schizophrenia, major depressive disorder, autism spectrum disorder and attention deficit hyperactivity disorder (Kabir et al., 2017). Also, mutations in the *Cacna1d* gene coding for the Ca$_v$1.3 channel have been associated with autism spectrum disorder, intellectual disability and epilepsy (Pinggera et al., 2017). Ca$_v$1.3 channels play a very important role in the mammalian auditory system. The Ca$_v$1.3 channel is the essential Ca^{2+} channel of inner hair cells as mice lacking Ca$_v$1.3 are congenitally deaf. There is a > 90 % loss of Ca^{2+} influx at the IHC synapse and subsequent loss of OHCs, IHCs and later SG neurons (Platzer et al., 2000). Furthermore, Ca$_v$1.3 is essential for neurons of the superior olivary complex and therefore represents a a central deafness gene (Satheesh et al., 2012). In humans, a loss-of-function mutation in Ca$_v$1.3 causes deafness and bradyarrhythmia (Baig et al., 2011).

Mutations in the *Cacna1a* gene coding for P/Q-type channels represents another example of channelopathies in the CNS leading to familial hemiplegic migraine type 1 (FHM1), episodic ataxia type 2 (EA2) and spinocerebellar ataxia type 6 (SCA6) (Kim, 2014). Till today, 21 FHM1 mutations are reported, all missense mutations in the Ca$_v$2.1 gene in the region of the pore lining and the voltage sensor. Characteristic for FHM1 are unilateral headache, often in combination with nausea, phonophobia, photophobia and motor weakness. In Ca$_v$2.1$^{-/-}$ mice the ataxic syndrome begins around postnatal day 12-16, which correlates with the time point when neurotransmitter release become exclusively dependent on P/Q-type channels (Iwasaki et al., 2000; Pietrobon, 2010). These Ca$_v$2.1$^{-/-}$ mice die at about 3 weeks of age.

1.4   Auxiliary subunits of voltage-gated Ca^{2+} channels

The α_1 subunit of HVA Ca^{2+} channels can be modified by the two auxiliary subunits $\alpha_2\delta$ and ß. The α_1 subunit and the auxiliary subunits form Ca^{2+} channel complexes in an ratio of 1:1:1, meaning that one of the seven HVA α_1 subunit is associated with only one of the four $\alpha_2\delta$ and one of the four ß subunits.

Four genes are known that code for 4 different isoforms of the ß subunit (Ca$_v$ß$_1$ – ß$_4$). The ß-subunit contains an SH3 as well as a GK domain, both common domains important for protein-protein interaction (Arikkarth and Campbell, 2003; Dolphin, 2016). The ß-subunit interacts with the alpha-interaction domain (AID) located at the cytoplasmic linker between repeat I and II of the α_1 subunit. It has been shown that the ß-subunit plays an important role in the expression of HVA channels at the cell surface since it supports the exit of the channel from the endoplasmic reticulum but also protects the channel from the degradation by the proteasome pathway. ß-subunits are involved in a variety of processes and its deletion has different consequences. Knockdown of either the ß$_1$ or the ß$_2$ subunit in mice result in non-viable offspring, while knockdown of ß$_4$ subunit results in viable mice- however, those mice show a severe phenotype (Buraei and Yang, 2010). Both, the ß-subunit as well as the $\alpha_2\delta$ subunit can significantly change the biophysical properties of the α_1 subunit, such as the voltage dependence of activation and the kinetics of the channel (Buraei and Yang, 2010; Dolphin, 2009; Dolphin 2016; Kadurin et al., 2016).

The auxiliary $\alpha_2\delta$ subunit is non-covalently associated with the α_1 subunit on the extracellular site of the channel and is anchored to the membrane by a GPI anchor (**Fig. 8**). Four different isoforms that are transcribed by different genes are known. The genes *Cacna2d1*, *Cacna2d2*, *Cacna2d3* and *Cacna2d4* code for the $\alpha_2\delta1$, $\alpha_2\delta2$, $\alpha_2\delta3$ and $\alpha_2\delta4$ subunit, respectively. The α_2 and the δ part are encoded by the same gene but the resulting pre-protein is posttranslationally cleaved into α_2 and δ, which remain connected via disulfide bridges. Characteristic for the $\alpha_2\delta$ subunit is the high degree of glycosylation, which is important to regulate the α_1 channel activity (Lazniewska and Weiss, 2017). The produced $\alpha_2\delta$ pre-protein contains a N-terminal signaling sequence, which is when expressed co-translationally cleaved. As a consequence, the resulting α_2 protein is inserted into the lumen of the ER and becomes later exclusively extracellular. As a mature protein, $\alpha_2\delta$ displays several features. First, the von Willebrand factor A (VWA) domain, present in the α_2 part of the protein. The VWA domain containing a so-called MIDAS motif and is a known site for protein-protein interaction. Second, the CACHE domain (Ca^{2+} channel and chemotaxis receptor), which is of bacterial origin and assumed to be acquired by the $\alpha_2\delta$ subunit (Dolphin, 2012, 2013). The domain is located

downstream of the VWA domain and is used for small molecule recognition. Due to the presence of a VWA and a CACHE domain and the in general large and highly glycosylated structure, the $\alpha_2\delta$ subunits are well suited for protein-protein or interactions with extracellular matrix proteins (Dolphin, 2013). Figure **8** shows the interplay of the auxiliary subunits and the α_1 subunit of HVA Ca^{2+} channels.
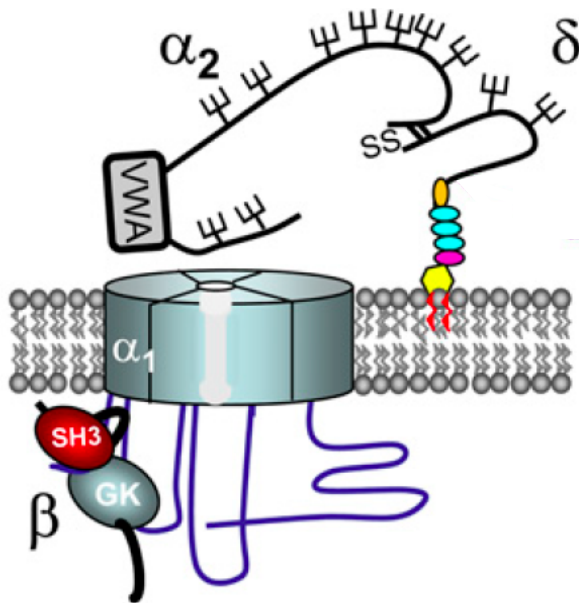
Figure 8. Structure of voltage-gated Ca^{2+} channels
Voltage-gated Ca^{2+} channels consist of an α_1 subunit, which is a transmembrane spanning protein that forms the channel pore. The α_1 subunit of the VGCC families Ca_v1 and Ca_v2 can be modulated by the 2 auxiliary subunits $\alpha_2\delta$ and ß. The ß subunit is located on the intracellular site of the channel, whereas the $\alpha_2\delta$ subunit is located on the extracellular site. The $\alpha_2\delta$ subunit is transcribed by the same gene, but is posttranslationally cleaved into α_2 and δ, which remain connected with disulfide bonds (marked with SS). The δ part of the $\alpha_2\delta$ subunit is linked to the membrane via a GPI anchor; α_2 is localized exclusively extracellular and is highly glycosylated. Both auxiliary subunits can modify the biophysical properties of the channel, and may have additional functions. Picture taken from Davies et al., 2010.

The four auxiliary subunits show different expression pattern sites. $\alpha_2\delta1$ is found in skeletal, cardiac and smooth muscles, endocrine tissue as well as in the CNS and the PNS. $\alpha_2\delta2$-3 are found only in neuronal tissue including the CNS and PNS. $\alpha_2\delta4$ is found only in retinal and endocrine tissue and is termed as the only non-neuronal auxiliary subunit of these four (Dolphin, 2013). Mutations in *Cacna2d1*, *Cacna2d2* and *Cacna2d4* gene have been linked to neuropsychiatric disorders like bipolar disorders and schizophrenia. Most of the mutations are single nucleotide polymorphisms (SNP) found in introns of the gene and it is unclear how the SNPs affect the expression of the splice variants. In patients with bipolar disorder, increased expression of *Cacna1s*, *Cacna2d4* or *Cacna1f* were found in hippocampal neurons (Simms and Zamponi, 2014; Zamponi, 2016). A rare germline mutation in *Cacna2d3* gene producing

a premature stop codon or aberrant splicing has been associated with different neurological disorders including autism, schizophrenia and Asperger's syndrome (Dolphin, 2016; Landmann et al., 2018; Simms and Zamponi, 2014; Zamponi et al., 2015).

The auxiliary subunit $\alpha_2\delta1$ is encoded by the *Cacna2d1* gene and is highly expressed in skeletal, cardiac (Patel and Dickenson, 2016) and smooth muscles, the central and peripheral nervous system. $\alpha_2\delta1$ knockout mice are viable and show only a cardiac phenotype. Following nerve injury, levels of $\alpha_2\delta1$ are elevated in damaged sensory neurons, e.g. in trigeminal neurons or dorsal root ganglion neurons. Overexpression of $\alpha_2\delta1$ is associated with neuropathic phenotypes hyperalgesia and tactile allodynia. These studies showed that $\alpha_2\delta1$ is important for the proper processing of neuronal signals even in the presence of nerve damage. In humans, mutations in the *Cacna2d1* gene are associated with cardiac dysfunctions and result in the Brugada and short QT syndrome (Antzelevitch et al., 2007). It has been shown that the $\alpha_2\delta1$ subunit, can interact with thrombospondin-2. Thrombospondins are produced in the brain by astrocytes and are important for synapse formation. Thrombospondin-induced synaptogenesis was found to require $\alpha_2\delta1$. The anti-epileptic drug gabapentin was found to disrupt the interaction between $\alpha_2\delta1$ and thrombospondin-2 and thereby disrupting synaptogenesis (Eroglu et al., 2009; Mendus et al., 2014). Worth mentioning, gabapentin did not affect already formed synapses and has no effect on mice pups exposed to chronic gabapentin exposure (Dolphin, 2016).

$\alpha_2\delta2$ encoded by the *Cacna2d2* gene is highly expressed in the cerebellum, in particular in Purkinje neurons. Ducky mice (du/du) carry a spontaneous mutation in this gene resulting in episodic waves of epilepsy and cerebellar ataxia. Ducky mice have deformed and smaller dendritic trees in Purkinje cells, which reduces the spontaneous activity. In addition du/du mice show a very severe phenotype, characterized by ataxia and episodic seizures starting around postnatal day 16 and mice die between postnatal weeks 2 – 3. The phenotype is only visible in homozygous mice (du/du), while heterozygous mice are viable and behave like their wildtype siblings. Fell et al. (2016) showed that $\alpha_2\delta2$ plays a crucial role in the composition of IHC calcium channel complexes and its deletion leads to an auditory processing disorder (Fell et al., 2016).

In humans, mutations in the *Cacna2d2* gene have also been associated with epilepsy and familial hemiplegic migraine (FHM). The $\alpha_2\delta1$ as well as the $\alpha_2\delta2$ subunit were identified to

contain ligand-binding sites to bind two drugs used to treat epilepsy and neuropathic pain, gabapentin and pregabalin.

Cacna2d3 encodes for auxiliary subunit $\alpha_2\delta3$, which is highly expressed in the central and peripheral nervous system including the auditory system. The function of the auxiliary subunit $\alpha_2\delta3$ has been intensively studied in Drosophila (Kurshan et al., 2009; Wang et al., 2016) and in mice by various groups (Neely et al., 2010; Pirone et al., 2014; Wang et al., 2016). In Drosophila, $\alpha_2\delta3$ is referred to as *straightjacket (CG12295; stj)* and was identified to be involved in synapse formation and modulation of VGCCs. Deletion of $\alpha_2\delta3$ leads to lethality in a late stage of embryonic development (Kurshan et al., 2009). Further investigations of the phenotype showed that knockout of $\alpha_2\delta3$ leads to deformed synapses at the neuromuscular junction (NMJ). The $\alpha_2\delta3$ subunit plays important roles in the formation of synaptic boutons independent of the presence of its α_1 subunit (Kurshan et al., 2009). Recently it has been shown that $\alpha_2\delta3$ is indispensable for presynaptic homeostasis, regardless of the severity of the $\alpha_2\delta3$ mutation (Kurshan et al., 2009). In addition it was revealed that mutations in the $\alpha_2\delta3$ gene lead to a significant reduction of the pre-synaptic $Ca_v2.1$ current without changing the channels activation or inactivation (Wang et al., 2016). The $\alpha_2\delta3$ knockout mice was intensively studied regarding its pain- and auditory-processing abilities by Neely et al. and Pirone et al. (Neely et al., 2010; Pirone et al., 2014). Consequences of $\alpha_2\delta3$ deletion with respect to its auditory function will be described in section 1.5.1.

The auxiliary subunit $\alpha_2\delta4$ is encoded by the *Cacna2d4* gene and is the only auxiliary subunit that has a restricted expression site namely, the retina. Therefore the subunit is referred to as non-neuronally expressed. Mutations in this gene are associated with dysfunctions of photoreceptors leading to night blindness (Zamponi et al., 2015).

1.4.1   Importance of VGCCs and $\alpha_2\delta$ subunits in the auditory system

Voltage-gated Ca^{2+} channels are widely distributed and are involved in many important cellular processes. As described previously, HVA Ca^{2+} channels play an important role in various neuronal processes. This chapter will highlight the importance of VGCCs and $\alpha_2\delta$ subunits with respect to their function in the auditory system and especially its function in sensory hair cells, primary auditory neurons (SG neurons) and at the endbulb of Held synapse (**Fig. 9**).

The sensory hair cells in the cochlea receive afferent innervation from nerve endings of SG neurons. At the basal pole of the inner hair cell, peripheral dendrites of SG neurons form the inner hair cell ribbon synapse whose task is to transmit incoming sound signals in a precise and fast manner. The most important Ca^{2+} channel at the inner hair cell ribbon synapse is the L-type Ca^{2+} channel $Ca_v1.3$, which covers more than 90 % of the total I_{Ca}.

$Ca_v1.3^{-/-}$ mice were studied by Platzer et al. who elucidated that deletion of this channel led to more than 90 % loss of Ca^{2+} current influx at the IHC synapse (Platzer et al., 2000). Also OHC, whose exact function has not been intensively studied, showed degradation in the most apical turn of the cochlea. Deletion of $Ca_v1.3$ leads to congenital deafness in mice and humans (Baig et al., 2011). So far other Ca_v channel mutations have not been described for inner or outer hair cells.

HVA Ca^{2+} channels are associated with various $\alpha_2\delta$ and ß subunits. Recently, Fell et al. described the importance of the $\alpha_2\delta2$ subunit for the function of the IHC (Fell et al., 2016). They showed that deletion of the $\alpha_2\delta2$ subunit led to reduced Ca^{2+} currents at the IHC and to impaired synaptic coupling of pre-synaptic Ca^{2+} channels and AMPA receptors.

Another important finding with respect to the function of $\alpha_2\delta3$ was made by Pirone et al. (2014) who showed that deletion of $\alpha_2\delta3$ led to decreased expression of P/Q-type channels ($Ca_v2.1$) in primary auditory neurons. Furthermore they found malformed endbulb of Held synapses in the AVCN. The different findings of Ca_v channel and $\alpha_2\delta$ with respect to the auditory system are summarized in Figure **9** below.

Sensory hair cells
$\alpha_2\delta2^{-/-}$: reduced Ca^{2+} currents at IHC synpases & impaired trans-synaptic coupling of presynaptic Ca^{2+} channels & AMPA receptors

IHC

AVCN

SGN

Sensory hair cells
$Ca_v1.3^{-/-}$: < 90% loss of Ca^{2+} influx at IHC synapse, degradation of apical OHCs

Primary auditory neurons
$\alpha_2\delta2^{-/-}$: reduced expression of $Ca_v2.1$ channels and currents

Endbulb of Held synapse
$\alpha_2\delta2^{-/-}$: malformed synapses
$\alpha_2\delta3^{-/-}$: malformed synapses

Figure 9. Consequences of known VGCC and $\alpha_2\delta$ deletions in the auditory system
At the IHCs more than 90% of the total I_{Ca} flow through L-type channels ($Ca_v1.3$). Mutations or deletion of the channel causes congenital deafness in mice and humans (Baig et al, 2011). From own data we know that especially $\alpha_2\delta3$ is required for the proper expression of P/Q-type channels. Analysis of mature and immature endbulb of Held synapses in du/du mice and $\alpha_2\delta3^{-/-}$ mice showed that both subunits are required for a proper synapse development. Picture taken and modified from Stephani et al., unpublished (Fell et al., 2016; Platzer et al., 2000; Striessnig et al., 2014).

1.5   Mouse models

1.5.1   The *Cacna2d3*-deficient mouse

The $\alpha_2\delta3$ knockout mouse is a constitutive mouse model, carrying a mutation in the *Cacna2d3* gene coding for the auxiliary subunit $\alpha_2\delta3$ of voltage-gated Ca^{2+} channels. The mouse line was generated by Deltagen (San Mateo, California, USA) and purchased via Jax® mice (Sulzfeld, Germany). The gene is located on chromosome 14 at position 28,904,943 – 29,721,864 and consists of 38 exons. The knockout mice was generated by the deletion of 11 base pairs at position 1521 – 1531 corresponding to exon 15. Figure **10** shows the scheme of the $\alpha_2\delta3^{-/-}$ mouse construct.

Cacna2d3
Chr.14
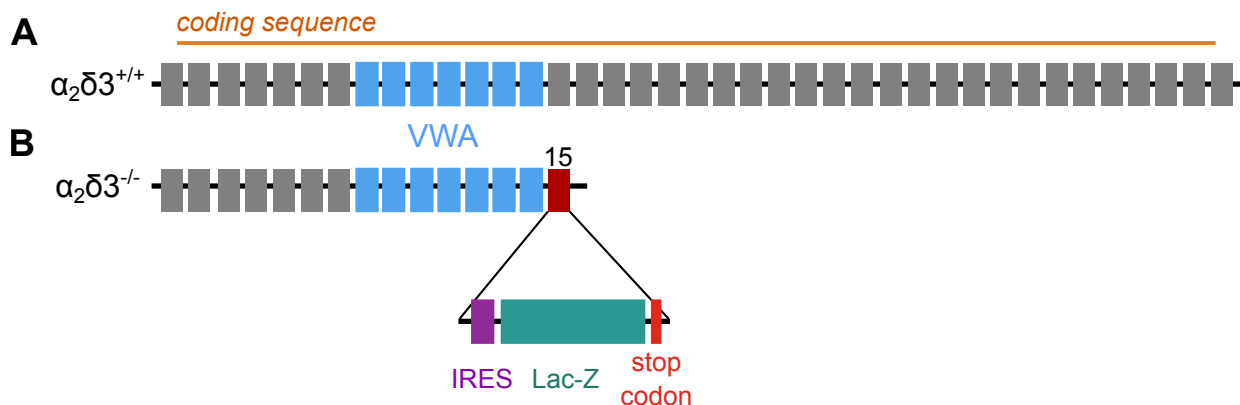
Figure 10. Construct of the $\alpha_2\delta3$ knockout mouse
The *Cacna2d3* gene consists of 38 exons and is located on chromosome 14. The von Willebrand factor A domain, shown here in light blue is located at the beginning of the gene between the exons 8 and 14. At exon 15 (red), 11 bp were deleted and a lacZ-Neo cassette was inserted. The vector contains a IRES sequence followed by a SV40 domain, the LacZ cassette and at the end a stop codon. The LacZ cassette runs under the endogenous gene promoter. An immature or premature $\alpha_2\delta3$ protein is presumably produced because exons 1 to 14 are also expressed in the knockout mouse. Vector map of the inserted LacZ-Neo cassette can be found in. (Reference: https://www.jax.org/strain/005780)

The mouse was first described 2010 by Neely and colleges (Neely et al., 2010) where they showed that mice carrying a mutation for $\alpha_2\delta3$ are not able to properly transmit thermal pain evoked signals from the thalamus to higher pain centers. Furthermore they found activation in the visual cortex, the auditory cortex and the olfactory brain regions. A detailed analysis of hearing performance was done 2014 by Pirone and colleges (Pirone et al., 2014). They analyzed the cochlea and found intact inner hair cells and a normal expression of $Ca_v1.3$ channels, the dominant Ca^{2+} channel at the inner hair cell synapse. Analysis of distortion products of otoacoustic emissions (DPOAE) showed no difference between both genotypes indicating normal OHC function. Auditory brainstem response (ABR) measurements showed a reduced wave II and distortion of wave III and IV. Furthermore SG neurons of $\alpha_2\delta3^{-/-}$ mice showed a strong reduction of $Ca_v2.1$ channel expression at the age of 4 – 5 weeks. Electron

microscopic analysis and measurement of the size of the Endbulb of Held synapse showed a deformation and a reduced number of synaptic boutons in the $\alpha_2\delta3^{-/-}$ mice (Pirone et al., 2014). These mutation dependent phenotypes make the $\alpha_2\delta3^{-/-}$ mice a good candidate for the analysis of auditory processing disorders.

1.5.2 The ducky mouse

The ducky mice, also called du/du mice, carry a spontaneous mutation in the *Cacna2d2* gene that codes for the auxiliary $\alpha_2\delta2$ subunit of voltage-gated Ca^{2+} channels. These mice have a severe phenotype, which is detectable around postnatal day 15. Compared to their wildtype or heterozygous siblings, homozygous du/du mice are smaller, have a wiggly walk and episodic seizures. Homozygous mice die around postnatal day 25. Previous characterization of these mice revealed a neurodevelopmental disorder affecting especially the cerebellum. Barclay et al. showed that the accessory $\alpha_2\delta2$ subunit is highly expressed in the Purkinje cells in the cerebellum of wildtype mice (Barclay et al., 2001). They found that branching of Purkinje cell dendrites was smaller and less complex in ducky mice. Furthermore, dendritic trees were shorter and most of the time did not reach the outer layer of the cerebellar cortex (Brodbeck et al., 2002). Electrophysiological recordings in Purkinje cells showed that Ba^{2+} currents were reduced by approx. 30 % (Barclay et al., 2001).
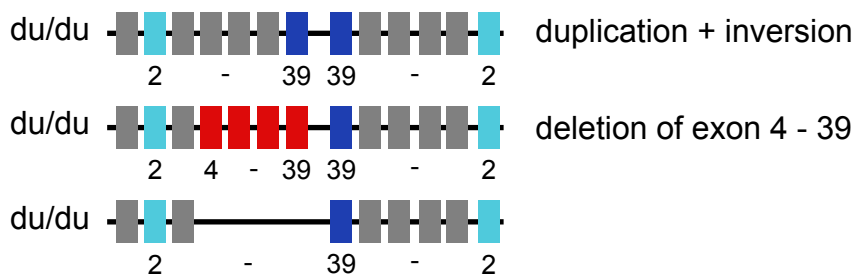
Figure 11. Genomic rearrangement of the spontaneous *Cacna2d2* mutation in du/du mice
The *Cacna2d2* gene undergoes 2 genetic rearrangements, first a head to tail duplication of exons 2 – 39 that affects an additional region of unknown length and second a deletion of the exons 4 – 39 in the original *Cacna2d2* gene. This spontaneous mutation results in 2 transcripts, which are assumed to result in a non-functional protein (Reference: https://www.jax.org/strain/012889), (Barclay et al., 2001).

Fell et al. investigated the hearing performance of du/du mice and found elevated click and frequency-dependent hearing thresholds as assessed with auditory brainstem response audiometry (ABR). Ca^{2+} currents of IHCs were reduced by 30 – 40 % in 3-week-old du/du mice. Immunohistochemical analysis of inner hair cell ribbon synapses showed an altered coupling of presynaptic $Ca_v1.3$ clusters and postsynaptic GluA4 receptor and PSD-95

clusters, suggesting a novel role for $\alpha_2\delta2$ in trans-synaptic coupling (Fell et al., 2016). Edvardson et al. described a family with three children suffering from epileptic seizures and mental retardation that was attributed to a point mutation in the human *Cacna2d2* gene. The hearing performance of the children was not investigated (Edvardson et al., 2013).

1.6 Working hypothesis and aim

Auxiliary $\alpha_2\delta$ subunits of voltage-gated Ca^{2+} channels have become of recent interest regarding their influence on the α_1 subunit of VGCCs and their potential role in synaptogenesis (Arikkath and Campbell, 2003; Kurshan et al., 2009; Pirone et al., 2014). Previous work has shown that the four auxiliary subunits $\alpha_2\delta 1 - 4$ can modulate and shape the biophysical properties of VGCCs (Dolphin, 2013, 2016; Kadurin et al., 2016).

Preliminary work by Pirone et al. (2014) showed that deletion of $\alpha_2\delta 3$ led to a decreased expression of P/Q type Ca^{2+} channels ($Ca_v 2.1$) at the soma of spiral ganglion neurons and measurements of auditory brainstem responses indicated a reduced wave II and distorted wave 3 indicating that the transmission from auditory nerve fiber terminals onto the bushy cell is hampered. This was confirmed by high resolution electron microscopic images from the endbulb of Held synapse showing smaller and malformed auditory nerve fiber terminals at bushy cells in the anteroventral cochlear nucleus of mature mice, indicating that deletion of $\alpha_2\delta 3$ lead to an auditory processing disorder and is essential for normal hearing.

Spiral ganglion neurons, which form the auditory nerve, are located within the cochlea and express the three different $\alpha_2\delta$ isoforms - $\alpha_2\delta 1$, $\alpha_2\delta 2$ and $\alpha_2\delta 3$. Previous work showed that the loss of $\alpha_2\delta 3$ could not be compensated by $\alpha_2\delta 1$ or $\alpha_2\delta 2$ at the level of mRNA in SG neurons (personal communication with Prof. Obermair, Dr. Scheuer and Prof. Engel).

For achieving the following goals we characterized the Ca^{2+} channel composition in primary cultures of spiral ganglion neurons along the tonotopic axis of the cochlea in pre-hearing (P5) as well as hearing mice (P20). In addition, brain cryosections were prepared to analyze the endbulb of Held synapse in neonatal and mature $\alpha_2\delta 3$ wildtype and knockout mice.

Within this thesis I tried to answer the following questions:

1. What is the Ca^{2+} current composition of spiral ganglion neurons in pre-hearing and hearing mice?

2. Which effect has a deletion of $\alpha_2\delta 3$ on the different Ca^{2+} current types in spiral ganglion neurons?

3. How does lack of $\alpha_2\delta 3$ affects the morphology of auditory nerve fiber terminals in hearing and pre-hearing mice?

This work gives new insights into the composition of Ca^{2+} currents in spiral ganglion neurons of pre-hearing and hearing mice and shows that $\alpha_2\delta 3$ is important for maintenance of the

normal Ca^{2+} current composition in mature SG neurons and furthermore necessary for the development of the auditory nerve fiber (ANF) terminals.

For the first time, we were able to show that proper development of ANF terminals require the presence of $\alpha_2\delta3$ even before the onset of hearing. Moreover we showed that the deletion of $\alpha_2\delta3$ specifically affected the Ca^{2+} current composition in SG neurons from hearing mice (P20), by a massive lack of P/Q type Ca^{2+} currents, which was not compensated by other Ca^{2+} currents. Overall this project shows the importance of the auxiliary Ca^{2+} channel subunit $\alpha_2\delta3$ with respect to Ca^{2+} channel currents and the development of auditory nerve fiber terminals in neonatal as well as mature mice.

2. Material and Methods

2.1 Mouse lines

All mice used in this study were housed according to the regional board for scientific animal experiments of the Saarland (TierSchG § 4). Animals were kept under a 12 h day – night circle with permanent access to food (Ssniff®, animal food for rats and mice) and water. Beside the knockout specific mouse lines, NMRI and C57BL/6N mice (Charles River, Sulzfeld, Germany) were used for control experiments or pre-tests as for example immunohistochemical labeling. In this project the following mouse lines were used:

Cacna2d3-deficient mice (Neely et al., 2010; Pirone et al., 2014)
Mice bred in the C57BL/6N background with a mutation in the auxiliary subunit $\alpha_2\delta3$. Described in detail in chapter 1.5.1.

Cacna2d2 mutant mice (Barclay et al., 2001; Brodbeck et al., 2002)
Mice bred in the C57BL/6N background with a mutation in the auxiliary subunit $\alpha_2\delta2$. Described in detail in chapter 1.5.2.

Cacna1d-deficient mice (Platzer et al., 2000)
Mice bred in the C57BL/6N background with a mutation of the pore-forming α_{1D} subunit of the $Ca_v1.3$ channel.

Cacna1b-deficient mice (Ino et al., 2001)
Mice bred in the C57BL/6N background with a mutation of the pore-forming α_{1B} subunit of the $Ca_v2.2$ channel. The mouse was generated by Yasuo Mori and was kindly provided by Prof. Dr. Leinders-Zufall with permission.

2.2 Genotyping of mouse lines

Table 2 summarizes all chemicals and kits used for genotyping of various mouse lines.

Table 2. Chemicals and kits used for genotyping

Chemical / kits	Company	Cat. No.
Acetic acid	VWR International, Darmstadt, Germany	700876
Agarose	Carl Roth, Karlsruhe, Germany	HP30.1
EDTA	Fluka, Morris Plains, NJ, USA	03679
Go Taq Green Master Mix	New England Biolabs, Ipswich, MA, USA	M0482 S
NucleoSpin® tissue extraction kit	Macherey Nagel, Düren, Germany	740952.50
Primer	Biomers.net	Custom made
TrackIt 100 bp DNA ladder	Invitrogen, Carlsbad, CA, USA	10488058
TRIS-Base	Sigma-Aldrich, St. Louis, MO, USA	T1503
PlusBlue DNA ladder 100 bp	GeneOn, Ludwigshafen, Germany	304-125

2.2.1 Genotyping of *Cacna2d3*-deficient mice

DNA was isolated from tissue taken from the ear or tail and processed in 50 µl BE buffer according to the protocol of the NucleoSpin® tissue kit. For each PCR mix, 2 µl DNA, 0.5 µl forward primer (5'-GCAGAAGGCACATTGCCATACTCAC-3'), 0.5 µl reversed primer (5'-TAGAAAAGATGCACTGGTCACCAGG-3'), 0.5 µl mutant primer (5'-GGGCCAGCTCAT TCCCACTCAT-3'), 6.5 µl ddH$_2$O and 10 µl Go Taq Green Master Mix were mixed and amplified using the PCR cycler (PeqStar Peqlab, Erlangen, Germany). DNA was amplified according to the settings mentioned in Table 3.

Table 3. PCR program used for genotyping of *Cacna2d3*-deficient mice
* go back to step 2 and repeat 34 times.

Step	Temperature (°C)	Time
1	94	3 min
2	95	15 s
3	60	15 s
4	72	30 s*
5	72	5 min
6	8	∞

After amplification of the DNA, 10 µl of the PCR mix were loaded onto a 1.8 % agarose gel embedded in TAE buffer (2 M TRIS-Base, 50 mM EDTA (pH 8), 5.71 % (v/v) pure acetic acid). DNA fragments were separated by applying 120 V to the gel electrophoresis chamber. Pictures were taken using an EBox-VX2 (Vilber Lourmat Deutschland GmbH, Eberhardzell). The expected band sizes for genotyping of different *Cacna2d3* genotypes are listed below (**Tab. 4**).

Table 4. Expected band size of a *Cacna2d3* genotyping

Genotype	Band size (bp)
Homozygous (tg/tg)	331
Heterozygous (tg/wt)	331 and 183
Wildtype (wt)	183
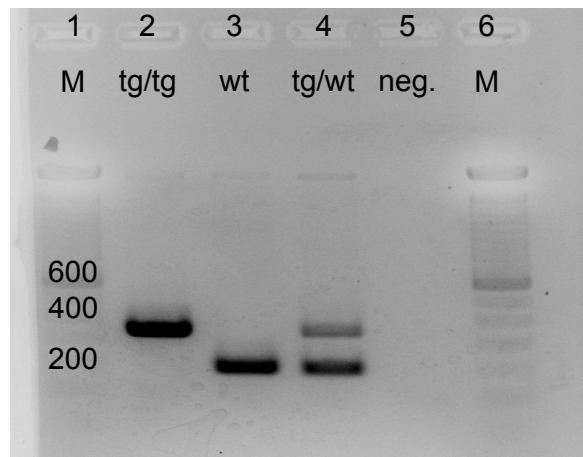
Figure 12. Example picture of a *Cacna2d3* genotyping gel
Lane 1 and Lane 6 show the TrackIt 100 bp DNA ladder (1µl; M). Lane 2 with a band at approximately 331 bp represents a homozygous knockout mouse abbreviated tg/tg. Lane 3 shows a wildtype animal (wt) giving a band at approximately 183 bp. Lane 4, a heterozygous animal (tg/wt) giving a band at approx. 331 bp and 183 bp. Lane 5 shows the negative control (neg.) containing only the master mix without DNA.

2.2.2 Genotyping of *Cacna2d2*-mutant mice

Tissue samples were isolated and processed as described formerly (chapter 2.2.1). For the amplification 0.5 µl forward primer (5'-ACCTATCAGGCAAAAGGACG-3') and 0.5 µl reverse primer (5'-AGGGATGGTGATTGGTTGGA-3') were used. The DNA was amplified using the following PCR program (**Tab. 5**).

Table 5. PCR program used for the genotyping of *Cacna2d2*-mutant mice
* go back to step 2 and repeat 34 times.

Step	Temperature (°C)	Time
1	95	3 min
2	95	30 s
3	56	25 s
4	72	30 s*
5	72	5 min
6	8	∞

After DNA amplification 5 µl enzyme mix were added to the PCR product consisting of 3 µl cut smart buffer and 1 µl BspH I (New England BioLabs, Cat. No.: R0517L) restriction enzyme and 1 µl H_2O. The PCR product was incubated together with the enzyme mix at 70 °C for 30 min. Afterwards the sample was loaded onto a 2 % agarose gel and the PCR products were separated by applying 120 V. One example image of a *Cacna2d2* genotyping is shown in Figure 13. The table below gives the expected band sizes.
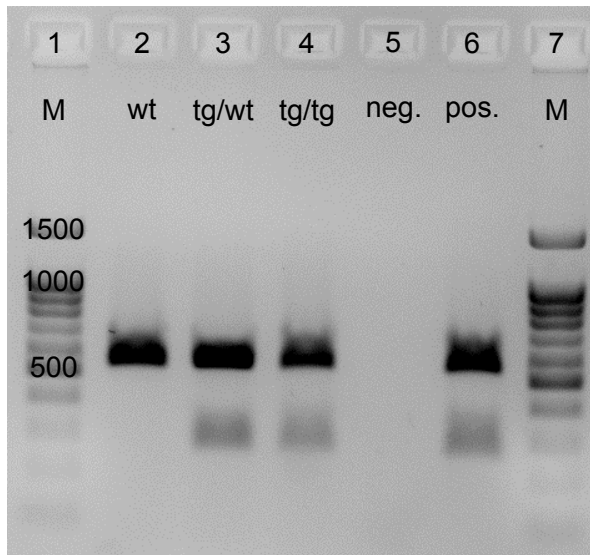
Figure 13. Example picture of a *Cacna2d2* genotyping gel
Lane 1 and 7 shows the PlusBlue 100 bp DNA ladder (3 µl; M). Lane 2 with a band at approximately 541 bp represents a wildtype (wt). Lane 3 shows a heterozygous animal (tg/wt) giving 2 bands at approximately 541 bp and 280 bp. Lane 4 shows a homozygous animal giving 2 bands at approximately 541 bp and 280 bp. Using standard PCR, homozygous animals can not be distinguished from heterozygous animals. Lane 5 represents a negative control (neg.), containing only the master mix without DNA. Lane 6 represents a positive control (pos.) with a pool of different tg/wt samples.

Table 6. Expected band sizes of the *Cacna2d2* genotyping

Genotype	Band size (bp)
Homozygous (tg/tg)	541 and 280
Heterozygous (tg/wt)	541 and 280
Wildtype (wt)	541

2.2.3 Genotyping of *Cacna1d*-deficient mice

Tissue samples were taken and processed as described formerly (chapter 2.2.1). For the amplification 0.3 µl sense primer (5'-GCAAACTATGCAAGAGGCACCAGA-3'), 0.3 µl antisense primer (5'-TACTTCCATTCCACTATACTAATGCAGGCT-3') and 0.3 µl nonsense primer (5'-TTCCATTTGTCACGTCCTGCACCA-3') were used and the DNA was amplified using the program described in Table 7.

Table 7. PCR program used for genotyping of *Cacna1d*-deficient mice
* go back to step 2 and repeat 34 times.

Step	Temperature (°C)	Time
1	95	3 min
2	95	30 s
3	61	40 s
4	72	45 s*
5	72	5 min
6	8	∞

The amplified PCR product was loaded onto a 1.8 % agarose gel and DNA fragments were separated by applying 120 V. Table 8 shows the expected band size for each genotype. Figure 14 shows one example picture of a *Cacna1d* genotyping.

Table 8. Expected band size of a *Cacna1d* genotyping

Genotype	Band size (bp)
Homozygous (tg/tg)	450
Heterozygous (tg/wt)	450 and 311
Wildtype (wt)	311
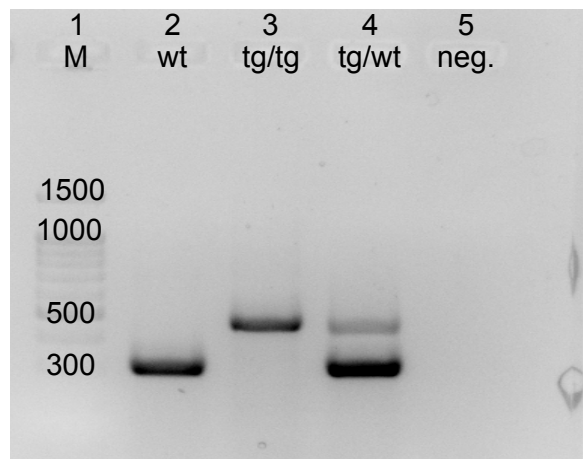
Figure 14. Example of a *Cacna1d* genotyping gel
Lane 1 shows the 100 bp DNA ladder PlusBlue (4 µl; M). Lane 2 represents a wildtype animal (wt) with an expected band size at 311 bp. Lane 3 shows a knockout animal (tg/tg) with an expected band size of 450 bp. Lane 4 represents a heterozygous sample (tg/wt) giving 2 bands, one at 311 bp and the other at 450 bp. Lane 5 shows the negative control (neg.) containing only the master mix without DNA.

2.3   Dissection of the cochlea

In this study, mice at 2 different developmental stages (P5 and P20) were examined. In rare cases, mice were also used at P4-P6 and P19-P21. Mice were handled and killed according to the regional board for scientific animal experiments (TierSchG § 4) of the Saarland. P5 mice were killed by decapitation, P20 mice were first anaesthetized using 500 µl Isofluran® followed by decapitation. Afterwards, the head was cut sagittally using a fine scissor, and the brain was removed using a forceps. For the dissociated SG neuron culture the tissue was processed differently from hereon, which is described in detail in chapter 2.6. For immunofluorescence studies the head halves were placed into cold physiological solution (referred to as B-49) and stored on ice until further use. Subsequent dissection steps were performed under a stereomicroscope SZX-16 (Olympus, Deutschland GmBH, Hamburg). Using 2 forceps, the cochlea was separated from the surrounding tissue and transferred into cold B-49 solution.

2.4 Immunohistochemical staining of whole-mount samples

The cochlea was isolated as described before. For fixation with one of the chemicals outlined below (**Tab. 9**) a small petri dish was filled with the fixative and the cochlea was placed into the solution. After poking a small whole into the most apical part of the cochlea with the cannula of a fine ($\varnothing$ 0.40 x 20 mm) syringe (VWR International, Darmstadt, Germany; Cat. No.: BDAM324891), 1 ml of the fixative was slowly injected through the round window. The cochlea was incubated in the same fixation solution for a given time at a given temperature (**Tab. 9**). Different fixatives were used to achieve optimal immunolabeling results.

Table 9. Overview of fixatives used

Fixative	Concentration	Temperature (°C)	Time (min)	Company	Cat. No.
Ethanol abs.	100 %	-20	20	VWR International, Darmstadt, Germany	700892
Methanol abs.	100 %	-20	20	Merck KGaA, Darmstadt, Germany	1.06009.1000
PFA	2 %, 4 % or 8 %	4	10	Life Technology, Carlsbad, CA, USA	28908
Zamboni	--	4	10	Custom-made	--

Zamboni's fixative (Stefanini et al., 1967) was prepared using the following chemicals summarized in the table below and stored at 4 °C protected from light.

Table 10. Preparation of Zamboni's fixative

Chemical	Concentration	Volume / Weight
PFA	8 %	50 ml
PFA	2 %	50 ml
PBS (10X)	10 x	2.5 ml
H_2O	---	25 ml
NaCl	---	1.70 g
NaOH	1 M	500 µl
Picric acid	Supernatant of a saturated solution	22.5 ml

After fixation, the cochlea was placed into cold PBS (1X), and the remaining fixative was removed by rinsing the cochlea with 1 ml PBS (1X) applied through the round window. The cartilage-like (at P5) or bony shell of the cochlea (at P20) was removed piece-by-piece starting at the most apical part of the cochlea. The lateral wall was removed until the organ of Corti was visible. For the isolation of the apical turn, the cochlea was clipped at the medial turn and carefully transferred to a new petri dish filled with PBS (1x). The tectorial membrane located above the hair cells was carefully removed and the bone covering the SG neurons was removed as well. The tissue pieces were transferred to an object slide and attached to the surface using 1 µl Cell-Tak® (1 mg/ml; Corning, Corning NY, USA; Cat.No.: 734-1081). To prevent dehydration during the immunolabeling procedure, the tissue was covered with 50 µl

46

PBS (1X) and stored in a humidified chamber. Table 11 gives an overview about the buffers used for immunohistochemical analysis. All buffers were freshly prepared before each experiment and stored on ice during the immunolabeling procedure.

Table 11. Buffers used for immunofluorescence labeling of whole-mount samples

Buffer	Composition
Blocking buffer (BP)	1 % BSA in PBS (1x)
Permeabilization buffer (PP)	0.5 % Triton X-100 in PBS (1x)
Reaction buffer (RP)	0.5 % BSA, 0.2 % Triton X-100 in PBS (1x)
Washing buffer (WP)	0.1 % Triton X-100 in PBS (1x)

In a first step the tissue was permeabilized for 10 min with 0.5 % TX-100 (Sigma-Aldrich, St. Louis, MO, USA; Cat. No.: SIALX100) to allow primary antibodies to attain their target structure. Unspecific binding sites were blocked by 1 % BSA (Sigma-Aldrich, St. Louis, MO, USA; Cat. No.: A3912) for 30 min. The blocking solution (BP) was prepared from a 10 % BSA stock solution, diluted with PBS (1x) to a final concentration of 1 % BSA. Meanwhile primary antibodies (PAB) were diluted in RP-buffer as mentioned in Table 12. Primary antibodies were incubated either for 1 h 30 min at room temperature or overnight at 4 °C. After incubation with the PAB the tissue was washed twice with washing buffer (WP) for 15 min. The secondary antibodies (SAB) were diluted in RP-buffer as described in Table 13, centrifuged at 6000 rpm for 3 min and incubated for 1 h 10 min at room temperature protected from light.

Table 12. List of primary antibodies

Target protein	Host	Company	Cat. No.	Lot	Dilution
Beta Tubulin	Mouse	Covance, Princeton, NJ USA	MMS-435P	B205807	1:250
$Ca_v1.2$	Rabbit	Alomone, Jerusalem, Israel	ACC-003	AN-08	1:200
$Ca_v1.3$	Rabbit	Alomone, Jerusalem, Israel	ACC-311	AN-15	1:200
$Ca_v2.1$	Rabbit	Synaptic Systems, Göttingen, Germany	152203	152203/7	1:500
$Ca_v2.2$	Rabbit	Alomone, Jerusalem, Israel	ACC-002	AN-37	1:500
$Ca_v2.3$	Rabbit	Abcam, United Kingdom	ab63705	673316	1:500
VGLUT1	Guinea Pig	Synaptic Systems, Göttingen, Germany	135304	135 304/33	1:300
$\alpha_2\delta3$	Rabbit	Alomone, Jerusalem, Israel	ACC-103	AN0125	1:200
$\alpha_2\delta3$	Rabbit	Novus, Centennial, CO, USA	NBP1-20111	05012012	1:200
$\alpha_2\delta3$	Rabbit	Sigma Aldrich, St. Louis, MO, USA	SAB1303793	Aliquot H.Seiter	1:400
$\alpha_2\delta3$	Rabbit	Abcam, Cambridge, United Kingdom	ab102939	GR79700-1	1:250
NF 200	Rabbit	Sigma Aldrich, St. Louis, MO, USA	N4142	Aliqout AG Knipper	1:500
GM 130 kDa	Mouse	BD Biosciences, Franklin Lakes, NJ, USA	610822	Aliquot AG Knipper	1:50

Table 13. List of secondary antibodies

Epitope	Host	Company	Cat. No..	Lot	Dilution
Alexa Fluor® 488	Donkey anti-mouse	Invitrogen, Carlsbad, CA, USA	A-21202	898250	1:500
Alexa Fluor® 488	Donkey anti-guinea pig	Invitrogen, Carlsbad, CA, USA	A11073	1737010	1:500
Alexa Fluor® 647	Donkey anti-guinea pig	Jackson ImmunoResearch, Cambridgeshire, United Kingdom	706-605-148	106585	1:500
Cy3	Donkey anti-rabbit	Jackson ImmunoResearch, Cambridgeshire, United Kingdom	711-166-152	94967	1:1500

Unbound SAB was removed by washing twice with WP for 15 min. Staining of the nucleus was performed with 4′,6-Diamidin-2-phenylindol (DAPI). A stock solution (0.5 mg/ml Cat. No.: D9542; Sigma-Aldrich, St. Louis, MO, USA) was diluted in PBS (1X) to 1.5 µg/ml with which the tissue was incubated for 10 min. The samples were washed with PBS (1X) and mounted with ~ 10 µl Vectashield® (Vector Laboratories Inc. Burlingame, CA, USA). To preserve the staining, slides were stored at 4 °C protected from light. Images were taken with a confocal laser-scanning microscope 710 (Zeiss LSM 710, Zeiss Microscopy GmbH, Göttingen, Germany) using a 20x/0.8 NA objective for overview images. Detailed images

were taken by acquiring a Z-stack (thickness 0.31 μm) of the tissue using a 63x/1.4 NA oil objective.

2.5   Deglycosylation assays

Chemical as well as enzymatic deglycosylation agents were used to enhance the antibody specificity of highly glycosylated epitopes. Table 14 summarizes the deglycosylation agents with corresponding concentrations and incubation times.

Table 14. Chemical and enzymatic deglycosylation agents

Compound	Concentration	Incubation time	Incubation Temp.	Company	Cat. No.
Periodic acid	20 mM	15 min	RT	Sigma Aldrich, St. Louis, MO, USA	P0430
PNGase F	5 & 0.5 units	15 min	37 °C		F8345-50U

First, a 1 M stock solution of periodic acid was prepared, diluted to 200 mM with acetate buffer (Cat.No.: VWRK760115, VWR International, Darmstadt, Germany) and stored at 4 °C. A final working concentration of 20 mM, diluted in acetate buffer was prepared. For the chemical deglycosylation using periodic acid, the sample was fixed as described previously (chapter 2.4). After fixation the sample was glued onto an object slide using Cell-Tak® and incubated for 15 min at room temperature with 20 mM periodic acid. Afterwards the sample was washed 3 times in PBS (1x). For further immunohistochemical analysis the samples were processed as described previously in chapter 2.4. For the enzymatic deglycosylation using PNGase F samples were fixed and glued onto a glass slide using Cell-Tak®. Enzymatic deglycosylation was followed using either 5 or 0.5 units PNGase F which was pipetted onto the samples and incubated at 37 °C for 15 min. For immunohistochemical labeling, samples were processed as described formerly (chapter 2.4).

2.6   Establishment of a dissociated spiral ganglion neuron culture

SG neurons were isolated from neonatal mice (P4-6) and mature mice (P19-21). Isolated cells were cultured on coated coverslips that were stored in a 4 well plate. To allow proper attachment of the isolated neurons, coverslips with a diameter of 13 mm were coated with poly-D-lysine and laminin. First, coverslips were cleaned with 70 % absolute ethanol, autoclaved and stored under sterile conditions. Coverslips were coated with poly-D-lysine (0.5 mg/ml Cat.No.: P6407, Sigma-Aldrich, St. Louis, MO, USA) for 7 h at 37 °C, washed with PBS (1X) and coated overnight with laminin (1 mg/ml Cat.No.: L2020, Sigma-Aldrich, St. Louis, MO, USA). During the incubation steps, the plate was stored at 37 °C. For the

isolation of SG neurons at P20, 50 ml MEM were supplemented with 10 mg kynurenic acid (Cat.No.: K3375, Sigma-Aldrich, St. Louis, MO, USA), 5 ml Neurobasal A were supplemented with 1 mg kynurenic acid. Both solutions were mixed and stored overnight at 4 °C. On the initial day of the culturing, the 50 ml MEM and 5 ml Neurobasal A were sterile filtered through a 0.2 µm filter (Cat. No.: 12840830; VWR International, Darmstadt, Germany). The cell culture medium was prepared as follows (**Tab. 15**).

Table 15. Cell culture medium

Solution	Volume	Concentration	Company	Cat. No.
Neurobasal A	5 ml	---	Life Technology, Carlsbad, CA, USA	10888022
B 27	100 µl	2 %	Life Technology, Carlsbad, CA, USA	17504044
Penicillin G	5 µl	100 U/µl	Sigma-Aldrich, St. Louis, MO, USA	044M4773V
L-Glutamine	12.5 µl	0.5 mM	Life Technology, Carlsbad, CA, USA	25030032

The lid of the 15 ml falcon (Cat. No.: 734-0046, VWR International, Darmstadt, Germany) was closed with parafilm and the medium was stored in the fridge at 4 °C until further use. For the preparation of the dissection solution 50 ml filtered MEM (Cat.No.: 11090-081; Life Technology, Carlsbad, CA, USA) were supplemented with 400 µl $MgCl_2$ (stock solution 1 M), 110 µl D-glucose (450 mg/ml) and 50 µl Penicillin G. The solution was mixed and 2 ml were taken away to prepare the digestion solution. Therefore, 2 ml dissection solution were supplemented with 40 µl B 27 (2 % v/v) and stored on ice until further use. 2 ml FBS (Cat.No.: 16000044; Life Technology, Carlsbad, CA, USA) were added to the dissection solution and mixed. To prepare the centrifugation solution, 3 ml dissection solution were taken away and mixed with the same volume of solution 2. Solution 2 is a high sucrose solution prepared as described in Table 16, which was used as density gradient to collect the cell pellet at the bottom of the Eppendorf tube.

Table 16. Preparation of solution 2 for density gradient
HBSS and sucrose were dissolved in H_2O to make a final volume of 500 ml. The pH was adjusted with 1 M HCl to 7.5. The solution was filtered under sterile conditions and stored at -20 °C.

Chemical	Volume	Company	Cat. No.
HBSS (1x)	25 ml	Life Technology, Carlsbad, CA, USA	14185045
Sucrose	154 g	Carl Roth, Karlsruhe, Germany	4621.1

The centrifugation solution was stored on ice until further use. For a primary culture of P20 SG neurons, tissue of 4 mice (8 ears) with the same genotype was pooled. For mice aged P5, tissue from 3 mice (6 ears) was sufficient. Mice were killed as described in chapter 2.3 and the head halves were stored in ice cold pure MEM. Under sterile conditions the skull halves were transferred to dissection solution.
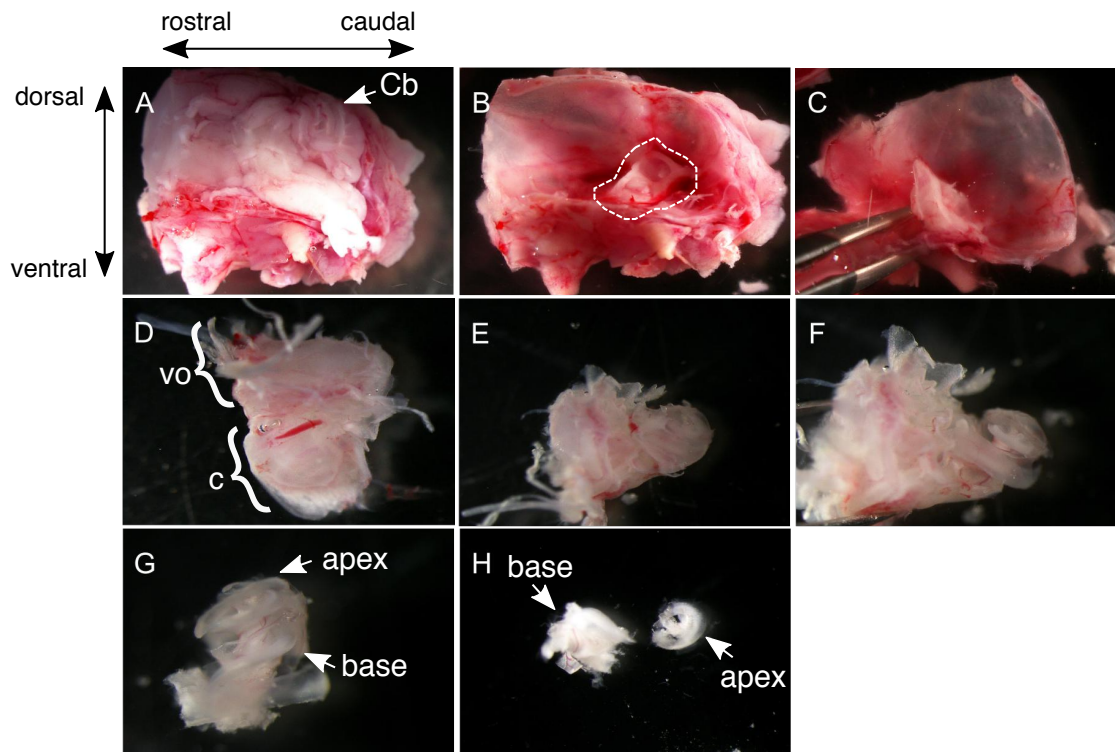
Figure 15. Dissection of the cochlea for the isolation of spiral ganglion neurons
A, The fur was removed and the head was cut in the sagittal plane. **B,** After removal of the brain with a coarse forceps the location of the cochlea and the vestibular organ within the skull is visible (dashed line). **C,** The cochlea was carefully cut out from the skull. **D,** Isolated cochlea (c) (facing upwards) with the vestibular organ (vo) is shown. **E,F,** The capsule of the cochlea was opened at the apex and carefully removed until the complete turns were visible. **G,** The cochlea was separated from the vestibular organ by clipping at the most basal turn. **H,** The cochlea was separated into apical and basal parts. Each tissue pieces was further disintegrated into smaller pieces and transferred into digestion solution for further processing. Abbreviations: Cb – cerebellum, vo – vestibular organ, c – cochlea

All dissection steps were performed in dissection solution. The cartilage-like (P5) or bony shell (P20) of the cochlea was carefully removed and the cochlea was separated into an apical-medial and a medial-basal part, later referred to as "apical" or "basal". The apical and basal halves were transferred into separate petri dishes filled with 1 ml digestion solution. The tissue pieces were disintegrated and affiliated in 400 µl digestion solution collected in a 2 ml Eppendorf tube. In a first digestion step, 50 µl DNase I (1000 U/ml, Cat.No.: D4527, Sigma-Aldrich, St. Louis, MO, USA) and 50 µl collagenase type I (10 mg/ml, Cat.No.: C0130, Sigma-Aldrich, St. Louis, MO, USA)) were added to the tubes. The tissue was incubated in a 37 °C water bath (VLSB12, Cat. No.: 462-0493; VWR International, Darmstadt, Germany) for 15 min with a constant shaking speed of 180/min. In a second digestion step 50 µl 2.5 % trypsin (Cat.No.: 15090046; Life Technology, Carlsbad, CA, USA) were added to each tube and the tissue was incubated for 10 min at 37 °C with a constant shaking speed of 180/min. To allow better performance of trypsin, 1 µl 0.25 M NaOH was added to each tube prior to the 10 min incubation step. To stop the enzyme digestion, 400 µl FBS were added to each tube. The remainders of the tissue were carefully triturated and 800 µl centrifugation solution

was added to each tube. Cells were centrifuged at room temperature for 5 min at 3000 rpm (5424R, VWR International GmbH, Darmstadt Germany). During the 5 min centrifugation step the cell culture medium was pre-warmed in the water bath. After centrifugation, the supernatant was aspirated and the cell pellet was dissolved in 400 µl cell culture medium. After the cell pellet had been carefully re-suspended and filtered through a cell strainer the cell suspension was plated onto two wells (400 µl/well). Each well was supplemented with 1 µl NT3 (Cat.No.: N1905; Sigma-Aldrich, St. Louis, MO, USA) and 1 µl BDNF (Cat.No.: B3759; Sigma-Aldrich, St. Louis, MO, USA) at 10 ng/µl respectively. When SG neurons from mature mice were isolated 40 µl FBS were added to each well in addition. The well plate was placed back to the incubator and the medium was exchanged completely after one day. At the second day, only half of the medium was exchanged. For each change, the culture was supplemented with 1 µl BDNF and 1 µl NT3 at 10 ng/µl respectively. SG neurons isolated at P5 were cultured for 2 days, SG neurons isolated at P20 were cultured for 3 days.

2.7   Establishing brain cryosections from the cochlear nucleus

Brain cryosections were prepared from P7 and P20 $\alpha_2\delta3^{+/+}$ and $\alpha_2\delta3^{-/-}$ mice and from P20 du/du and WT mice. Mice were killed according to the animal protection law of the Saarland as described previously (chapter 2.1). The skin at the head was gingerly removed using a fine scissor. A small incision at the spinal cord was made and the upper skull bone was removed using a fine forceps. After cutting the optical nerves with a high precision scissor the brain was removed from the remaining skull. Brains isolated at P20 were fixed in 4 % PFA for 4 h, brains isolated at P7 were fixed in 8 % PFA for 4 h. During the fixation process, brains were kept at 4 °C. After the fixation, brains were transferred to 30 % sucrose solution and incubated overnight at 4 °C.
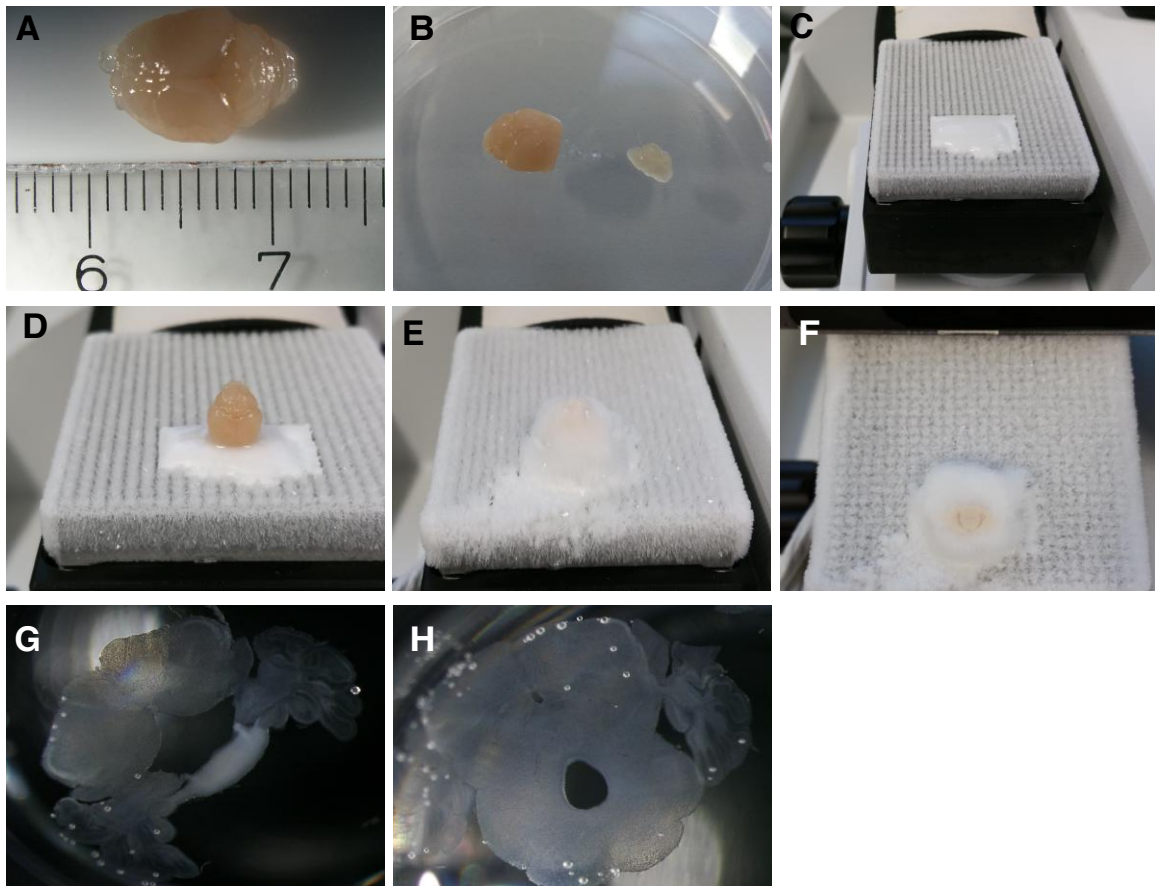
Figure 16. Experimental setup for the preparation of brain cryosections
A, Mouse brain after fixation in 4 % PFA for 4 h and incubated in 30% sucrose overnight. **B,** Using a scalpel the olfactory bulb and part of the cortex was cut off to obtain a planar surface. **C,D,** A socket of sucrose was generated to freeze the brain onto the cutting block. **E,** The brain was frozen onto the cutting block and completely covered by sucrose. **F,** Coronal sections with a cutting size of 30 µm were produced. **G,H,** Example of 2 sections from the brain stored in PBS (1X).

Cryosections were prepared using the HM 430 Micron microtome (Thermo Fisher, Waltham, MA,USA). Optimal cutting temperatures were determined to be between -26 and -23 °C. The brain was horizontally frozen to the cooling plate and fully embedded with 30 % sucrose (Cat.No.: 107687, MerckMillipore, Burlingtion, MS, USA) (**Fig. 16**). Coronal sections of 30 µm thickness were prepared and transferred to a 48 well plate filled with PBS (1X). The brain was cut until Bregma position ~ - 4.96 mm according to the mouse brain atlas (Franklin and Paxinos, 2008). The immunofluorescence labeling procedure was the same as described in chapter 2.4 with the only difference that the primary antibody was always incubated overnight at 4 °C. Fluorescence images of the slices were taken using the confocal LSM 710 (Zeiss). Overview images were acquired with the 20x/0.8 NA objective whereas the 63x/1.4 NA oil objective was used for the detailed analysis of the endbulb of Held synapses at bushy cells.

2.8 Analysis of auditory nerve fiber terminals

For the analysis of auditory nerve fiber terminals, Z-stacks with a slice thickness of 0.31 μm trough individual bushy cells were taken using the 63x/1.4 NA oil objective. Images were taken with a frame size 66.5 x 66.5 μm^2 and a pixel length of 0.07 μm. Cells were analyzed using Fiji Version 2.0.0 (Schindelin et al., 2012). For the analysis, the slice of the largest diameter of a bushy cell was determined and the image was duplicated as single image, showing VGLUT1 labeling only. The contrast was adjusted and the image was converted into an 8-bit image. Using the tool "Auto local threshold" a suitable threshold was chosen. All following bushy cells of the frame were treated with the same threshold. A line was drawn surrounding the bushy cell to be analyzed. Under "analyze", "analyze particles" the following settings were chosen: "size (μm^2): 0.1 – infinity", "circularity 0.00 – 1.00", "show outlines". Both the number of boutons as well as the total VLGUT1 labeled area (μm^2) was analyzed. Statistical analysis was performed with the Wilcoxon rank test using the IgorPro software (Version 6.12; Wavematrics, Orgeon, USA).

2.9 Whole cell patch clamp recordings

For the recording of Ca^{2+} currents from SG neurons, the patch clamp amplifier Axopatch 200B was used (Molecular Devices GmbH, Sunnyvale, CA, USA). Cells were visualized using an upright Olympus BX51WI microscope with a 40x/0.80 NA water objective LUMPlanFN (Olympus) and a BFWCAMXM camera (Scientifica, United Kingdom). The software IC Capture Version 2.3.394.1917 (Bremen, Germany) was used to monitor the cells on the screen. Data acquisition was performed using the software PatchMaster V2x69,27 Sep.2012 (Heka Electronics). The Axopatch 200 B amplifier was used with the following settings: V_{hold} at -80 mV, V_{clamp} mode, low pass Bessel filter at 10 kHz, output gain 1 and whole cell configuration ß=1. The protocols were generated with PatchMaster V2x69,27 Sep.2012 (Heka Electronics) with the help of Dr. Münkner. The following pulse protocol was used for recording of Ca^{2+} currents.
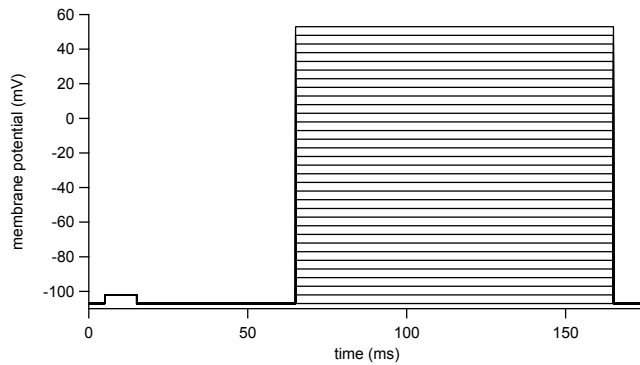
Figure 17. Pulse protocol used to record Ca^{2+} currents from SG neurons
Cells were initially held at -80 mV following a stepwise depolarization in 5 mV steps to 75 mV. Due to the large liquid junction potential, the effective holding potential was calculated to be -107 mV (chapter 2.9.2) and cells depolarized to 40 mV. Between 0 ms und 65 ms a 10 ms pre-pulse of 5 mV for off-line determination of the leak was applied. Altogether, there was in interval of 75 ms between consecutive depolarizations.

2.9.1 Solutions for electrophysiology

Three solutions were used to record Ca^{2+} currents from SG neurons. The bath solution (B-49) represents a standard extracellular Ringer-like solution consisting of: 1.3 mM CaCl$_2$, 10 mM HEPES acid, 5.6 mM glucose, 5.8 mM KCl, 0.9 mM MgCl$_2$, 143 mM NaCl and 0.9 mM NaH$_2$PO$_4$xH$_2$O, pH 7.35, $\sim$ 305 mOsmol. The internal solution (I-18) is an extracellular solution that partially mimicked the interior of the cell and on the other hand prevented ion influx through K$^+$ channels, consisting of: 0.1 mM CaCl$_2$, 20 mM CsCl, 5 mM EGTA acid, 0.3 mM GTP, 5 mM HEPES acid, 4 mM MgCl$_2$, 4 mM Na$_2$ATP, 10 mM Na-Phosphocreatine, 110 mM Cs-methanesulfonate, pH 7.35, $\sim$ 295 mOsmol. The application solution named B-58 was used for local superfusion of the neurons to isolate Ca^{2+} currents by blocking Na$^+$ and K$^+$ currents. Components of the application solution (B-58) were: 15 mM 4-AP, 1.3 mM CaCl$_2$, 2 mM CsCl, 5.6 mM glucose, 10 mM HEPES, 1 mM MgCl$_2$, 0.7 mM NaH$_2$PO$_4$ x H$_2$O, 30 mM TEA-Cl, 113 mM NMDG, pH 7.35, $\sim$ 305 mOsmol. Table 17 gives an overview about the chemicals that were used to prepare the bath, application and internal solution for patch clamp experiments.

Table 17. List of chemicals used for internal, bath and application solution

Chemical	Company	Cat. No.	LOT
$CaCl_2$	MerckMillipore, Burlingtion, MS, USA	208291	D00073408
HEPES acid	MerckMillipore, Burlingtion, MS, USA	1.10110.1000	K40249810949
Glucose	AppliChem GmbH, Darmstadt, Germany	A1349	9W003221
KCl	VWR International, Darmstadt, Germany	26764.298	13C250022
$MgCl_2$	MerckMillipore, Burlingtion, MS, USA	442611	D00076028
NaCl	VWR International, Darmstadt, Germany	1.06404.1000	17B234107
NaH_2PO_4	MerckMillipore, Burlingtion, MS, USA	1063460500	A995646938
4-AP	Sigma-Aldrich, St. Louis, MO, USA	A78403	MKBP9715V
CsCl	AppliChem GmbH, Darmstadt, Germany	A1098.0050	9B003226
TEACl	Sigma-Aldrich, St. Louis, MO, USA	86614	BCBP2382V
NMDG	Sigma-Aldrich, St. Louis, MO, USA	M2004	WXBB3510V
EGTA acid	Sigma-Aldrich, St. Louis, MO, USA	03779	30808161
GTP	Sigma-Aldrich, St. Louis, MO, USA	G8877	SLBL7184V
Na_2ATP	Sigma-Aldrich, St. Louis, MO, USA	A26209	10172203 TKSR
Na-Phosphocreatine	Sigma-Aldrich, St. Louis, MO, USA	P7936	SLBF2288V
Cesium methanesulfonate	Sigma-Aldrich, St. Louis, MO, USA	C1426	MKBQ0344V

The pH value was adjusted to 7.35 using 1 M NaOH for the bath solution, 1 M CsOH for the internal solution and 1 M HCl for the application solution. A pH-meter HI 221 (iHanna instruments, Vöhringen, Germany) was used and calibrated before each measurement. The osmolarity of the bath- and application solution was adjusted to ~ 305 mOsmol, the internal solution had an osmolarity of ~ 295 mOsmol. The osmolarity was measured using the Osmomat 030 from Gonotec (Berlin, Germany). The bath solution was stored at 4 °C, internal and application solution were stored at -20 °C.

2.9.2 Measurement and calculation of the liquid junction potential

Because recording of Ca^{2+} currents in SG neurons required a setting of three-solutions: pipette solution, bath solution and local superfusion solution containing ions with very different mobility, potentials had to be corrected for the different junction potentials (Neher, 1992). To determine the junction potential between two solutions, two clean bath chambers were filled with either internal or application solution (750 µl I-18 / B-58) and bath solution (750 µl B-49). A second pipette holder was attached to the setup that served as reference electrode. Both pipette holders were equipped with freshly chlorinated silver wires. Pipettes used for the reference electrode were pulled with a diameter opening of approx. 2 µm. The pipette was filled with 3 M KCl solution and little positive pressure was applied. The other pipette had a resistance similar to the ones used for patch clamp experiments. Both pipettes were placed into the bath chamber at the same height. Pipettes were placed apart from each other to avoid high chloride concentrations close to the patch pipette. The liquid junction potential (LJP)

was measured in the voltage clamp mode (VC). The bath chamber as well as the measurement electrode was filled with I-solution. The reference electrode filled with 3 M KCL was removed from the bath. The parameter at the Axopatch meter was set to "I" and the readout was 0. To test the chloride wires the patch pipette and the chamber were filled with I solution and the amplifier was changed to current clamp mode (CC); C = 0 and the readout was set to V_m. V was set to 0 using the pipette offset. After 10 min, V was supposed to be same or not differ by more than 1.0 mV. To record the LJP, the bath chamber filled with I solution was replaced by bath solution. The pipette (filled with I-solution) was placed into the bath chamber and after 1 min V_m was measured in the CC = 0 mode. To test the reversibility the mode was switched to VC and the bath chamber was filled with I solution (instead of bath solution). In CC = 0 mode V_m should be 0 or not differ more than 1 mV from 0. The measurements were repeated 3 times for each condition. Two conditions were measured, first B-49 versus I-18 and second B-58 versus I-18.

The LJP was determined and calculated according to Neher 1992 (Neher, 1992). The LJP for B-49 versus I-18 was -9.0 mV, for B-58 versus I-18 -18.8 mV. We used the following formula to calculate the LJP:

$$V_M = V - V_{LJ} - V_{2,1}$$
$$V_M = -80 \text{ mV} - (9.0 \, mV) - (18.8 \, mV)$$
$$V_M = -107.8 \, mV$$

A LJP of 27.8 mV was calculated. For the analysis of the recordings and for the generation of the I/V curve, the holding potential of -80 mV was corrected in IgorPro to -107.8 mV.

2.9.3 Ca^{2+} current recordings of cultured spiral ganglion neurons

Patch clamp recordings were performed on dissociated SG neurons isolated from the apical and basal parts of the cochlea. The recordings were performed at room temperature (21 ± 1 °C) in whole-cell configuration using the voltage clamp mode. A glass coverslip with SG neurons attached to it was carefully cracked into pieces by the back of a forceps. One of the pieces of the glass coverslip was attached to a dry bath chamber using a tiny amount of silicon gel, immediately immersed with B-49 and constantly perfused with it. Cells were visualized using an Olympus BX51WI microscope, with a 40x/0.80 W LUMPlamFN objective and a BFWCAMXM camera. Patch pipettes were pulled from quartz glass using a laser-based micropipette puller P-2000 (Sutter Instruments, Novato, CA, USA). The pipette was filled with I-18 stored on ice. The pipette resistance was between 6 and 8 MΩ using the two solutions mentioned before. To isolate Ca^{2+} currents, bath solution flow was stopped and the

cells were perfused for 1 min with application solution B-58. To isolate specific types of Ca^{2+} channels, a second channel of the application system was filled with B-58 supplemented with a specific Ca^{2+} channel blocker (**Tab. 18**). The application solution containing the blocker was also applied for 1 min before the voltage protocol was run.

Table 18. Ca^{2+} channel blocker

Toxin / blocker	Concentration	Company	Cat. No.	LOT
Nimodipine	10 μM	Sigma Aldrich, St. Louis, MO, USA	482200	#B45226
ω-agatoxin IVA	1 μM	Alomone, Jerusalem, Isreal	STA-500	#STA500TX0601
ω-conotoxin GVIA & MVIIA	1 μM	Alomone, Jerusalem, Isreal	C-300 / C-670	#C670CN1501
SNX-482	1 μM	Alomone, Jerusalem, Isreal	RTS-500	#RTS500SX1701

To ensure that the recorded Ca^{2+} current is stable over the recording time, run-down / run-up experiments were performed. The isolated Ca^{2+} current was repetitively measured over 3 min. Figure 18 shows example recordings of two SG neurons with repetitively measured Ca^{2+} currents.
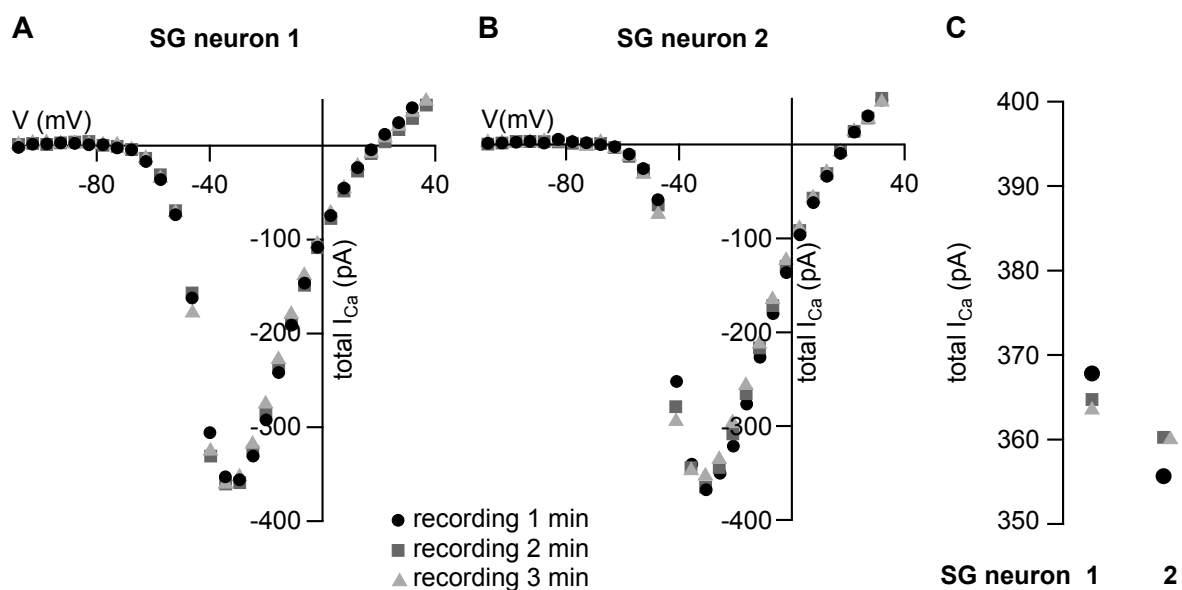
Figure 18. Analysis of potential run-down / run-up of the whole-cell Ca^{2+} current in cultured SG neurons
A,B, I-V curves of repetitive recordings at 1, 2 and 3 minutes after superfusion of the application solution that isolates I_{Ca} for 2 SG neurons aged P20 3 DIV. Both SG neurons showed neither run-down nor run-up of the peak I_{Ca}. C, Peak I_{Ca} amplitudes of the 3 recordings for SG neurons 1 and 2 indicate negligible, non-systematic differences of 2 % after 3 minutes.

The example recordings show that there was neither run-up nor run-down of the Ca^{2+} current within 3 min.

2.9.4 Analysis of patch clamp data

Patch clamp data were analyzed using the software IgorPro (Wavematrics, Lake Oswego, USA). For the analysis different plugins designed and programmed by Dr. Münkner were used. Although an automatic routine for determination of the leak resistance existed by fitting the current response to a rectangular 10 mV prepulse in the stimulation protocol it often did not yield suitable results. Therefore, leak subtraction was performed manually by using an I-V taken between 80 – 100 ms after start of depolarization (**Fig. 19A,B**) from the family of raw currents. The linear leak resistance was determined as DV/DI in the linear part of the I-V at very negative voltages where all channels were still closed, e.g. between -107 mV to -77 mV shown by the green symbols in Figure 19B. Using the calculated leak resistance all current traces were leak-subtracted automatically (**Fig. 19C**).
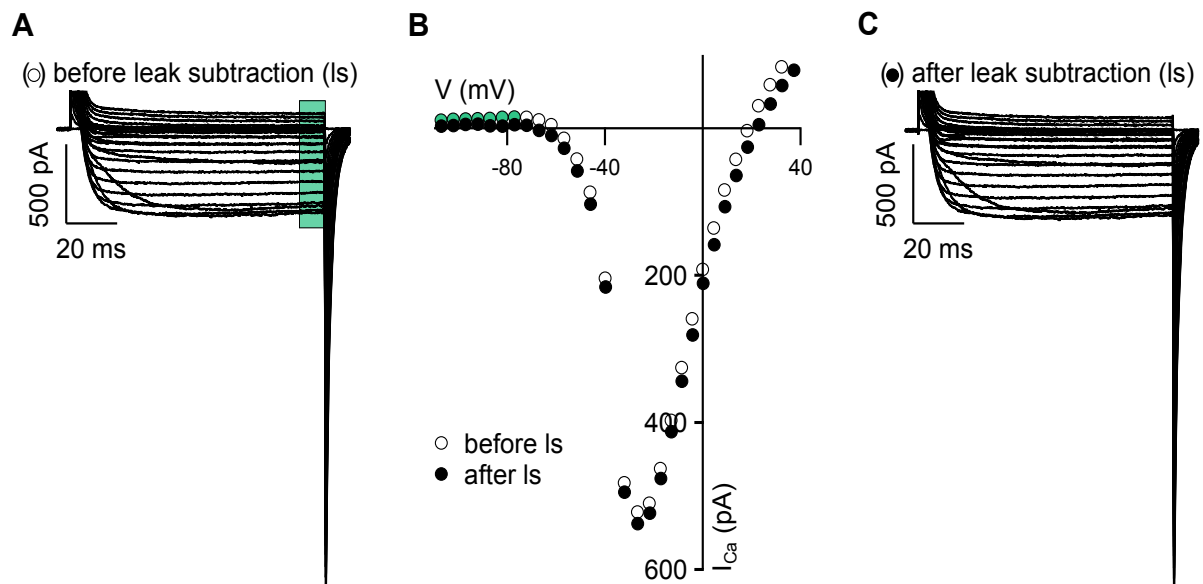
Figure 19. Determination of the manual leak subtraction
A, Left current trace represents the current before leak subtraction (ls). The green line at the end of the current trace indicates the 10 ms range used to generate the I-V curve shown in the middle (B before ls). **B,** The linear range of the beginning of the I-V curve (light green dots) was used to determine the leak. The greenish dots indicate the range. The first dot and the last dot were used to calculate Δx and Δy. In this example a leak of 7734.4 MΩ was calculated. **C,** Current trace after leak subtraction (**B** after ls). From this processed trace the I-V curve during the last millisecond was determined for further analysis.

2.10 Statistic Analysis

All statistic tests were performed using the software IgorPro (Wavematrics). For recorded Ca^{2+} currents from the apex or base and the response to the blocker the Wilcoxon Signed test (paired samples) was used. For the comparison of the portion of currents between the apex and base of $\alpha_2\delta3^{+/+}$ and $\alpha_2\delta3^{-/-}$ mice the Wilcoxon Rank test was used. For the comparison of the VGLUT1 labeled area and the number of boutons between $\alpha_2\delta3^{+/+}$ and $\alpha_2\delta3^{-/-}$ mice the

Wilcoxon Rank test was used. The significance was defined as followed *** $p < 0.001$, ** $p < 0.01$ and * $p < 0.05$.

3 Results

3.1 Localization of high voltage-activated Ca^{2+} channels in spiral ganglion neurons

Voltage-gated Ca^{2+} channels can be categorized into high voltage-activated (HVA: Ca$_v$1.1-Ca$_v$1.4 or L-type and Ca$_v$2.1-Ca$_v$2.3 or P/Q-, N- or R-type) and low voltage-activated (LVA: Ca$_v$3.1-3.3 or T-type) Ca^{2+} channels, based on the voltage required to activate these channels (Catterall, 2000). mRNA and protein expression of L-type, P/Q-type, N-type and R-type channels were reported for neonatal and mature SG neurons by various groups in the past (Davies et al., 2007; Lv et al., 2014; Pirone et al., 2014). For this project, we focused on HVA Ca^{2+} channels because their α_1 subunits are associated with the auxiliary subunits $\alpha_2\delta$ and β. The family of LVA Ca^{2+} channels that comprise the T-type channels was neglected because those are not associated with any auxiliary subunit (Dolphin, 2016).

Acutely isolated SG neurons from P5 (**Fig. 20**) and from P20 (**Fig. 21**) NMRI mice were labeled for the expression of L-type, P/Q-type, N-type and R-type Ca^{2+} channels. Table 19 summarizes the antibodies used with their corresponding amino acid epitope sequences. Different fixation agents were used to obtain optimal staining results, and are mentioned for each staining separately.

Images represent single optical slices of 0.3 µm acquired with a 63x/1.4 NA oil objective using a confocal LSM 710. Images were processed using Fiji (2.0.0-rc.43/1.15K) (Schindelin et al., 2012).

Table 19. Epitope sequence of tested HVA Ca^{2+} channel antibodies
Antibodies against Ca$_v$1.2, 1.3 and 2.2 were purchased from Alomone, against Ca$_v$2.3 from Abcam and against Ca$_v$2.1 from Synaptic Systems. All tested antibodies were polyclonal rabbit antibodies.

Antibody	Epitope
Ca$_v$1.2	TTKINMDDLQPSENEDKS
Ca$_v$1.3	DNKVTIDDYQEEAEDKD
Ca$_v$2.1	KAKKLQAMREEQNRTPLMFQRMEPPSPTQEGGPSQNALPSTQLDPGGGLMAQESSMKES PSWVTQRAQEMFQKTGTWSPERGPPIDMPNSQPNSQSVEMREMGTDGYSDSEHYLPMEG QTRAASMPRLPAENQRRRGRPRGNNLSTISDTSPMKRSASVLGPKARRLDDYSLERVPPEE NQRYHQRRRDRGHRTSERSLGRYTDVDTGLGTDLSMTTQSGDLPSKDRDQDRGRPKDRK HRPHHHHHHHHHHPPAPDRERYAQERPDTGRARAREQRWSRSPSEGREHATHRQ
Ca$_v$2.2	RHHRHRDRDKTSASTPA
Ca$_v$2.3	SASQERSLDEGVSIDG
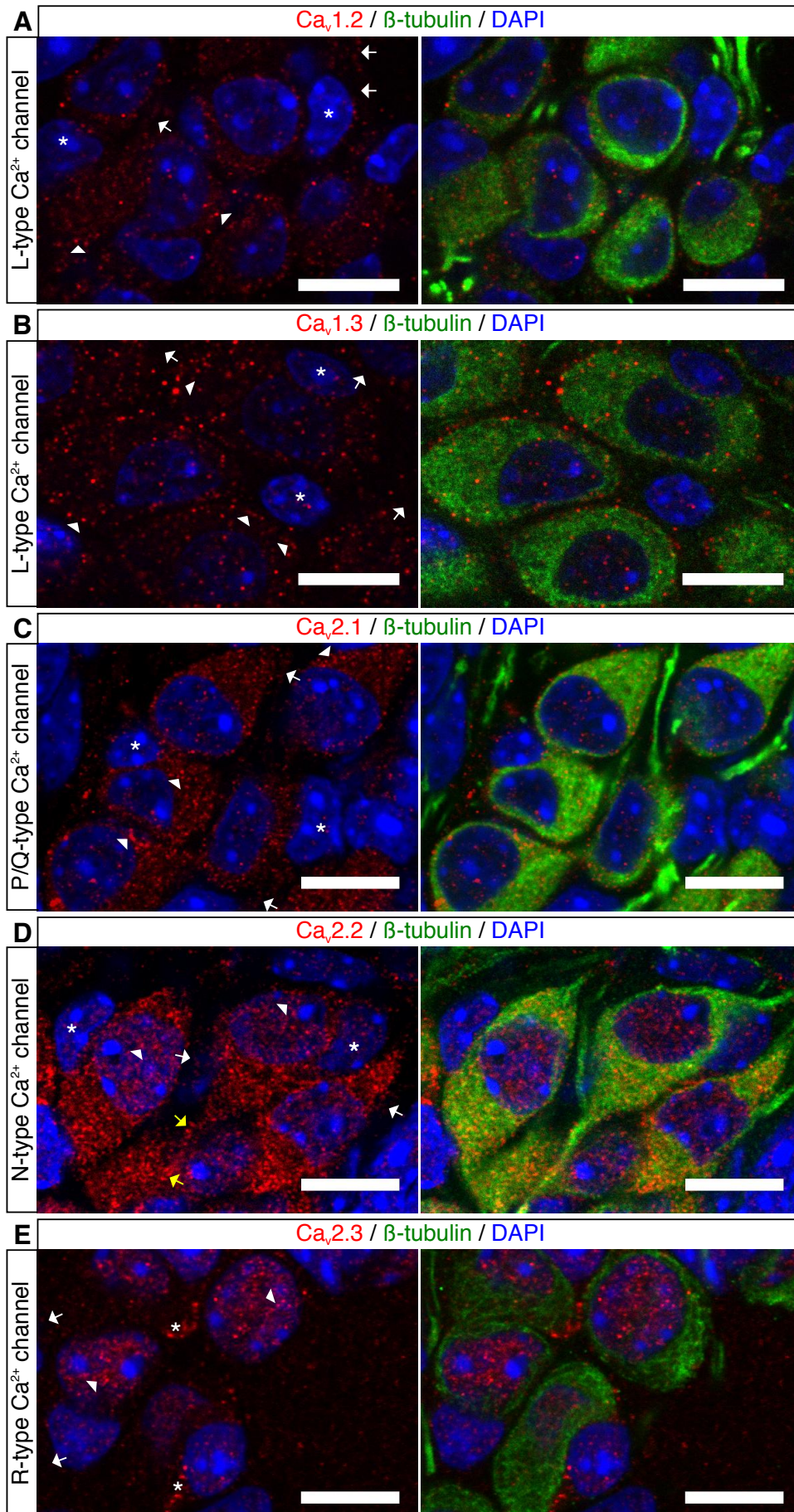
Figure 20. Localization of HVA Ca^{2+} channels in acutely isolated SG neurons from neonatal mice
Images **A-E** represent single optical slices of 0.3 μm acquired using a confocal LSM 710 with a 63x/1.4 NA oil objective; scale bar = 10 μm. SG neurons were labeled for ß-tubulin (green), the different Ca$_v$ channel types are shown in red and the nucleus was stained with DAPI (blue). White arrowheads mark the soma of SG neurons, white asterisks mark satellite cells and arrows (white or yellow) mark neurites. **A,B,** Labeling for the expression of the L-type Ca^{2+} channels Ca$_v$1.2 and Ca$_v$1.3. **A,** Methanol-fixed sample showed a weak labeling for Ca$_v$1.2 that was predominantly found in the soma of SG neurons (white arrowhead). In satellite cells (asterisk) and neurites (white arrows) no labeling of Ca$_v$1.2 was found. **B,** In samples fixed with ethanol, the membrane of SG neurons showed labeling for Ca$_v$1.3 (arrowhead). Labeling was absent in satellite cells (asterisk) and neurites (white arrows). **C,** Labeling for Ca$_v$2.1 performed on ethanol-fixed cells was found in the soma of SG neurons (arrowhead). Satellite cells (asterisk) and neurites (white arrows) showed no labeling. **D,** SG neurons fixed with Zamboni's fixative showed a strong labeling for Ca$_v$2.2 in the soma but also around the nucleus (arrowhead). In most neurites no Ca$_v$2.2 labeling was found (white arrow), however some neurites (yellow arrow) showed a strong labeling. Satellite cells showed a weak labeling mostly at the nucleus (asterisk). **E,** SG neurons fixed with methanol showed no labeling for Ca$_v$2.3 at the soma. A strong labeling for Ca$_v$2.3 was found at the nucleus of SG neurons (arrowhead). In the soma of satellite cells, labeling for Ca$_v$2.3 was detected (asterisk). Labeling was absent in neurites (arrows).

Immunofluorescence labeling of different HVA Ca^{2+} channels was performed on acutely isolated tissue of neonatal NMRI mice using different fixation chemicals. All types of HVA Ca^{2+} channels were identified in neonatal SG neurons, showing differential expression patterns (**Fig. 20**). Somatic labeling was predominantly found for L-type and P/Q-type Ca^{2+} channels (**Figs. 20A, B, C**). A strong immunoreactivity was found for N-type Ca^{2+} channels in the soma, the nucleus of SG neurons and satellite cells (**Fig. 20D**). Labeling for R-type channels was confined to the nuclei of SG neurons and satellite cells (**Fig. 20E**). The specificity of Ca$_v$1.3 and Ca$_v$2.2 antibodies was tested using 3-week old Ca$_v$1.3$^{-/-}$ and Ca$_v$2.2$^{-/-}$ mice. The results are shown in Fig.22 and 23 and will be discussed later. The specificity of the other Ca$_v$ channels (Ca$_v$1.2, Ca$_v$2.1 and Ca$_v$2.3) could not be tested because the respective knockout animals were not available to us. To test how the expression of Ca$_v$ channels changes during the development the stainings were repeated using acutely isolated SG neurons from P20 NMRI mice (**Fig. 21**).

A   Ca$_v$1.2 / ß-tubulin / DAPI
L-type Ca^{2+} channel

B   Ca$_v$1.3 / ß-tubulin / DAPI
L-type Ca^{2+} channel

C   Ca$_v$2.1 / ß-tubulin / DAPI
P/Q-type Ca^{2+} channel

D   Ca$_v$2.2 / ß-tubulin / DAPI
N-type Ca^{2+} channel

E   Ca$_v$2.3 / ß-tubulin / DAPI
R-type Ca^{2+} channel
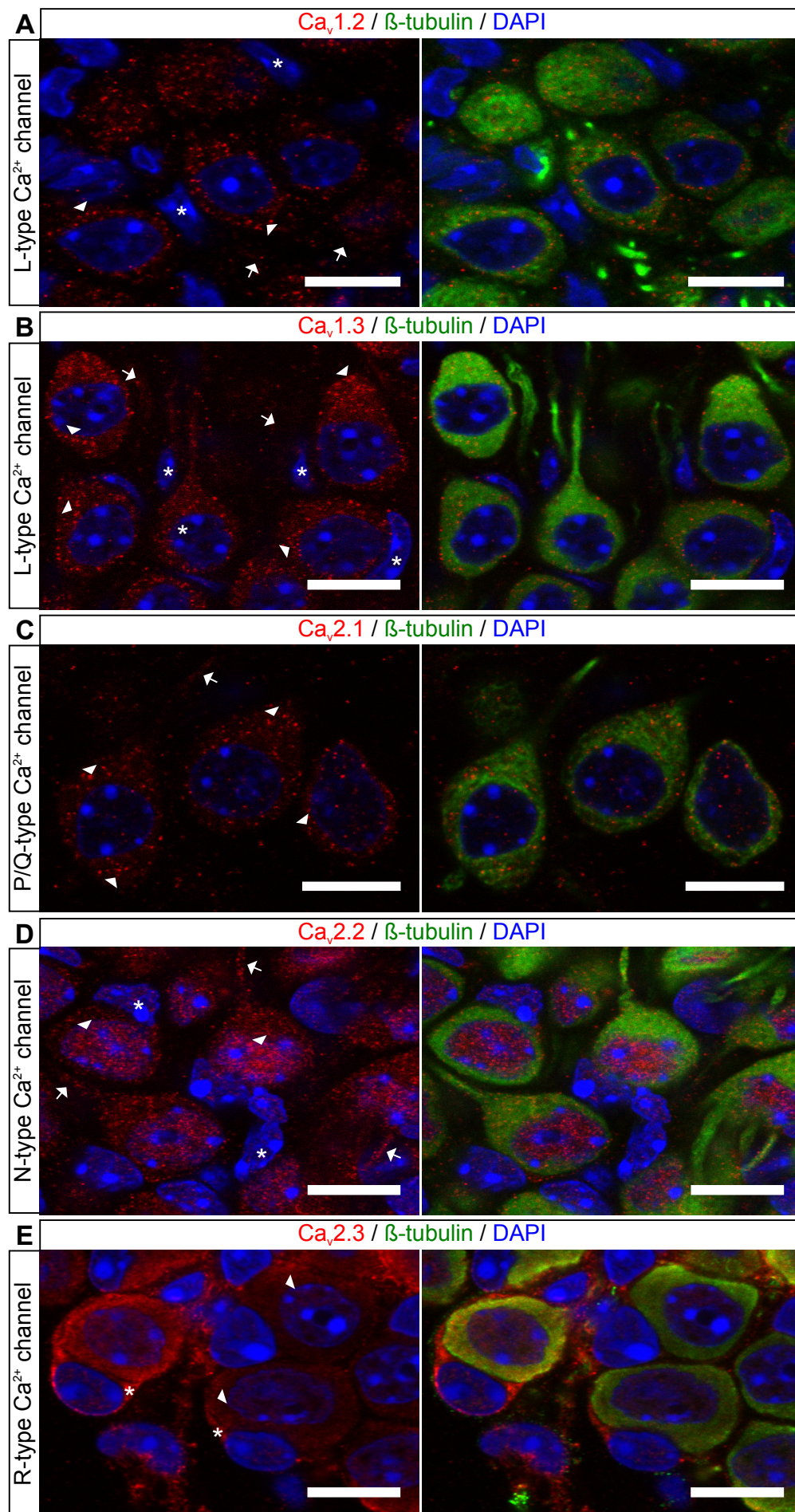
Figure 21. All types of high voltage activated Ca^{2+} channels were detected in the mature cochlea
Images **A-E** represent single optical slices of 0.3 μm that were acquired using a confocal LSM710 using a 63x/1.4 NA oil objective; scale bar = 10 μm. SG neurons were labeled for ß-tubulin (green), the different Ca$_v$ channel types are shown in red and the nucleus was stained with DAPI (blue). **A,B,** Labeling for the L-type channels Ca$_v$1.2 (methanol fixation) and Ca$_v$1.3 (ethanol fixation). **A,** A weak labeling for Ca$_v$1.2 was found in the soma of SG neurons (arrowhead) whereas Ca$_v$1.2 was absent from satellite cells (asterisk) and neurites (arrow). **B,** Labeling of Ca$_v$1.3 resulted in a punctate staining pattern in the soma and membrane of SG neurons. No signal was found in satellite cells (asterisk) or neurites (arrow). **C,** Labeling for P/Q-type channels after ethanol fixation resulted in a strong dot-like staining pattern in the soma and membrane of SG neurons. No staining was detected on neurites (arrow). **D,** N-type channel immunoreactivity after fixation with Zamboni's fixative was almost exclusively found at the nucleus of SG neurons. Satellite cells (asterisks) and neurites (arrows) showed faint labeling for Ca$_v$2.2. **E,** R-type channels were predominantly found in satellite cells (asterisks) and likely their myelin surrounding the SG neurons. SG neurons showed only a very weak labeling (arrowhead). Cells were fixed using methanol.

The images show that the expression of HVA Ca^{2+} channels changes within quantity and labeling pattern during the development. In deaf mice (P5), mainly the L-type Ca^{2+} channel Ca$_v$1.3 is expressed on the soma of SG neurons, while only a weak labeling for Ca$_v$1.2 is found. In mature mice (P20), after the onset of hearing, an increase in Ca$_v$1.2 labeling was found, however Ca$_v$1.3 channels were stronger expressed. From the Ca$_v$2 family, only P/Q-type channels were found on the soma of SG neurons isolated from mature mice, indicating that these channels might be the predominant channel type at this age (**Fig. 21C**). In neonatal mice, a strong signal for N-type channels was found on the soma and neurites of SG neurons, but also on the satellite cells. At P20, the signal was mainly restricted towards the nucleus. The specificity of the Ca$_v$1.3 and Ca$_v$2.2 labeling was tested using specific knockout mice (**Fig. 22, 23**).

3.1.1 Specificity test of anti-Ca$_v$1.3 and anti-Ca$_v$2.2 antibodies in acutely isolated spiral ganglion neurons from *Cacna1d*- and *Cacna1b*-deficient mice

Several possibilities exist to prove the specificity of an antibody. The best way is to perform immunohistochemistry in parallel on tissue from wildtype mice and on tissue from gene-specific knockout mice as a negative control. The Ca$_v$1.3$^{-/-}$ mice is a constitutive knockout mice that carries a premature stop codon at the N-terminus after exon 1 in the *Cacna1d* gene (Platzer et al., 2000). The Ca$_v$2.2$^{-/-}$ mouse carries a premature stop codon near segment 6 of domain II in the *Cacna1b* gene (Ino et al., 2001). Rabbit polyclonal anti-Ca$_v$1.3 and anti-Ca$_v$2.2 antibodies were purchased from Alomone Labs (Israel). The Ca$_v$2.2 antibody with the lot number AN-31 was previously tested and proven to be specific by Weiss and colleague (Weiss et al., 2014). Unfortunately this lot number was no longer available, so an antibody with the lot number AN-37 was tested. The tissue was isolated, fixed and stained as described previously (chapter 2.4).

3.1.1.1 Antibody test using *Cacna1d*-deficient mice

The epitope of the $Ca_v1.3$ antibody targets the intracellular loop of segment 2-3 (**Fig. 22A**) of the α_1 channel pore. The mutation in $Ca_v1.3^{-/-}$ mice is at the beginning of the N-terminus, so even if in the knockout a small protein was produced it would not contain the epitope sequence of the anti-$Ca_v1.3$ antibody.
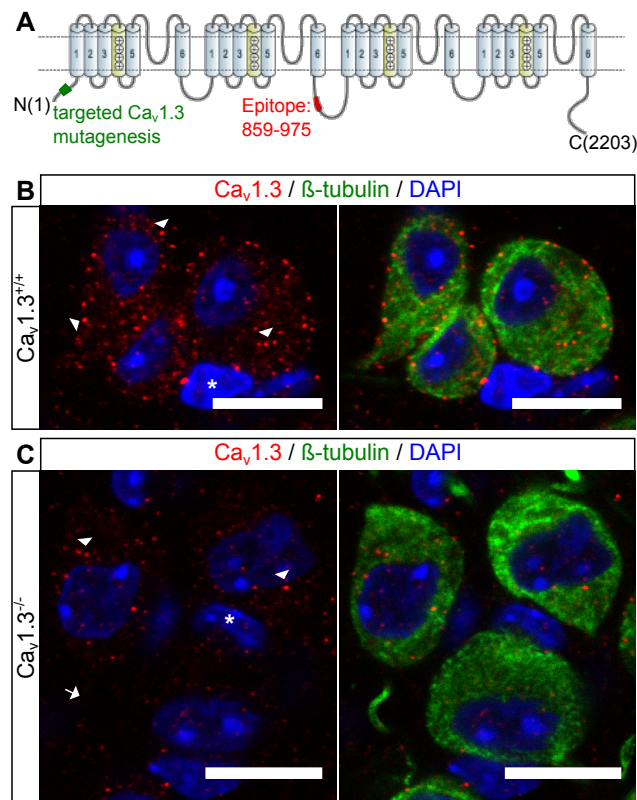
Figure 22. Specificity test of the $Ca_v1.3$ antibody on SG neurons from $Ca_v1.3^{-/-}$ mice aged P20
A, Topology of the transmembrane spanning domains of the $Ca_v1.3$ α_1 subunit showing the binding epitope of the $Ca_v1.3$ antibody in red and the genomic mutation of the knockout in green. Numbers represent position of amino acid residues. The sketch was taken from the Alomone homepage and modified. **B,C,** Labeling of $Ca_v1.3$ in wildtype and $Ca_v1.3^{-/-}$ mice. In the wildtype (**B**), punctate $Ca_v1.3$ labeling was mainly found at the membrane and soma of SG neurons (arrowhead) whereas satellite cells (asterisk) showed no labeling. In tissue of the $Ca_v1.3^{-/-}$ mouse (**C**), the punctate labeling of the SG neurons was markedly reduced and mostly confined to the soma of the SG neurons (arrowhead). Satellite cells (asterisk) and neurites (arrow) showed no staining for $Ca_v1.3$. The images represent single optical slices of 0.3 µm taken using a confocal LSM 710 at 63x/1.4 NA oil objective, scale bar = 10 µm (**B,C**).

Acutely isolated SG neurons from P20 $Ca_v1.3$ wildtype and knockout mice were labeled for the expression of $Ca_v1.3$ to test the specificity of the used antibody. The results show (**Fig. 22B**) that in the wildtype, $Ca_v1.3$ is predominantly found in the soma and the membrane of SG neurons. In the knockout (**Fig. 22C**) the labeling was massively reduced and the $Ca_v1.3$ puncta were smaller compared to the wildtype. In addition, $Ca_v1.3$ puncta were mainly found on the soma rather than at the membrane. In summary, the anti-$Ca_v1.3$ antibody, lot number

AN-15 (Alomone Laboratories, Israel; Cat. No.: ACC-311), seems to recognize its epitope but shows some unspecific labeling in addition. The remaining labeling for $Ca_v1.3$ in $Ca_v1.3^{-/-}$ SG neurons indicates a substantial background of the antibody, which makes interpretations of true $Ca_v1.3$ labeling in wildtype tissue impossible

3.1.1.2 Antibody test using *Cacna1b*-deficient mice

The $Ca_v2.2$ subunit was labeled using a polyclonal anti-rabbit antibody from Alomone (Israel). The initial antibody lot that had been shown to be specific by Weiss et al., was no longer available, so a new antibody lot was tested (AN-37). The samples were processed as described before and the results were summarized below (**Fig. 23**).
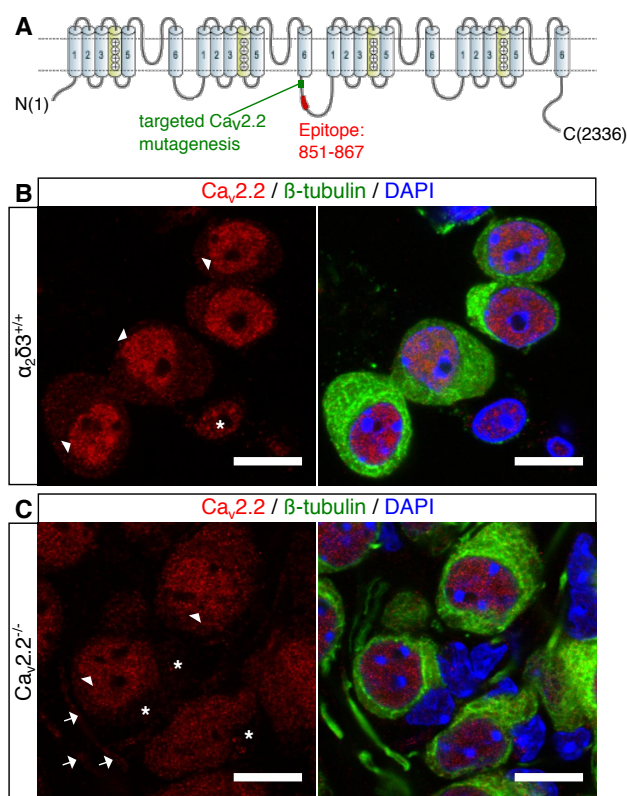
Figure 23. Specificity test of the $Ca_v2.2$ antibody using $Ca_v2.2^{-/-}$ mice at P20
A, Topology of the $Ca_v2.2$ subunit showing the transmembrane spanning segments of the channel with the voltage sensors shown in yellow (+). Both N and C terminus are located on the intracellular side of the channel. Numbers represent amino acid residues and the red label indicates the antigenic epitope. The site of the premature stop codon of the knockout is indicated in green. **B,C,** Fluorescence labeling of $Ca_v2.2$ (red), ß-tubulin (green) and DAPI (blue) in mature wildtype and $Ca_v2.2^{-/-}$ mice. **B,** In tissue of the $\alpha_2\delta3^{+/+}$ mouse, a strong labeling for $Ca_v2.2$ was found in the nucleus of SG neurons (arrowhead) and also in satellite cells (asterisk). In the $Ca_v2.2^{-/-}$ mice the nuclear labeling was absent from satellite cells (asterisks) but unchanged in SG neurons (**C**). Images represent single optical slices of 0.3 μm taken using a confocal LSM 710 at 63x/1.4 NA oil objective. Scale bar = 10 μm (**B,C**).

The specificity of the $Ca_v2.2$ antibody was tested using $\alpha_2\delta3^{+/+}$ and $Ca_v2.2^{-/-}$ mice aged P20. In the $\alpha_2\delta3$ wildtype, $Ca_v2.2$ labeling was predominantly found at the nucleus of SG neurons and

satellite cells (**Fig. 23B**). In the $Ca_v2.2$ knockout, the labeling was absent in satellite cells but remained at the nucleus of SG neurons (**Fig. 23C**). To conclude, the tested $Ca_v2.2$ antibody (lot number AN-37) from Alomone Laboratories (Israel) is unspecific for $Ca_v2.2$ and the nuclear labeling seems to be an artifact.

3.2 Specificity test of different $\alpha_2\delta3$ antibodies

Different $\alpha_2\delta3$ antibodies were tested regarding their specificity using acutely isolated whole-mount samples from $\alpha_2\delta3^{+/+}$ and $\alpha_2\delta3^{-/-}$ mice aged P20. The knockout construct of the $\alpha_2\delta3^{-/-}$ mouse introduced a premature stop codon behind exon 15 of the *Cacna2d3* gene (Neely et al., 2010). The expression of a residual peptide comprising exon 1 to 15 is theoretically possible if nonsense-mediated RNA decay is not 100 % efficient (Kurosaki and Maquat, 2016). To make sure that anti-$\alpha_2\delta3$ antibodies bind only in regions that are not expressed in the knockout, we chose antibodies with epitope positions behind exon 15. Table 20 gives an overview about the peptide sequences and their corresponding binding positions in the *Cacna2d3* gene. Acutely isolated whole-mount samples were isolated and stained as described previously (chapter 2.4). The samples were analyzed using a confocal LSM 710 with a 63x/1.4 NA oil objective.

Table 20. Binding positions and peptide sequence of $\alpha_2\delta3$ antibodies
Binding positions were determined using the UCSC genome browser blat search (https://genome.ucsc.edu/cgi-bin/hgGateway).

Company	Cat. No.	Peptide sequence	Binding position
Novus	NBP1-20111	KYKLGIHGYAFAITNNGYILTHPELRLL YEEGKKRRKPNYSSVDLSEVEWE	Exon 17 - 18
Alomone	ACC-103	KWIMTELVLFLVEFNLCSWWH	Part of exon 34
Sigma-Aldrich	N4142	WHSDMTAKAQKLKQTLEPCDTEYPAFVSER TIKETTGNIACEDCSKSFVIQQIPSSNLFMVVVD	Exon 35
Abcam	Ab102939	TMAPIEIRYNESLKCERLKAQKIRRRP ESCHGFHPEENAR	Exon 37

The following figures (**Figs. 24 – 27**) show the results of antibody specificity tests performed on acutely isolated SG neuron tissue from $\alpha_2\delta3^{+/+}$ and $\alpha_2\delta3^{-/-}$ mice.
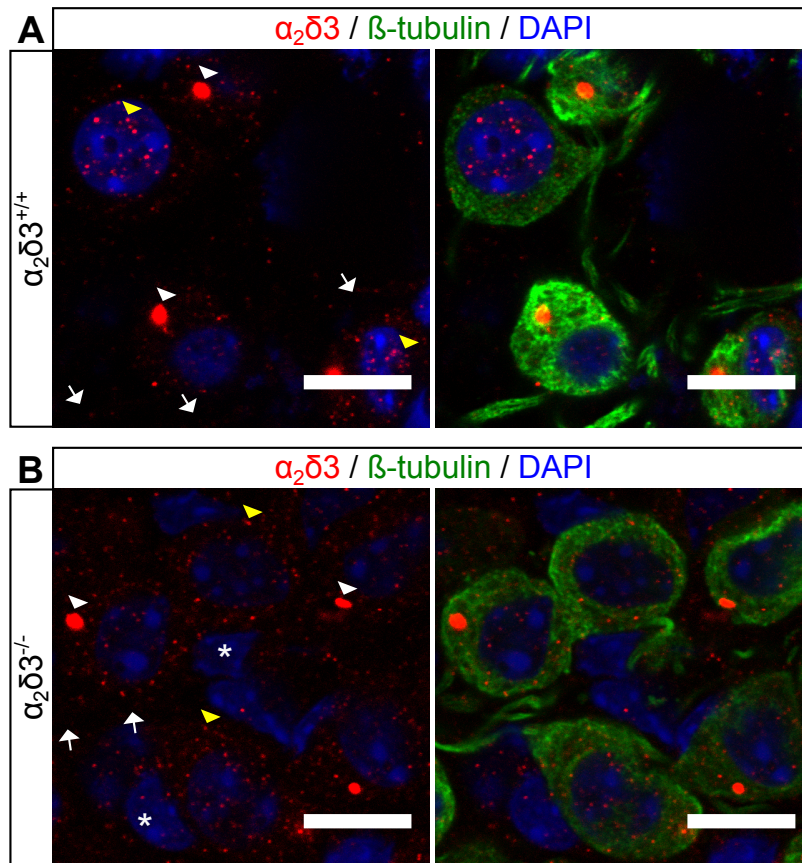
Figure 24. Immunolabeling of $\alpha_2\delta3$ in acutely isolated SG neurons using an antibody from Sigma Aldrich
The polyclonal antibody N4142 produced by Sigma Aldrich was directed against a region of exon 35 of the *Cacna2d3* gene. **A,** Labeling of $\alpha_2\delta3$ in SG neurons isolated from $\alpha_2\delta3^{+/+}$ mice. **B,** Labeling of $\alpha_2\delta3$ in SG neurons isolated from $\alpha_2\delta3^{-/-}$ mice. In **A** and **B** yellow arrowheads mark small puncta, white arrowheads mark large prominent dots and the white arrow indicate labeling of $\alpha_2\delta3$ in fibers. In tissue isolated from both genotypes labeling for $\alpha_2\delta3$ resulted in a very similar pattern. In almost each SG neuron a very prominent dot (white arrowhead) as well as several smaller puncta (yellow arrowhead) were found. No labeling for $\alpha_2\delta3$ was found in neurites. In the knockout a weak labeling for $\alpha_2\delta3$ was found on satellite cells (asterisk). Zamboni fixation; images represent single optical slices acquired using a confocal LSM 710 with a 63x/1.4 NA oil objective; scale bar = 10 μm.
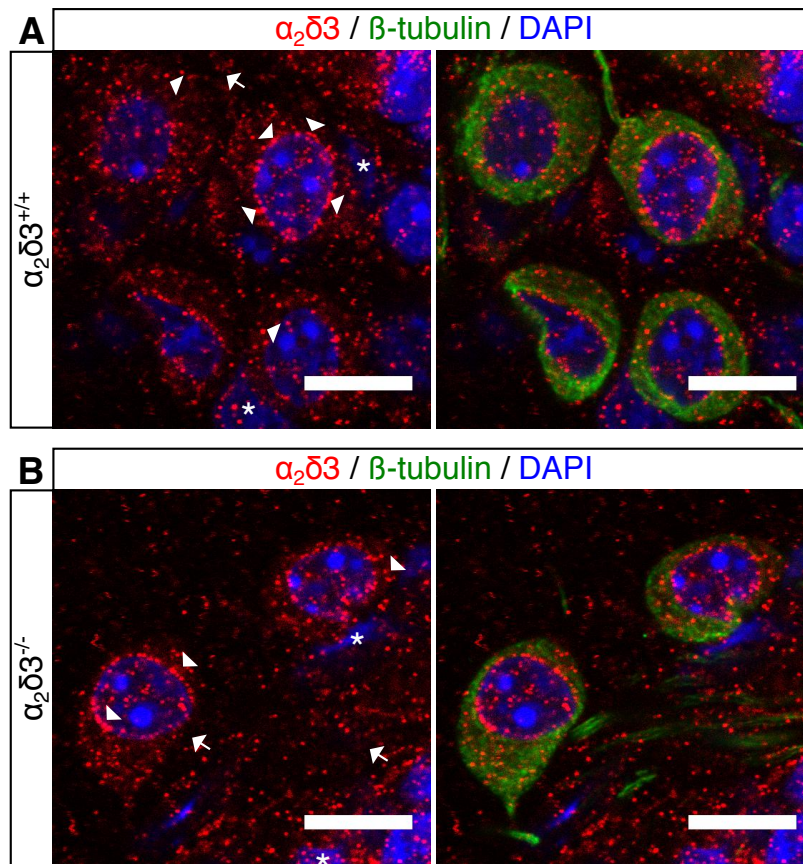
Figure 25. Immunolabeling of $\alpha_2\delta3$ in acutely isolated SG neurons using an antibody from Abcam
The polyclonal antibody (Cat. No.: ab102939; Abcam) was directed against a region of exon 37. **A,** Labeling of $\alpha_2\delta3$ in SG neurons isolated from $\alpha_2\delta3^{+/+}$ mice resulted in a strong punctate labeling around the nucleus (arrowheads) as well as in the soma. Labeling of $\alpha_2\delta3$ was also found in satellite cells (asterisk). **B,** Labeling of $\alpha_2\delta3$ in SG neurons isolated from $\alpha_2\delta3^{-/-}$ mice resulted in a similar staining pattern as described in **A**. A weak $\alpha_2\delta3$ labeling was found on neurites (arrow). Both images show a high background labeling. Zamboni fixation; images represent single optical slices acquired using a confocal LSM 710 with a 63x/1.4 NA oil objective; scale bar = 10 µm.
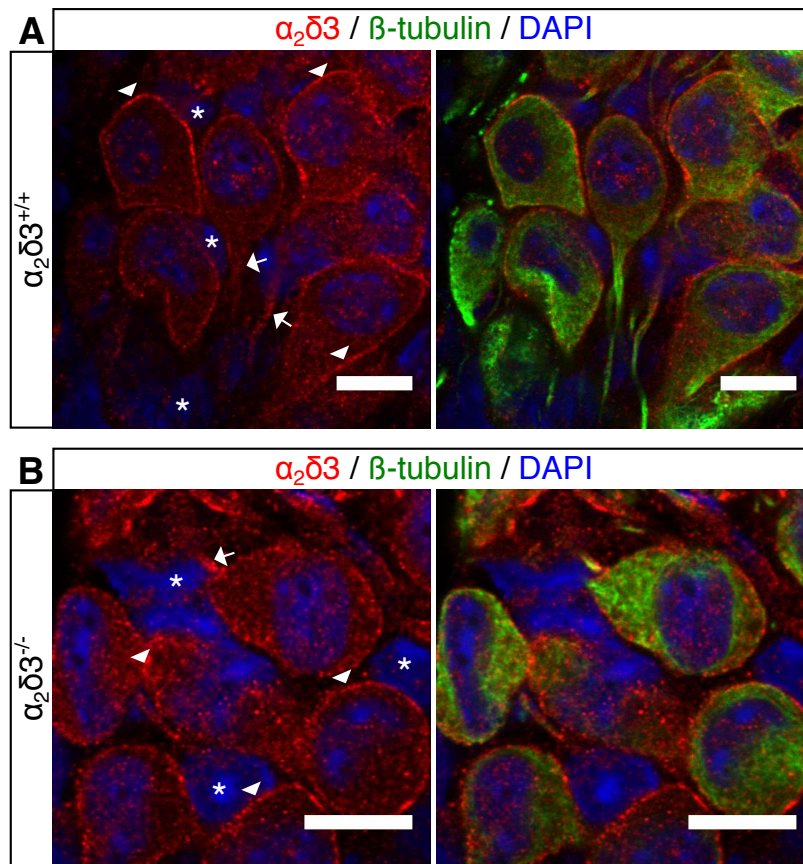
Figure 26. Immunolabeling of α₂δ3 using an antibody from Alomone Laboratories

The polyclonal antibody (Cat. No.: ACC-103; Alomone Laboratories) was directed against a part of exon 34. **A,** Labeling of α₂δ3 in SG neurons isolated from α₂δ3$^{+/+}$ mice outlined the membrane of SG neurons (arrowheads). A diffuse labeling was also detected in the soma of SG neurons and in the proximal neurites (arrows). No α₂δ3 labeling was present in satellite cells (asterisks). **B,** Labeling of α₂δ3 in SG neurons isolated from α₂δ3$^{-/-}$ mice showed clear labeling at the membrane (arrowheads) and weaker labeling in the soma and in proximal neurites (arrow, left). No labeling for α₂δ3 was detected in satellite cells (asterisks). Ethanol fixation; images represent single optical slices acquired using a confocal LSM 710 with a 63x/1.4 NA oil objective; scale bar: 10 = μm.
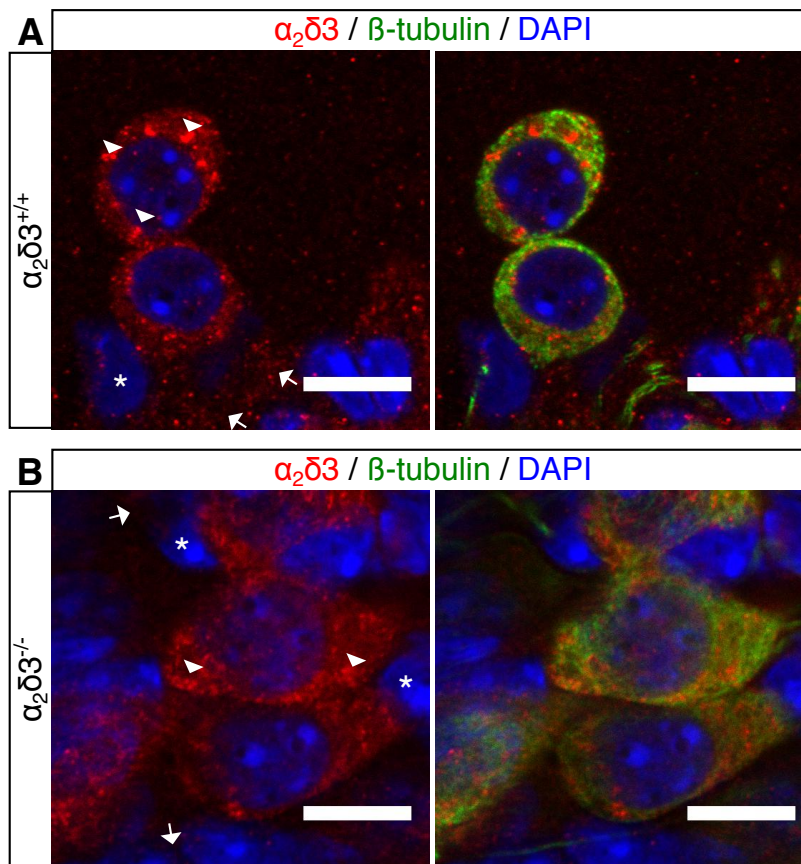
Figure 27. Immunolabeling of $\alpha_2\delta3$ in acutely isolated SG neurons using an antibody from Novus
The polyclonal antibody (Cat. No.: NBP1-20111; Novus) from Novus was directed against exons 17 and 18 of the *Cacna2d3* gene. **A,** Labeling of $\alpha_2\delta3$ in SG neurons isolated from $\alpha_2\delta3^{+/+}$ mice. Immunoreactivity was found as puncta or larger clusters in the cytoplasm surrounding the nucleus of SG neurons (arrowheads). No staining was detected in satellite cells (asterisk) and neurites (arrows). **B,** Labeling of $\alpha_2\delta3$ in SG neurons isolated from $\alpha_2\delta3^{-/-}$ mice resulted in a diffuse labeling in the soma (arrowheads, left), partially surrounding the nucleus. Satellite cells (asterisk) and neurites (arrow) did not show immunoreactivity for $\alpha_2\delta3$. Ethanol fixation; images represent single optical slices acquired using a confocal LSM 710 with a 63x/1.4 NA oil objective, scale bar = 10 μm.

Four different polyclonal anti-$\alpha_2\delta3$ antibodies directed against different epitopes were tested for specificity in labeling the auxiliary subunit $\alpha_2\delta3$. All antibodies were directed against regions that are absent in the $\alpha_2\delta3^{-/-}$ mice. To our dismay, the four antibodies resulted in complete different staining patterns with different localization of $\alpha_2\delta3$ (nuclear, somatic and membrane, **Figs. 24 – 27**). The comparison of the staining results in $\alpha_2\delta3^{+/+}$ with those in $\alpha_2\delta3^{-/-}$ tissue revealed almost identical (**Figs. 24 – 26**) or very similar (**Fig. 27**) labeling patterns for each individual antibody. All tested $\alpha_2\delta3$ antibodies showed unspecific labeling and are therefore not specific.

A hallmark of $\alpha_2\delta$ proteins is their high degree of glycosylation, which is a very important post-translational modification but can hamper antibody specificity and thereby influence the outcome of the staining. Because antigenic peptides lacking glycosylation are often used for injection of for example rabbits, the produced antibody might not be specific for native

protein being highly glycosylated. To overcome the problem of non-specificity caused by glycosylation, chemical as well as enzymatic deglycosylation agents were tested with the goal to improve the antibody specificity. Because we hypothesized that $\alpha_2\delta3$ predominantly localizes with the P/Q-type channels $Ca_v2.1$ (Pirone et al., 2014) and we knew that $Ca_v2.1$ protein and $Ca_v2.1$ channels are expressed in the membrane of SG neurons (**Figs. 21C, 37C**) the antibody from Alomone was chosen to further improve the labeling for $\alpha_2\delta3$ because it labeled the membrane of SG neurons (**Fig. 26A**). From the immunofluorescence labeling for $Ca_v2.1$ and the electrophysiology recordings it was known that $Ca_v2.1$ is expressed at the membrane. Therefore the antibody from Alomone was used to further improve the labeling for $\alpha_2\delta3$ because the staining resulted in a nice membrane localization of the auxiliary subunit.

3.3 Chemical and enzymatic deglycosylation assays

Glycosylation is the linkage of sugar residues to amino acids within a polypeptide chain and represents one of the most complex post-translational modifications, necessary for a plethora of processes, which among others increases the protein diversity. However, glycosylation can lead to masking of antibody epitopes or unspecific binding to antibodies, resulting in unspecific labeling. All $\alpha_2\delta$ proteins represent highly glycosylated proteins and so far no specific antibodies for the $\alpha_2\delta3$ subunit exist. Here we tested chemical as well as enzyme deglycosylation. To improve antibody specificity, the chemical agent periodic acid (H_5IO_4) and as an enzymatic agent Peptide:N-Glycosidase F (PNGase F) were used. PNGase F is an enzyme that removes N-linked glycans thereby leaving an intact protein structure. It is assumed that the glycosylation of the auxiliary subunit is N- rather than O-glycosylation (Lazniewska and Weiss, 2017). An assay for the deglycosylation of whole-mount samples was developed since no protocols for deglycosylation and subsequent immunolabeling was found. Whole-mount samples from NMRI mice aged P20 were dissected from the cochlea as described before (chapter 2.3). After fixation of the tissue with ethanol, cells were treated with different concentrations of PNGase F (chapter 2.5). Afterwards cells were labeled for ß-tubulin (green), $\alpha_2\delta3$ (red) and DAPI (blue). The results are summarized below in figure 28.
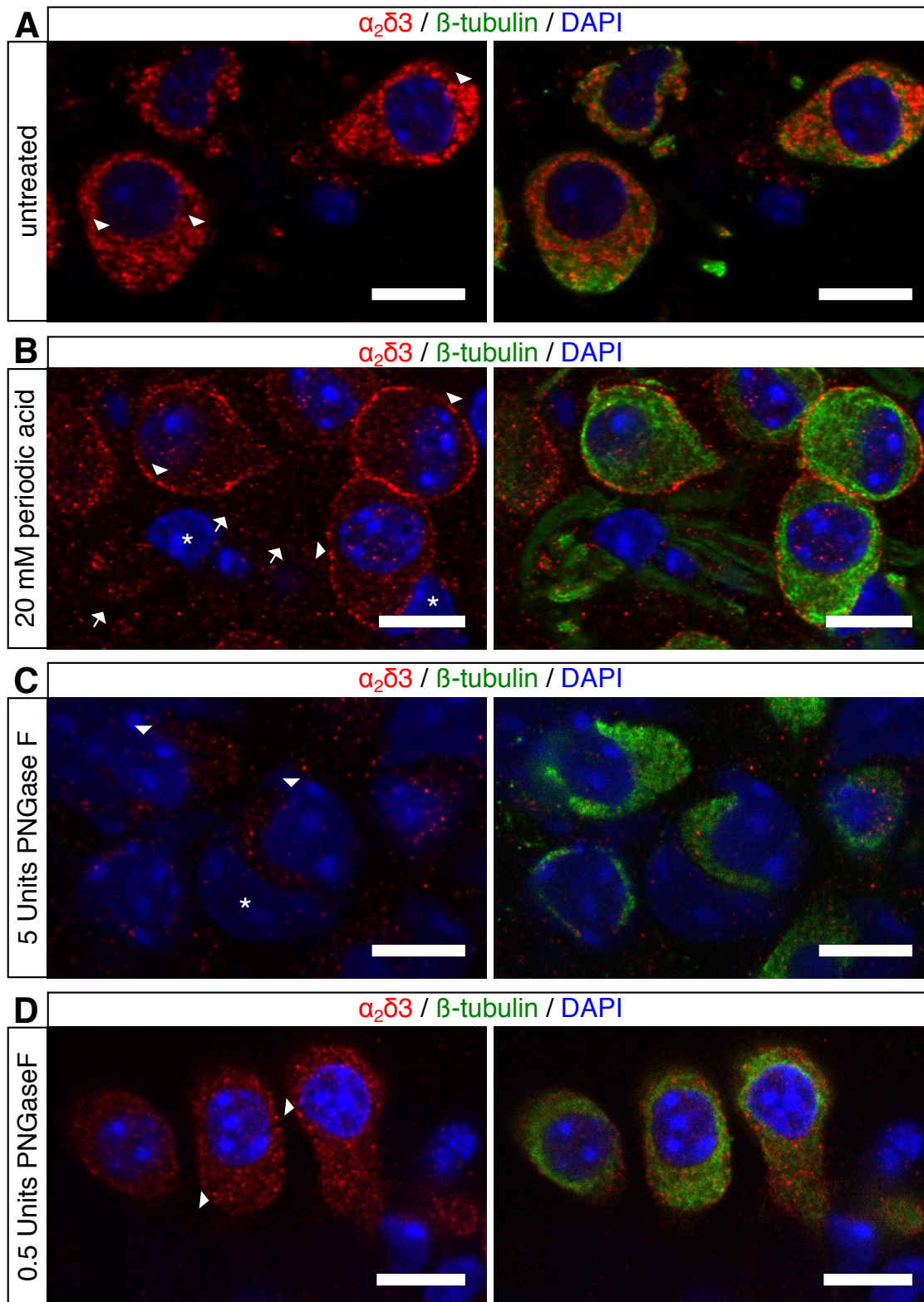
Figure 28. Effects of chemical or enzymatic deglycosylation agents on α₂δ3 immunolabeling

A, Labeling for α₂δ3 with polyclonal anti-α₂δ3 (Alomone Laboratories, 1:200) under normal conditions (no deglycosylation). Strong immunoreactivity was found in the soma of SG neurons, with a particular intense labeling around the nucleus of SG neurons (arrowheads, left). **B,** Effect of 20 mM periodic acid. After the treatment the staining was predominantly found at the membrane of SG neurons (arrowhead, left). No labeling was found in satellite cells (asterisk, left) or neurites (arrows, left). **C,** Effect of treatment with 5 Units PNGase F. Cells were swollen (arrowhead, left) and disintegrated (arrowhead, right) **D,** Treatment with 0.5 Units PNGase F treatment resulted in an almost evenly distributed labeling for α₂δ3 in the soma with some

more intense dots (arrowheads, left). However treatment at this lower concentration resulted in an elongated cell shape. Ethanol fixation; images represent single optical slices of 0.3 μm taken with a confocal LSM 710 with a 63x/1.4 NA oil objective; scale bar = 10 μm.

It turned out that the concentration of 5 units PNGase F was a too high because cells were swollen and in part bursted (**Fig. 28C**). For further treatment, a concentration of 0.5 units was used which caused an elongation of SG neurons (**Fig. 28D**). Treatment with 20 mM periodic acid resulted in a clear membrane labeling for $\alpha_2\delta3$ in SG neurons (**Fig. 28B**). Surprisingly, the untreated samples displayed a different staining pattern than obtained previously (**Fig. 26**). To figure out if the chemical or enzymatic treatment improves the specificity of the $\alpha_2\delta3$ labeling, tissue samples from $\alpha_2\delta3^{+/+}$ and $\alpha_2\delta3^{-/-}$ mice were treated with both deglycosylation agents, which is summarized in Figure 29.
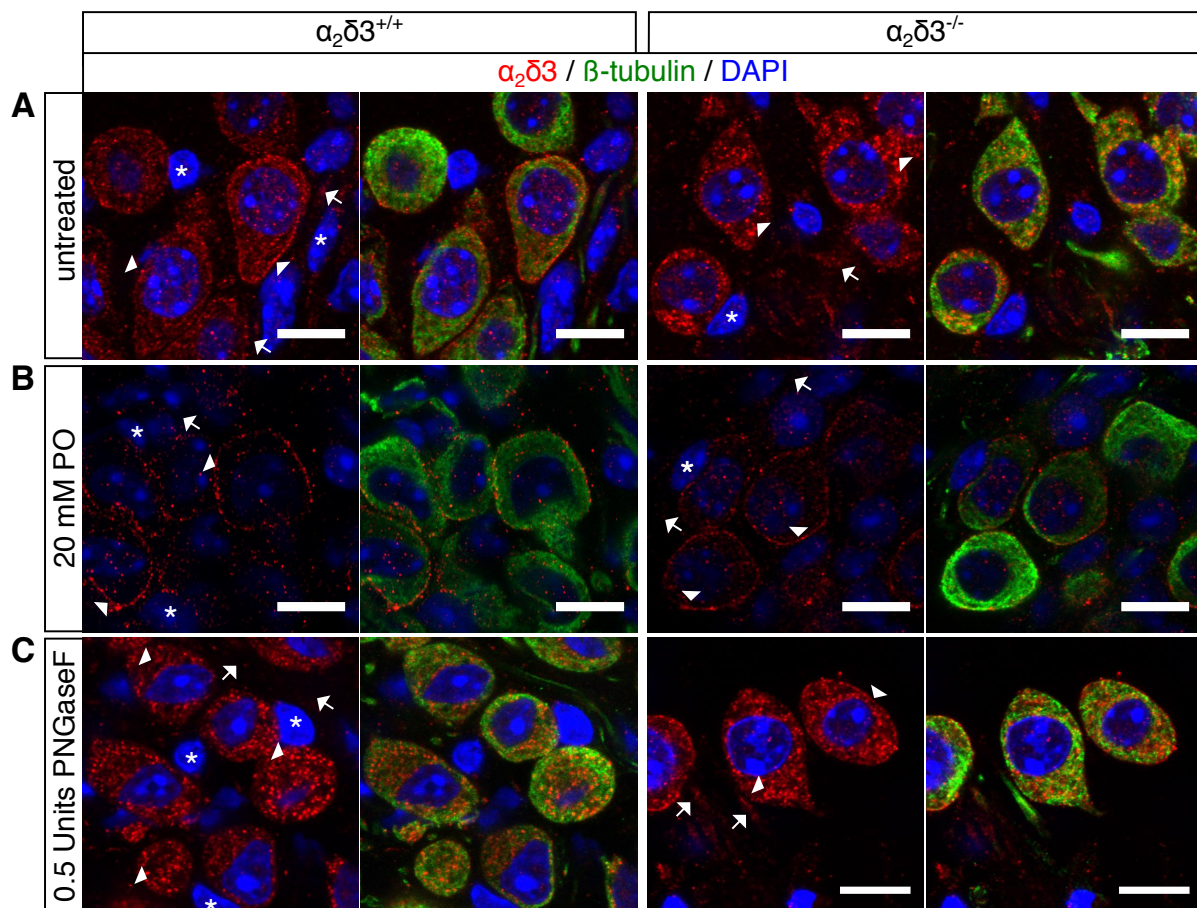
Figure 29. Effects of deglycosylation on the specificity of $\alpha_2\delta3$ immunolabeling in $\alpha_2\delta3^{+/+}$ and $\alpha_2\delta3^{-/-}$ mice SG neurons were labeled for $\alpha_2\delta3$ (Cat. No.: ACC-103; Alomone antibody; red), ß-tubulin (green) and nuclei were stained with DAPI (blue). **A,** Control staining without deglycosylation for $\alpha_2\delta3^{+/+}$ (left two images) and $\alpha_2\delta3^{-/-}$ (right two images). Left panels show predominant $\alpha_2\delta3$ labeling in the membrane (arrowheads), which was absent from satellite cells (asterisks) and neurites (arrows). In the knockout (right images) $\alpha_2\delta3$ labeling was more redistricted to the soma and appeared in clusters. No $\alpha_2\delta3$ labeling was seen in neurites (arrow) and satellite cells (asterisks). **B,** Treatment with 20 mM periodic acid led to sparse membrane labeling (arrowheads) in both $\alpha_2\delta3^{+/+}$ (left two images) and $\alpha_2\delta3^{-/-}$ SG neurons (right images) and lack of labeling from satellite cells

(asterisks) and neurites (arrows). **C,** After treatment with 0.5 Units PNGase F $\alpha_2\delta3$ labeling appeared as prominent clusters in the entire soma of both $\alpha_2\delta3^{+/+}$ and $\alpha_2\delta3^{-/-}$ SG neurons (arrowheads). Single optical slices acquired with a confocal LSM with a 63x/1.4 NA oil objective, scale bar = 10 μm.

The treatment with PNGase F and periodic acid showed no improvement in the specificity of the antibody. Although the labeling pattern changed after treatment with different deglycosylation agents compared with the untreated control, the resulting staining patterns were almost identical between $\alpha_2\delta3^{+/+}$ and $\alpha_2\delta3^{-/-}$ mice. From Fig. 29B,C we cannot judge whether deglycosylation worked with either PNGase F or periodic acid, because labeling patterns were very different in $\alpha_2\delta3^{+/+}$ tissue. The results of Figure 29 however confirm our findings from Figure 26 that the anti-$\alpha_2\delta3$ antibody from Alomone is not specifically recognizing $\alpha_2\delta3$ but other epitopes.

3.4 Immunohistochemical labeling of $\alpha_2\delta3$ and GM130

Immunolabeling without deglycosylation treatment resulted in the formation of clusters of $\alpha_2\delta3$ immunoreactivity (**Figs. 28A, 29A**). To ascertain if the labeled $\alpha_2\delta3$ was located intracellularly, specimen were co-labeled with GM130, a marker for the Golgi apparatus. The results are shown in Fig. 30.
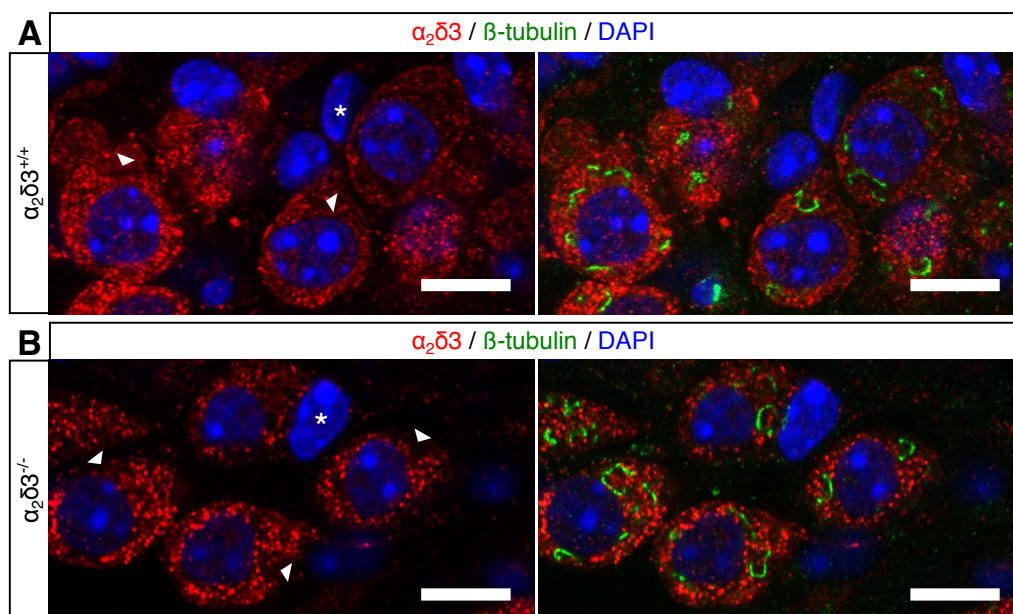
Figure 30. Immunoreactivity of $\alpha_2\delta3$ is not co-localized with GM130 immunolabeling
A,B, Immunolabeling for $\alpha_2\delta3$ (red; Antibody Alomone Cat.No.: ACC-103) resulted in an identical pattern in $\alpha_2\delta3^{+/+}$ and $\alpha_2\delta3^{-/-}$ mice, forming dots and clusters in the cytosol of SG neurons. GM130 labeling (green, right panels) did not overlap with labeling for $\alpha_2\delta3$, which is also indicated by the arrowheads in the left panels where no labeling for $\alpha_2\delta3$ was found at prominent GM130 expression sites. Satellite cells showed no staining for $\alpha_2\delta3$ and very sparse labeling for GM130. Nuclei were stained with DAPI (blue). Ethanol fixation; images represent single focal planes acquired using a confocal LSM with a 63x/1.4 NA oil objective, scale bar =10 μm.

A co-labeling of $\alpha_2\delta3$ and GM130 was done to test if the non-specific anti-$\alpha_2\delta3$ antibody labels part of the Golgi apparatus in $\alpha_2\delta3^{+/+}$ and $\alpha_2\delta3^{-/-}$. Again it was noticeable that the $\alpha_2\delta3$ labeling was somewhat different in the $\alpha_2\delta3$ wildtype compared to previous experiments (**Figs. 26, 28, 29**) and did not co-localized with GM 130.

In summary, four different anti-$\alpha_2\delta3$ antibodies from different companies were tested for their specificity. The binding regions of the antibodies were located behind exon 15 to exclude false-positive staining results in $\alpha_2\delta3^{-/-}$ mice. All tested antibodies were found to be non-specific for $\alpha_2\delta3$. Different approaches to improve antibody specificity by deglycosylation protocols failed. Further, the antibody from Alomone Laboratories used in a number of optimization experiments showed different labeling patterns varying from strong membrane and weak somatic labeling to lack of membrane labeling and pronounced somatic clusters in SG neurons although the tissue was treated always with the same procedure, i.e. using the same fixing chemical, incubation time and dilution. To our dismay, no specific labeling for $\alpha_2\delta3$ was achieved.

3.5   Morphology and yield of the dissociated spiral ganglion neuron culture

SG neurons were isolated and cultured as described in chapter 2.6. Because I established the technique of primary dissociated cultures of SG neurons newly in our laboratory, the cultures needed to be characterized morphologically before patch clamp experiments could be conducted (**Fig. 31**). There were different cell types present in the cultures that extended processes. To unequivocally identify SG neurons and to estimate their yield after mechanical and enzymatic isolation, cultured cells were fixed and labeled with anti-ß-tubulin, a specific marker for type I SG neurons (green), and anti-neurofilament 200 (NF 200), a specific marker for neurites (red); nuclei were stained with DAPI (blue) (**Fig. 31A**).
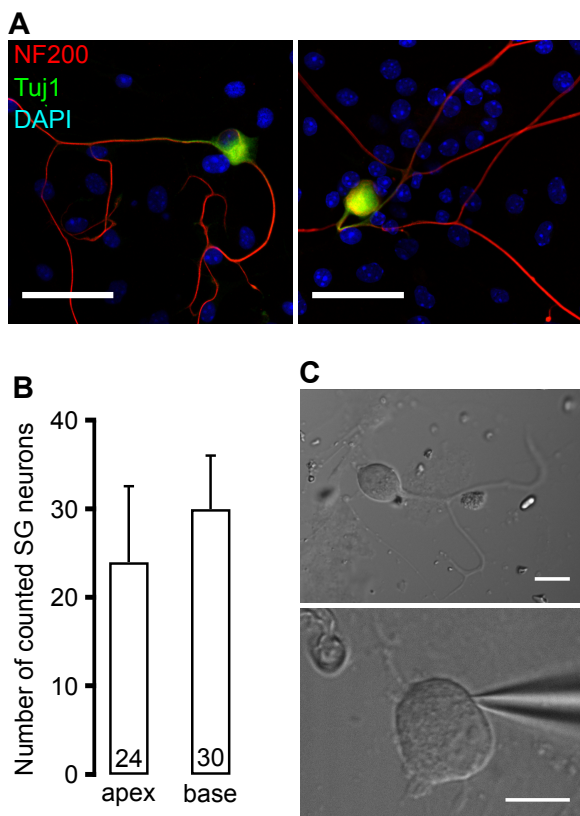
Figure 31. Morphology and yield of isolated SG neurons after 3 days in culture

A, Primary cultured, dissociated SG neurons isolated at P20 labeled for anti-ß-tubulin (green), anti-NF 200 (red) and DAPI (blue). Image on the left shows a bipolar SG neuron, the image on the right shows a monopolar SG neuron with branching neurites. Both morphologies are found predominantly in the culture. Images were taken using the confocal LSM 710 with 20x/0.8 NA objective; scale bar = 10 µm. **B,** Evaluation of the mean number ± S.D. of isolated SG neurons from 3 independent cultures. The number of SG neurons was counted for each coverslip containing SG neurons from either the apical half (apex) or the basal half (base) of the cochleae. **C,** Two examples images of isolated SG neurons before (upper image) and during (lower image) patch clamp recording. Scale bar: 10 µm. Images were taken using an upright microscope with DIC contrast (Olympus BX51WI, 40x/0.8 NA water objective).

In native tissue, SG neurons appear as bipolar neurons (Rusznák and Szucs, 2009). Dissection of the SG tissue, enzymatic digestion and mechanical isolation by trituration is a very stressful process, which kills many cells and can influence the morphology of isolated SG neurons. Type I SG neurons were identified based on the positive ß-tubulin labeling. In our culture, these cells had the largest cell bodies of all cells, were often lemon-shaped and appeared monopolar or bipolar (**Fig. 31A,C**) (Lv et al., 2012; Rusznák and Szucs, 2009). After 3 (P20 cultures) or 2 (P5 cultures) days in vitro (DIV), only a small proportion (< 5 %) of ß-Tubulin positive cells appeared multipolar or lacked any neurites. Because of their untypical morphology these cells were excluded for patch clamp recordings.

During the isolation process, the yield of neurons was estimated, by counting all ß-tubulin positive cells per coverslip. Figure 31B summarizes the counted SG neurons isolated from the apical and the basal region. A large number of cells was lost during the isolation process (Lv et al., 2012), resulting in the relative low number of isolated cells. The numbers given in Fig. 31B originate from early experiments in the establishment phase of the culture. Later the number of isolated SG neurons increased by approx. 1.5-2 fold for SG neurons isolated from the apex and by 2-2.5 fold for SG neurons isolated from the base. A quantitative evaluation of the number of isolated SG neurons by immunolabeling and counting was not repeated because isolated cells were exclusively used for patch clamp experiments.

3.6 Ca^{2+} current recordings in SG neurons from $\alpha_2\delta3^{+/+}$ and $\alpha_2\delta3^{-/-}$ mice aged P5

The recording of various currents from SG neurons represents a very difficult task since a myelin sheath, present as early as P0 makes direct recoding impossible (Wang et al., 2013). The myelin sheath surrounds 95 % of the total neuron population, making a dissociated SG neuron culture indispensable for patch clamp recordings. Today, two different techniques are commonly used to record from these cells. The first technique is the preparation of cultured whole-mount explants, the second is the preparation of dissociated SG neuron culture. This preparation allows the recording and analysis of single cells. For the dissociated culture of SG neurons, the cochlea was cut in the middle and separated into 2 parts referred to as apex and base.

$\alpha_2\delta3$ wildtype and knockout mice were analyzed before (P4-6; referred to as P5) the onset and after (P19-21; referred to as P20) the onset of hearing. Except for SNX-482; identical Ca^{2+} channel blocker concentrations have been used to isolated the fractions of the different Ca^{2+} currents (Lv et al., 2012). Here a concentration of 1µM SNX-482 instead of 200 nM was used to specifically block R-type currents, since it had been reported that some R-type currents were not fully blocked by concentrations between 200-500 nM.

For the recording of Ca^{2+} currents, cells were patched and a pulse protocol (chapter 2.9) was recorded three times under different conditions. First, cells were patched in B-49 (standard physiological solution with ~ 305 mOsmol, pH 7.34) to identify neurons by their characteristic Na^+ current. Na^+ and K^+ currents were suppressed by superfusing cells with application solution (B-58), which contained 113 mM NMDG and various K^+ channel blockers (30 mM TEA, 15 mM 4-AP and 2 mM Cs). The application solution was applied for 1 min to ensure the recording of pure Ca^{2+} currents. The same application solution was applied a 2nd time, now containing a specific Ca^{2+} channel blocker (**Tab. 18**). The 2nd application solution was also applied for 1 minute. The first part of the results describes the analysis of L-type and P/Q-type in cultured SG neurons isolated from $\alpha_2\delta3^{+/+}$ and $\alpha_2\delta3^{-/-}$ mice aged P5. The second part of the results describes the analysis of L-type, P/Q-type, N-type and R-type currents in cultured SG neurons isolated from P20 $\alpha_2\delta3^{+/+}$ and $\alpha_2\delta3^{-/-}$ mice.

3.6.1 Analysis of L-type currents in neonatal SG neurons

For the analysis of L-type currents, the isolated SG neurons were superfused with 10 µM nimodipine which is a specific Ca^{2+} channel blocker of L-type Ca^{2+} channels. For the analysis of Ca^{2+} currents in neonatal mice, tissue from 3 mice were isolated and separated into apex and base to identify possible differences between both groups in wildtype and knockout mice.

Figure 32 summarizes the analysis of L-type currents in SG neurons isolated from P5 $\alpha_2\delta3^{+/+}$ and $\alpha_2\delta3^{-/-}$ mice. The Ca^{2+} current was recorded without antagonist (control = ctrl) and during the application of 10 μM nimodipine (nimo). From each current trace, an I-V curve was generated in the last millisecond of the recording, used to determine the total I_{Ca}. Figure 32 C,D shows the effect of nimodipine application on SG neurons isolated from the apex and base of $\alpha_2\delta3^{+/+}$ and $\alpha_2\delta3^{-/-}$ mice. Finally, the portion of L-type current was calculated and compared between both genotypes (**Fig. 32E**).
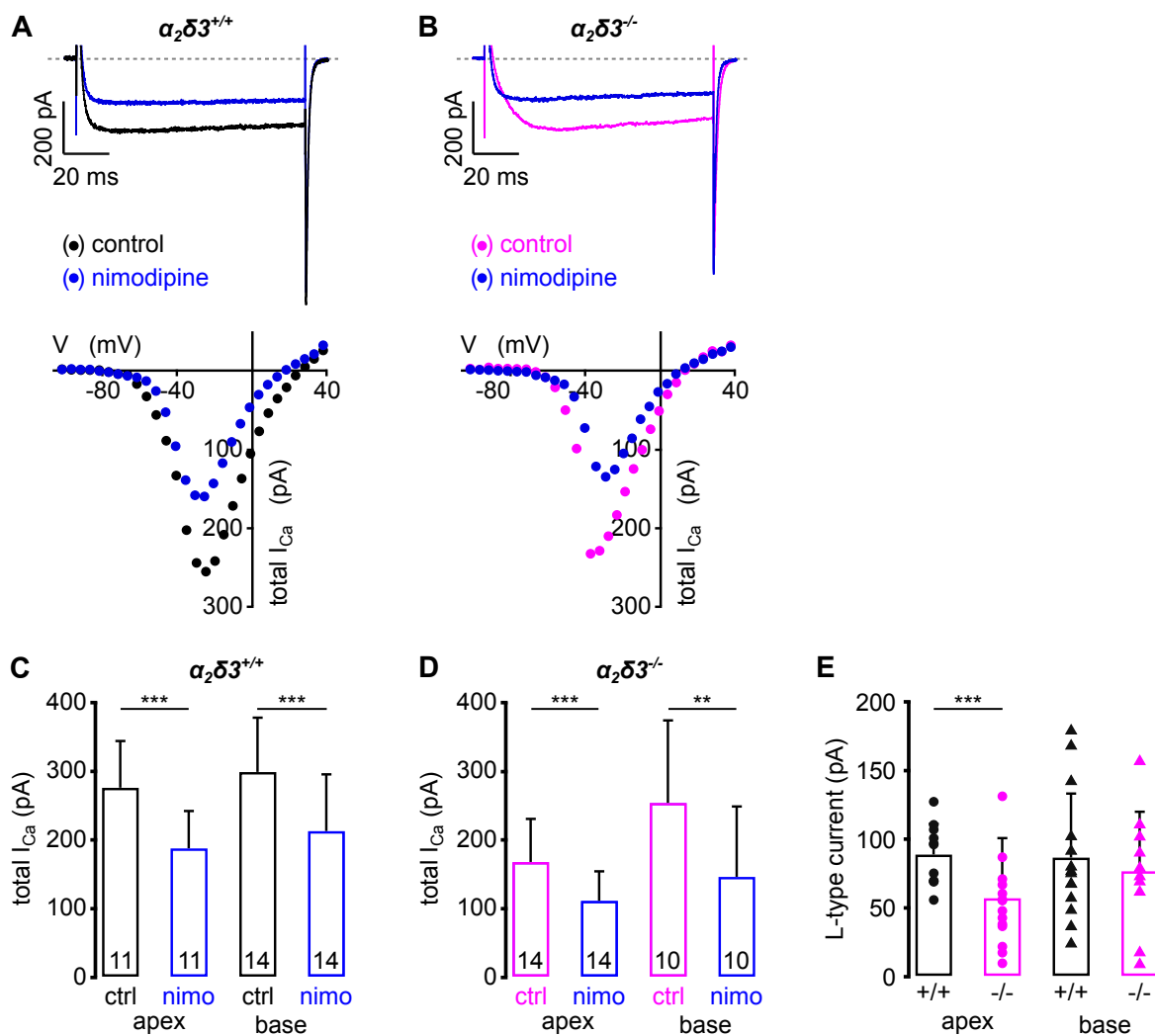
Figure 32. L-type currents were reduced in SG neurons isolated from the apical half of $\alpha_2\delta3^{-/-}$ mice aged P5

A,B, Whole cell patch clamp recordings of a P5 $\alpha_2\delta3^{+/+}$ (**A**) and $\alpha_2\delta3^{-/-}$ (**B**) SG neurons using 100 ms depolarizing voltage steps. Maximum I_{Ca} traces of a $\alpha_2\delta3^{+/+}$ (**A**) and $\alpha_2\delta3^{-/-}$ (**B**) before ($\alpha_2\delta3^{+/+}$: black; $\alpha_2\delta3^{-/-}$ magenta) and during the application of 10 uM nimodipine (blue). Corresponding steady-state I-V relations are shown below. Nimodipine (10 μM) blocked part of the total I_{Ca} in both genotypes. **C,D,** Average I_{Ca} (mean ± S.D.) and the effect of 10 μM nimodipine on SG neurons isolated from wildtype (**C**) and knockout (**D**) mice. The current reduced significantly in response to the blocker (**C,D**). The total I_{Ca} (ctrl) was reduced in SG neurons isolated from the apical turn of $\alpha_2\delta3^{-/-}$ mice (**D** apex) compared with SG neurons isolated from $\alpha_2\delta3^{+/+}$ mice (**C** apex). Statistic: Wilcoxon signed test *** p < 0.001, ** p < 0.01. **E,** Average contribution (mean ± S.D.) of the L-type current in SG neurons isolated from $\alpha_2\delta3^{+/+}$ and $\alpha_2\delta3^{-/-}$ mice. In neurons isolated from the apex, the current was significantly reduced in the $\alpha_2\delta3^{-/-}$ mice. The contribution of L-type currents was

unchanged in both genotypes of SG neurons isolated from the base. Numbers of cells are identical to the number of cells recorded in **C** and **D**. As statistical test the Wilcoxon rank test was used. *** p < 0.001

Nimodipine in a concentration of 10 µM specifically blocks L-type currents. The portion of L-type current was determined for each genotype by the subtraction of the blocked current from the total I_{Ca}. In the $\alpha_2\delta3$ wildtype, the total I_{Ca} was unchanged between neurons isolated from the apex or base of the cochlea (**Fig. 32C**). In both cochlear locations, the application of 10 µM nimodipine significantly reduced the current ($\alpha_2\delta3^{+/+}$ apex: ctrl 274 ± 68 pA, n = 11; nimo 186 ± 54 pA, n = 11; p = 0.001; base: ctrl 297 ± 78 pA n = 14, nimo 211 ± 82 pA; n= 14; p = 0.00012; **Fig. 32C**).

In the $\alpha_2\delta3$ knockout, the total I_{Ca} was reduced in neurons isolated from the apex (**Fig. 32D**) compared to neurons isolated from the apex of $\alpha_2\delta3$ wildtype mice (total I_{Ca} in $\alpha_2\delta3^{+/+}$ apex: 274 ± 68 pA; total I_{Ca} in $\alpha_2\delta3^{-/-}$ apex: 166 ± 62 pA). The total I_{Ca} recorded in neurons from the base of $\alpha_2\delta3$ knockout mice was similar to the wildtype.

Also in the $\alpha_2\delta3^{-/-}$, application of 10 µM nimodipine led to a significant reduction of the current ($\alpha_2\delta3^{-/-}$ apex: ctrl 166 ± 62 pA, n = 14; nimo 110 ± 42 pA, n = 14; p = 0.001; base: ctrl 252 ± 119 pA, n = 10; nimo 144 ± 102 pA, n = 10; p = 0.0019; **Fig. 32D**).

The L-type current was reduced in SG neurons isolated form $\alpha_2\delta3^{-/-}$ mice at P5 compared to $\alpha_2\delta3^{+/+}$ at the same age ($\alpha_2\delta3^{+/+}$ apex: 88 ± 22 pA; $\alpha_2\delta3^{-/-}$ apex: 56 ± 43 pA; p = 0.00102) but not for the base ($\alpha_2\delta3^{+/+}$ base: 86 ± 46 pA; $\alpha_2\delta3^{-/-}$ base: 76 ± 43 pA; p = 0.4091; **Fig. 32E**).

Noticeably, there was a tendency for increased L-type currents in SG neurons isolated from $\alpha_2\delta3^{-/-}$ mice aged P20 (**Fig. 35**), which was not found in neurons isolated from $\alpha_2\delta3^{-/-}$ mice at P5.

3.6.2 Analysis of P/Q-type currents in neonatal mice

P/Q-type currents belong to the group of HVA Ca^{2+} channels and are found at pre-synaptic sites of synapses, where they play an important role in neurotransmitter release and the coupling of neuronal excitation (Nimmrich and Gross, 2012b). The spider venom (from *Agelenopsis aperta*) ω-agatoxin IVA is a potent Ca^{2+} channel blocker and was used in a concentration of 1 µM to specifically block P/Q-type channels. Neurons were isolated and cultured as described previously. The portion of P/Q-type current was determined by the subtraction of the blocked current from the total I_{Ca}. The results are summarized in Figure 33.
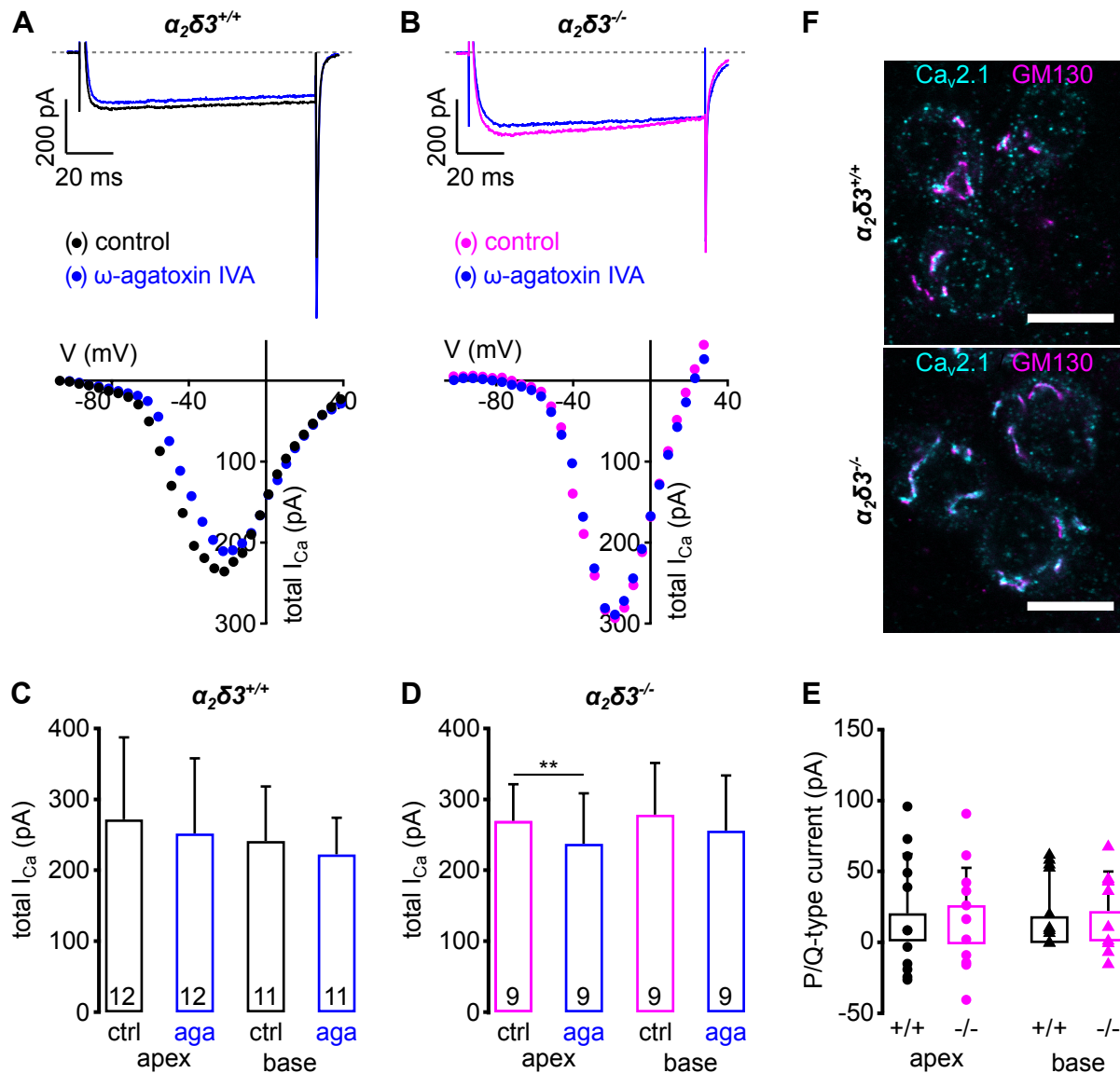
Figure 33. Only tiny P/Q-type currents are found in neonatal (P5) $\alpha_2\delta3^{+/+}$ and $\alpha_2\delta3^{-/-}$ mice

A,B, Whole cell patch clamp recordings of a P5 $\alpha_2\delta3^{+/+}$ (**A**) and $\alpha_2\delta3^{-/-}$ (**B**) SG neuron using 100 ms depolarizing voltage steps. Maximum I_{Ca} traces of a $\alpha_2\delta3^{+/+}$ (**A**) and $\alpha_2\delta3^{-/-}$ (**B**) SG neuron before ($\alpha_2\delta3^{+/+}$: black; $\alpha_2\delta3^{-/-}$ magenta) and during the application of 1 µM ω-agatoxin IVA (blue). Corresponding steady-state I-V relations are shown below. ω-agatoxin IVA (1 µM) blocked only a tiny part of the current in both genotypes. **C,D,** Average I_{Ca} (mean ± S.D.) and the effect of 1 µM ω-agatoxin IVA on SG neurons isolated from wildtype and knockout mice. The current showed no reduction in response to the blocker (**C**). In neurons isolated from the apex of $\alpha_2\delta3^{-/-}$ mice the current reduced significantly in response to the blocker (**D** apex). As statistical test the Wilcoxon signed test was used. ** $p < 0.01$. **E,** Comparison of the portion of P/Q-type currents between SG neurons isolated from the apex and base of $\alpha_2\delta3^{+/+}$ and $\alpha_2\delta3^{-/-}$ mice. In the wildtype P/Q-type currents make up approx. 20 - 30 pA in neurons isolated from the apex and base. Similar amounts of P/Q-type currents were found in the knockout. Numbers of cells are identical to the number of cells recorded in **C** and **D**. As statistical test the Wilcoxon rank test was used. No significant difference between the $\alpha_2\delta3$ wildtype and knockout was found. **F,** Immunolabeling of Ca$_v$2.1 (cyan) and GM130 kDa (magenta) in acutely isolated whole mount samples from $\alpha_2\delta3^{+/+}$ and $\alpha_2\delta3^{-/-}$ mice aged P5. In both genotypes, most of the Ca$_v$2.1 labeling was localized in the Golgi apparatus as determined via the Golgi specific marker GM130, resulting in a white overlay. Only a weak membrane labeling by Ca$_v$2.1 was found. Tissue was ethanol fixed and samples were acquired using a confocal LSM 710 with 63x/1.4 NA oil objective, scale bar = 10 µm. Images show a single optical plane.

The total I_{Ca} was unchanged between neurons isolated from the apex and base of $\alpha_2\delta3$ wildtype and knockout mice.

In the wildtype there was no significant reduction in response to the application of 1 µM ω-agatoxin IVA ($\alpha_2\delta3^{+/+}$ apex: ctrl 272 ± 115 pA, n = 12; aga 252 ± 105 pA, n = 12; p = 0.23; base: ctrl 241 ± 76 pA, n = 11, aga 222 ± 51 pA, n = 11; p = 0.17; **Fig. 33C**).

In the knockout the total I_{Ca} was unchanged between neurons isolated from the apex and base and only neurons isolated from the apex showed a significant reduction in response to the application of 1 µM ω-agatoxin IVA ($\alpha_2\delta3^{-/-}$ apex: ctrl 269 ± 51 pA, n = 9; aga 237 ± 71 pA, n = 9; p = 0.0078; base: ctrl 278 ± 72 pA, n = 9, aga 256 ± 77 pA, n = 9; p = 0.11; **Fig. 33D**). Analysis of the contribution of P/Q-type currents in wildtype and knockout mice revealed only tiny currents in both genotypes without significant difference ($\alpha_2\delta3^{+/+}$ apex: 19 ± 41 pA, $\alpha_2\delta3^{-/-}$ apex: 27 ± 26 pA, p = 0.1995; $\alpha_2\delta3^{+/+}$ base: 19 ± 38 pA, $\alpha_2\delta3^{-/-}$ base: 21 ± 27 pA, p = 0.365; **Fig. 33E**). Double immunolabeling on acutely isolated whole mount samples from $\alpha_2\delta3^{+/+}$ and $\alpha_2\delta3^{-/-}$ mice showed co-labeling of $Ca_v2.1$ (cyan) and GM130 (magenta) at the Golgi apparatus (white overlay; **Fig. 33F**). This could indicate that $Ca_v2.1$ channels are not yet expressed on the membrane but rather intracellular.

The data reveal that at neonatal ages P/Q-type channels are only present in a small number and are yet not fully up-regulated. This seems to be regardless of the presence of the $\alpha_2\delta3$ subunit.

3.6.3 Total I_{Ca} in neonatal $\alpha_2\delta3^{-/-}$ mice

VGCCs consist of several Ca^{2+} channel subtypes including LVA and HVA channels. In neonatal $\alpha_2\delta3^{+/+}$ and $\alpha_2\delta3^{-/-}$ mice, only L-type and P/Q-type currents were analyzed. For the comparison of the total I_{Ca} the recordings from the apex and base were taken together. Total I_{Ca}, was decreased in $\alpha_2\delta3^{-/-}$ mice compared based on the total amplitude and by histogram frequency distribution. The results are represented in Figure 34.
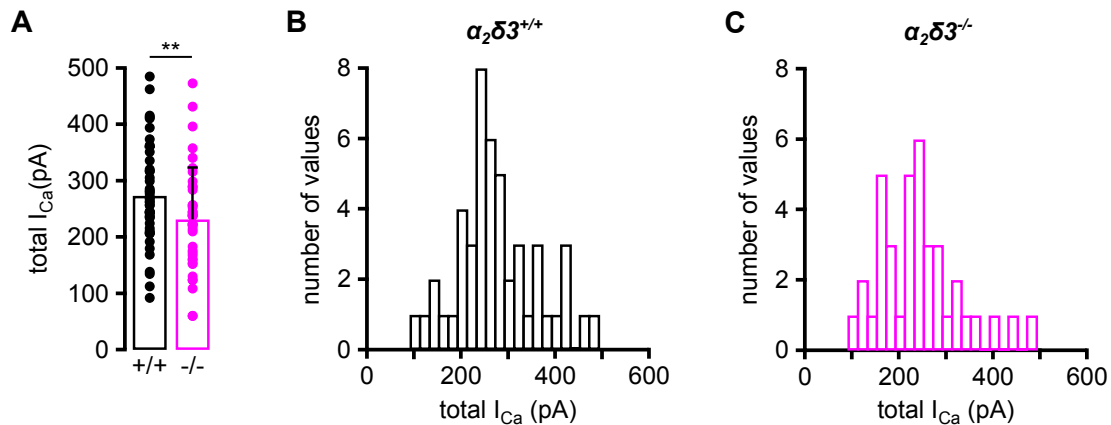
Figure 34. Isolated SG neurons from P5 – $\alpha_2\delta3^{+/+}$ and $\alpha_2\delta3^{-/-}$ mice showed a reduced total I_{Ca}
A, Average total $I_{Ca}\pm$ S.D. of SG neurons isolated from $\alpha_2\delta3^{-/-}$ mice were smaller compared to $\alpha_2\delta3^{+/+}$ mice (Wilcoxon rank test ** p < 0.01). **B,C,** Frequency distribution of I_{Ca} values for $\alpha_2\delta3^{+/+}$ and $\alpha_2\delta3^{-/-}$ SG neurons. Samples were grouped with a bin width of 20 pA, the number of values in those bins (events) are listed on the y-axis. Fewer events in the range of 250 pA were found in $\alpha_2\delta3^{-/-}$ SG neurons compared with $\alpha_2\delta3^{+/+}$. In total 48 SG neurons isolated from $\alpha_2\delta3^{+/+}$ mice and 42 SG neurons isolated from $\alpha_2\delta3^{-/-}$ mice were analyzed.

Total I_{Ca} was determined for $\alpha_2\delta3^{+/+}$ and $\alpha_2\delta3^{-/-}$ SG neurons in two experimental sets, i.e. in isolating L-type and P/Q type currents (shown in **Figs. 32, 33** as mean unblocked (ctrl) I_{Ca}). Total I_{Ca} was averaged for the two experimental groups for each cochlear location and compared between genotypes. In SG neurons isolated from $\alpha_2\delta3^{-/-}$ mice, the total I_{Ca} was significantly reduced as compared to the wildtype ($\alpha_2\delta3^{+/+}$: 273 ± 87 pA, n = 48; $\alpha_2\delta3^{-/-}$: 231 ± 92 pA, n = 40; p = 0.0115; **Fig. 34A**). Frequency distribution between both genotypes shows, that less neurons with an average I_{Ca} of ~ 250 pA are present in the $\alpha_2\delta3^{-/-}$ mice (**Fig. 34B, C**). However, it has to be considered, that the total I_{Ca} was smaller in neurons isolated from the apex of $\alpha_2\delta3^{-/-}$ mice and it cannot be excluded that this reduction leads to the significant difference between both genotypes. To unequivocally determine the Ca^{2+} current composition in both genotypes, N-type as well as R-type currents need to be determined in addition.

3.7 Ca^{2+} current recordings in SG neurons from $\alpha_2\delta3^{+/+}$ and $\alpha_2\delta3^{-/-}$ mice aged P20

Previous work by Pirone et al. showed a significant reduction of the number of immunopositive $Ca_v2.1$ puncta in the somata of SG neurons isolated from $\alpha_2\delta3^{-/-}$ versus $\alpha_2\delta3^{+/+}$ mice at 4-5 weeks of age (Pirone et al., 2014). This finding and the fact of impaired synaptic performance of the endbulb synapse suggested a reduction of P/Q-type currents in SG somata and at the endbulbs of Held in $\alpha_2\delta3^{-/-}$ mice (Pirone et al., 2014). Unfortunately, recording from the tiny endulbs in $\alpha_2\delta3^{-/-}$ mice is not feasible (personal communication with Dr. Taschenberger). Therefore we analyzed the expression of L-type, P/Q-type, N-type and R-

type Ca^{2+} channels in cultured SG neurons with patch clamp recordings and specific Ca^{2+} channel antagonists.

3.7.1 L-type currents of SG neurons isolated at P20

L-type currents were analyzed in SG neurons isolated from P20 day old $\alpha_2\delta3^{+/+}$ and $\alpha_2\delta3^{-/-}$ mice. For the isolation of L-type currents, isolated cells were superfused using 10 µM nimodipine and the portion of L-type current was determined by the subtraction of the blocked current from the total I_{Ca}. The results are summarized in Figure 35.
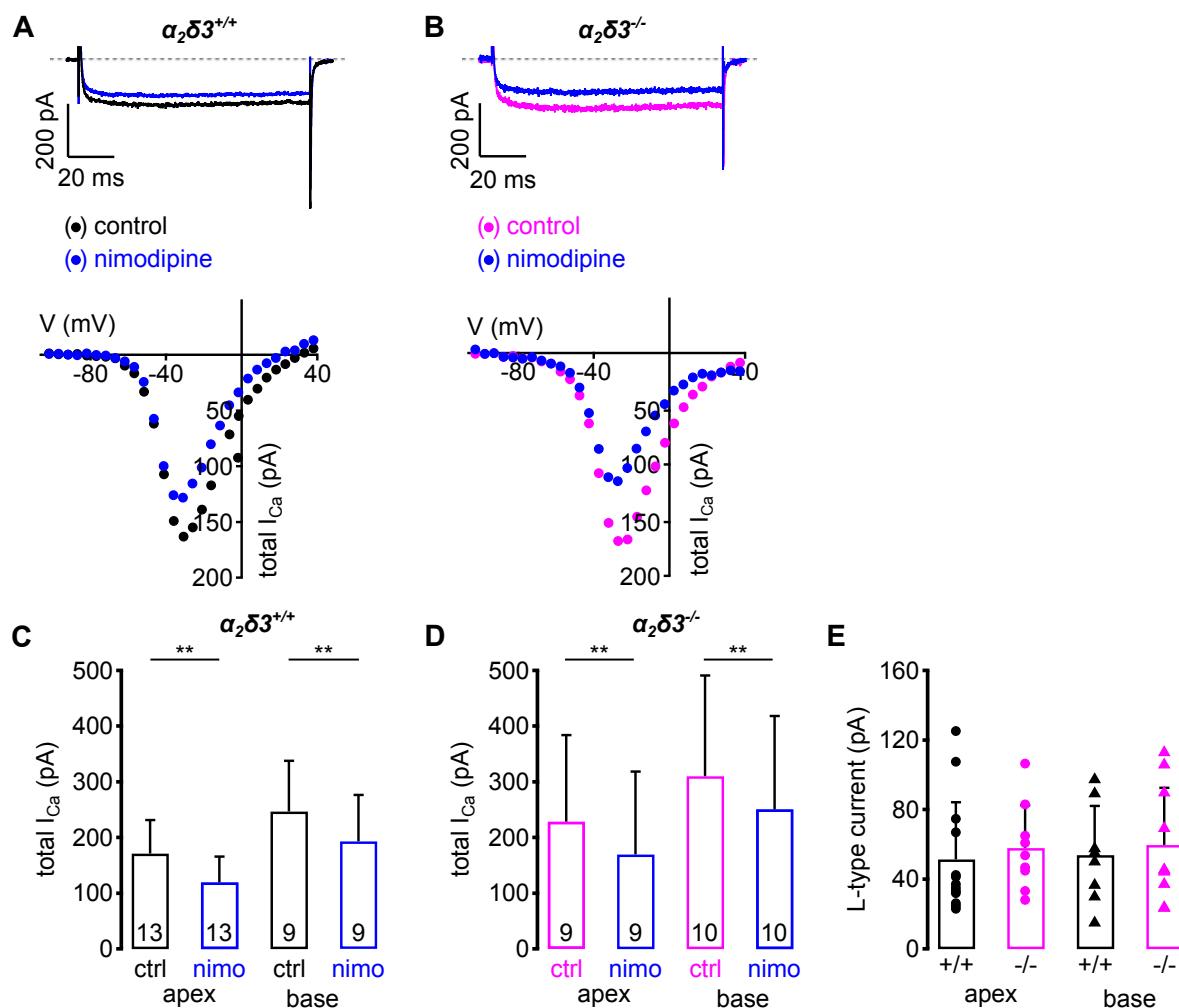
Figure 35. L-type Ca^{2+} currents in mature (P20) SG neurons were not affected by the deletion of $\alpha_2\delta3$
A,B, Whole-cell patch clamp recordings of I_{Ca} in a P20 $\alpha_2\delta3^{+/+}$ (black, **A**) and $\alpha_2\delta3^{-/-}$ (magenta, **B**) SG neuron in response to 100 ms depolarizing voltage steps. Maximum I_{Ca} traces of one example $\alpha_2\delta3^{+/+}$ (**A**) and $\alpha_2\delta3^{-/-}$ (**B**) SG neuron before ($\alpha_2\delta3^{+/+}$ black; $\alpha_2\delta3^{-/-}$ magenta) and during application of 10 µM nimodipine (blue). Corresponding steady-state current voltage relations are shown below. In both examples, application of 10 µM nimodipine blocked part of I_{Ca}. **C,D,** Average maximum I_{Ca} (mean ± S.D.) before (ctrl) and under superfusion of 10 µM nimodioine (nimo). Nimodipine significantly reduced I_{Ca} in SG neurons from both genotypes and cochlear locations, respectively (**C, D**). The number of neurons is indicated in the bars; Wilcoxon signed test, ** $p < 0.01$. **E,** Average contribution (mean ± S.D.) of L-type currents in SG neurons isolated from $\alpha_2\delta3^{+/+}$ and $\alpha_2\delta3^{-/-}$ mice. Statistical analysis performed using the Wilcoxon rank test. No significant difference was found

The total I_{Ca} was higher in SG neurons isolated from the apex and base of $\alpha_2\delta3^{-/-}$ mice compared to the wildtype ($\alpha_2\delta3^{+/+}$: apex, 171 ± 60 pA, n = 13; base, 246 ± 91 pA, n = 9; $\alpha_2\delta3^{-/-}$: apex, 228 ± 155 pA, n = 9; base, 310 ± 180 pA).

In the wildtype and the knockout, application of 10 µM nimodipine significantly reduced the current in SG neurons from both cochlear locations, respectively ($\alpha_2\delta3^{+/+}$ apex: ctrl 171 ± 60 pA, n = 13; nimo 119 ± 46 pA, n = 13; p = 0.0024; base, ctrl 246 ± 91 pA, n = 9; nimo 192 ± 83 pA, n = 9; p = 0.0078; $\alpha_2\delta3^{-/-}$ apex: ctrl 228 ± 155 pA, n = 9; nimo 170 ± 148 pA, n = 9; p = 0.0039; base, ctrl 310 ± 180 pA, n = 10; nimo 250 ± 167 pA, n = 10; p = 0.0019; **Fig. 35C, D**). The fractions of L-type currents were unchanged between both genotypes and cochlear locations ($\alpha_2\delta3^{+/+}$ apex: 51 ± 32 pA, n = 13; $\alpha_2\delta3^{-/-}$ apex: 58 ± 24 pA, n = 9; p = 0.15; $\alpha_2\delta3^{+/+}$ base: 53 ± 28 pA, n = 9; $\alpha_2\delta3^{-/-}$ base: 59 ± 32 pA, n = 10, p = 0.40; **Fig. 35E**).

3.7.2. P/Q-type currents of SG neurons isolated at P20

P/Q-type currents were analyzed in P20 day old $\alpha_2\delta3^{+/+}$ and $\alpha_2\delta3^{-/-}$ mice. They were pharmacologically isolated by superfusing isolated SG neurons with 1 µM ω-agatoxin IVA. The portion of P/Q-type current was determined by the subtraction of the blocked current from the total I_{Ca}. The results are pictured in Figure 36.
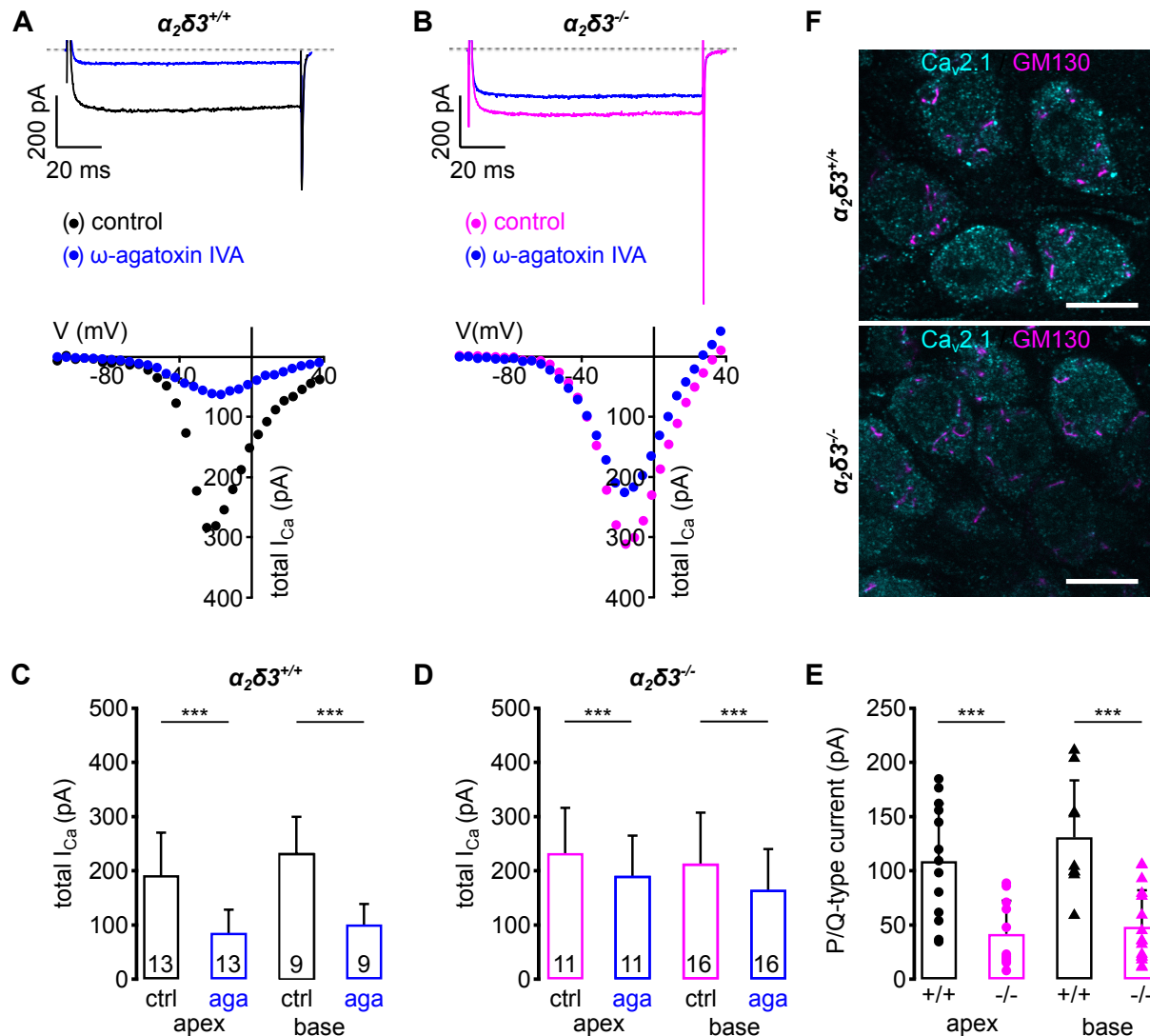
Figure 36. P/Q-type currents were severely reduced in SG neurons isolated from α₂δ3⁻/⁻ mice aged P20

A,B, Whole cell patch clamp recordings of a P20 $\alpha_2\delta3^{+/+}$ (**A**) and $\alpha_2\delta3^{-/-}$ (**B**) SG neurons using 100 ms depolarizing voltage steps. Maximum I_{Ca} traces of a $\alpha_2\delta3^{+/+}$ (**A**) and $\alpha_2\delta3^{-/-}$ (**B**) before ($\alpha_2\delta3^{+/+}$: black; $\alpha_2\delta3^{-/-}$ magenta) and during the application of 1 μM ω-agatoxin IVA (blue). Corresponding steady-state I-V relations are shown below. In the wildtype application of 1 μM ω-agatoxin IVA reduced the current by more than 60 % (**A**). In the knockout the response to the blocker was weaker (**B**). **C,D,** Average I_{Ca} (mean ± S.D.) and the effect of 1 μM ω-agatoxin IVA on SG neurons isolated from P20 $\alpha_2\delta3$ wildtype and knockout mice. In the wildtype, the current was significantly reduced in response to the blocker (**C**). In the knockout, neurons showed a significant reduction in response to the blocker, which was however weaker compared to the wildtype. As statistical test the Wilcoxon signed test was used. *** $p < 0.001$ **E,** Contribution of P/Q-type currents compared between neurons isolated from the apex and base of $\alpha_2\delta3^{+/+}$ and $\alpha_2\delta3^{-/-}$ mice. In neurons isolated from the wildtype, P/Q-type currents made up the majority of the current. In the knockout there was, a significant reduction in response to the blocker. As statistical comparison the Wilcoxon rank test was used. *** $p < 0.001$. **F,** Immunolabeling of $Ca_v2.1$ (cyan) and GM130 kDa (magenta) in acutely isolated whole mount samples from $\alpha_2\delta3^{+/+}$ and $\alpha_2\delta3^{-/-}$ mice aged P20. Wildtype SG neurons showed a strong soma and membrane labeling of $Ca_v2.1$ (cyan) and no co-labelling with GM130 (magenta). Reduced $Ca_v2.1$ labeling in the knockout. Tissue was ethanol fixed and samples were acquired using a confocal LSM 710 with 63x/1.4 NA oil objective, scale bar 10 um. Single optical slices are shown.

Application of 1 μM ω-agatoxin IVA strongly reduced the total I_{Ca} in SG neurons isolated from the apical and basal part of $\alpha_2\delta3^{+/+}$ mice, as shown for the maximum I_{Ca} traces and the respective I/V-curves (**Fig. 36A**).

In $\alpha_2\delta3^{+/+}$ mice, ω-agatoxin IVA blocked on average 50-55 % of the total I_{Ca} from apical and basal SG neurons, respectively (apex: ctrl 192 ± 78 pA, n = 13; aga 85 ± 42 pA, n = 13, p = 0.0007; base: ctrl 233 ± 66 pA, n = 9; aga 101 ± 37 pA, n = 9; p = 0.00018; **Fig. 36A, C**).

In $\alpha_2\delta3^{-/-}$ mice, the current reduction in response to ω-agatoxin IVA (1 μM) was much weaker, but still significant (apex: ctrl 233 ± 83 pA, n = 11; aga 191 ± 73 pA, n = 11; p = 0.0009; base: ctrl 213 ± 93 pA, n = 16; aga 165 ± 75 pA, n = 16; p = 0.0003; **Fig. 36B, D**).

The fraction of P/Q-type currents was determined for both genotypes by subtraction of the current after application of the blocker from the total I_{Ca}. In the wildtype, P/Q-type currents make up the majority of the total I_{Ca} ($\alpha_2\delta3^{+/+}$ apex: 109 ± 53 pA and base: 131 ± 52 pA). The knockout of $\alpha_2\delta3$ significantly reduced the expression of P/Q-type currents ($\alpha_2\delta3^{-/-}$: apex: 41 ± 30 pA, p = 0.00090 and base: 48 ± 33 pA, p = 0.00022; being equivalent to 20 – 21 % of the wildtype current). Our data show that normal P/Q-type current amplitudes require the presence of the auxiliary subunit $\alpha_2\delta3$ and its deletion severely affect the expression of P/Q-type currents (**Fig. 36E**). Co-labeling of $Ca_v2.1$ and GM130, showed a clear membrane labeling in SG neurons isolated from $\alpha_2\delta3^{+/+}$ mice (**Fig. 36F** upper image). The labeling was weaker in SG neurons isolated from $\alpha_2\delta3^{-/-}$ mice (**Fig. 36F** lower image) and no co-localization with GM130 was found in both genotypes.

3.7.3   N-type currents of SG neurons isolated at P20

For the isolation of N-type currents, two different toxins from the group of conotoxins were used. N-type currents were isolated using 1 μM ω-conotoxin MVIIa or GVIa. Because both blockers are highly effective and specific at this concentration (Ramírez et al., 2017) and the responses to both conotoxins were similar using both blockers, the data were combined for the analysis and are referred to as conotoxin or cono (**Fig. 37**).
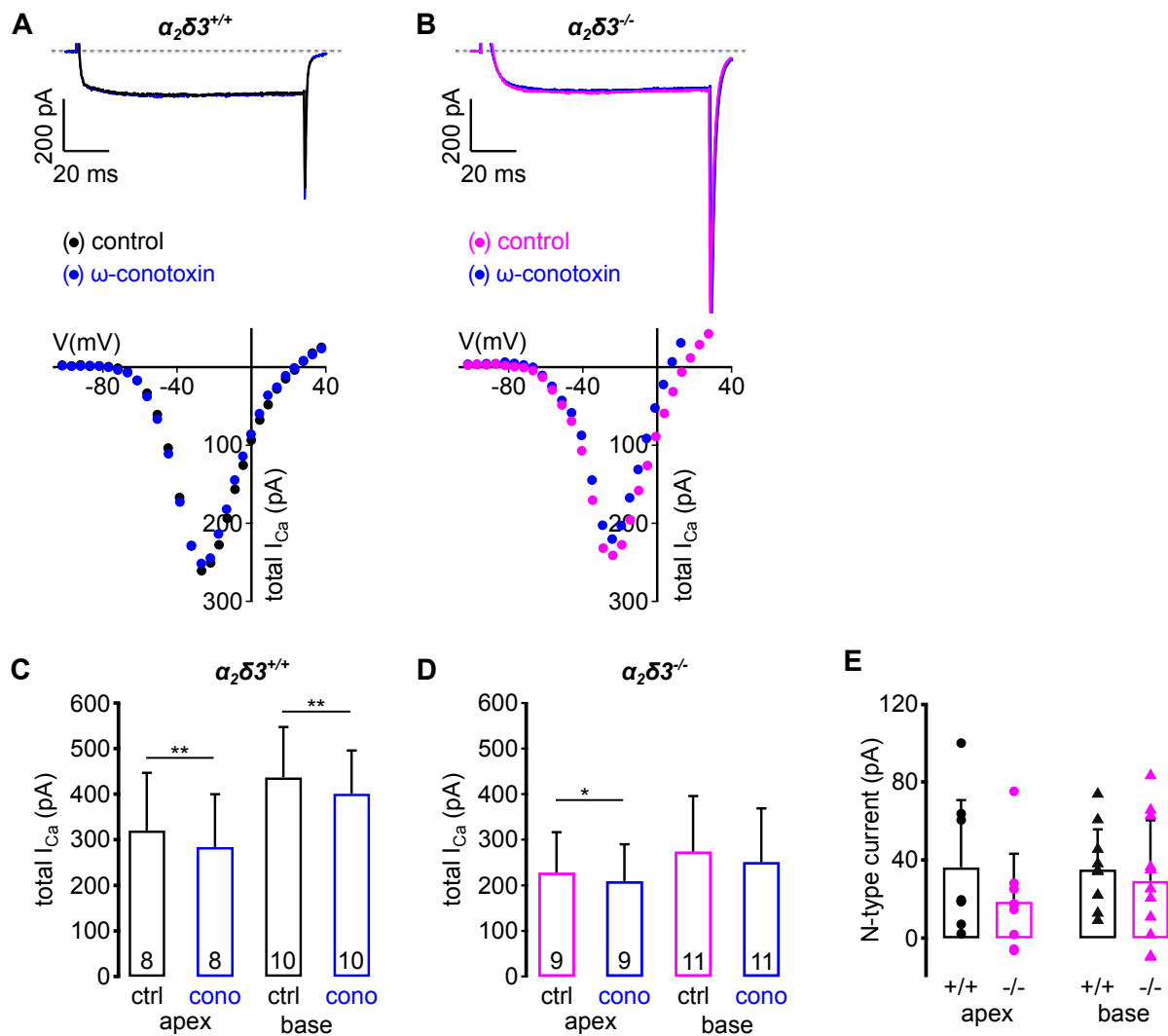
Figure 37. N-type currents in SG neurons of mice aged P20 were small and not affected by the deletion of α₂δ3

A,B, Whole cell patch clamp recordings of a P20 $\alpha_2\delta3^{+/+}$ (A) and $\alpha_2\delta3^{-/-}$ (B) SG neurons using 100 ms depolarizing voltage steps. Maximum I_{Ca} traces of a $\alpha_2\delta3^{+/+}$ (A) and $\alpha_2\delta3^{-/-}$ (B) before ($\alpha_2\delta3^{+/+}$: black; $\alpha_2\delta3^{-/-}$: magenta) and during the application of 1 μM ω-conotoxin (blue). Corresponding steady-state I-V relations are shown below. In both genotypes, I_{Ca} showed a minimal reduction under the superfusion with 1 μM ω-conotoxin (A,B). C,D, Average I_{Ca} (mean ± S.D.) and the effect of 1 μM ω-conotoxin on SG neurons isolated from P20 $\alpha_2\delta3$ wildtype and knockout mice. I_{Ca} showed a small but significant reduction in response to ω - conotoxin in SG neurons from the apex and base of $\alpha_2\delta3^{+/+}$ mice and from SG neurons isolated from the apex of $\alpha_2\delta3^{-/-}$ mice. As statistical test the Wilcoxon signed test was used. ** $p < 0.01$, * $p < 0.05$ E, Average contribution of N-type currents (mean ± S.D.) compared between neurons isolated from the apex and base of $\alpha_2\delta3^{+/+}$ and $\alpha_2\delta3^{-/-}$ mice. There was no significant difference between the genotypes for the same cochlear location. As statistical comparison the Wilcoxon rank test was used.

For unknown reasons, the mean total I_{Ca} recorded in neurons isolated from the base of $\alpha_2\delta3^{+/+}$ mice was unusually high ($\alpha_2\delta3^{+/+}$ base: 437 ± 110 pA) when compared to the total I_{Ca} recorded from neurons isolated from the apex of apical SG neurons ($\alpha_2\delta3^{+/+}$ apex: 320 ± 89 pA) and the total I_{Ca} recorded from basal SG neurons shown in Fig. 35 (L-type currents, total I_{Ca}: 246 ± 91 pA) and Fig. 36 (P/Q-type currents, I_{Ca}: 233 ± 66 pA).

We assume that this reflects the rather high variability of neurons in our culture. In the wildtype, the data showed a small but significant reduction of the current in response to the application of 1 μM ω-conotoxin ($\alpha_2\delta3^{+/+}$ apex: ctrl 320 ± 126 pA, n = 8, cono 284 ± 115 pA, n = 8; p = 0.0078; base: ctrl 437 ± 110 pA, n = 10, cono 401 ± 94 pA, n = 10; p = 0.0019; **Fig. 37C**)).

In the $\alpha_2\delta3$ knockout, the total I_{Ca} had the same amplitude as recorded formerly (**Fig. 37D**). The current was reduced only slightly in response to the blocker and the reduction was only significant for neurons isolated from the apex of $\alpha_2\delta3^{-/-}$ mice ($\alpha_2\delta3^{-/-}$ apex: ctrl 228 ± 88 pA, n = 9, cono 209 ± 80 pA, n = 9; p = 0.039; base: ctrl 274 ± 121 pA, n = 11, cono 251 ± 118 pA, n = 11; p = 0.067).

The analysis of the contribution of N-type currents showed no significant difference between neurons that were isolated from the apex or base of $\alpha_2\delta3^{+/+}$ and $\alpha_2\delta3^{-/-}$ mice for both cochlear locations ($\alpha_2\delta3^{+/+}$ apex: 36 ± 34 pA, n = 8; $\alpha_2\delta3^{-/-}$ apex: 18 ± 24 pA, n = 9; p = 0.108; $\alpha_2\delta3^{+/+}$ base: 35 ± 20 pA, n = 10; $\alpha_2\delta3^{-/-}$ base: 29 ± 31 pA, n = 11, p = 0.339; **Fig. 37E**). The data indicate that on average N-type currents in SG neurons of our preparation are equally small in both genotypes and that they are (i) not affected by the deletion of $\alpha_2\delta3$ (ii) nor compensate for the loss of P/Q-type channels in the $\alpha_2\delta3^{-/-}$ mice.

3.7.4 R-type currents of SG neurons isolated at P20

R-type channels can be specifically blocked by SNX-482, a peptide isolated from *Hysterocrates gigas* (Newcomb et al. 2000). Here SG neurons from $\alpha_2\delta3$ wildtype and knockout mice were isolated at P20 and cultured as previously described (chapter 2.6). SNX-482 (1 μM) was applied to specifically isolate R-type currents. The portion of R-type current was determined by the subtraction of the blocked current from the total I_{Ca}. The results are summarized in Fig. 38.
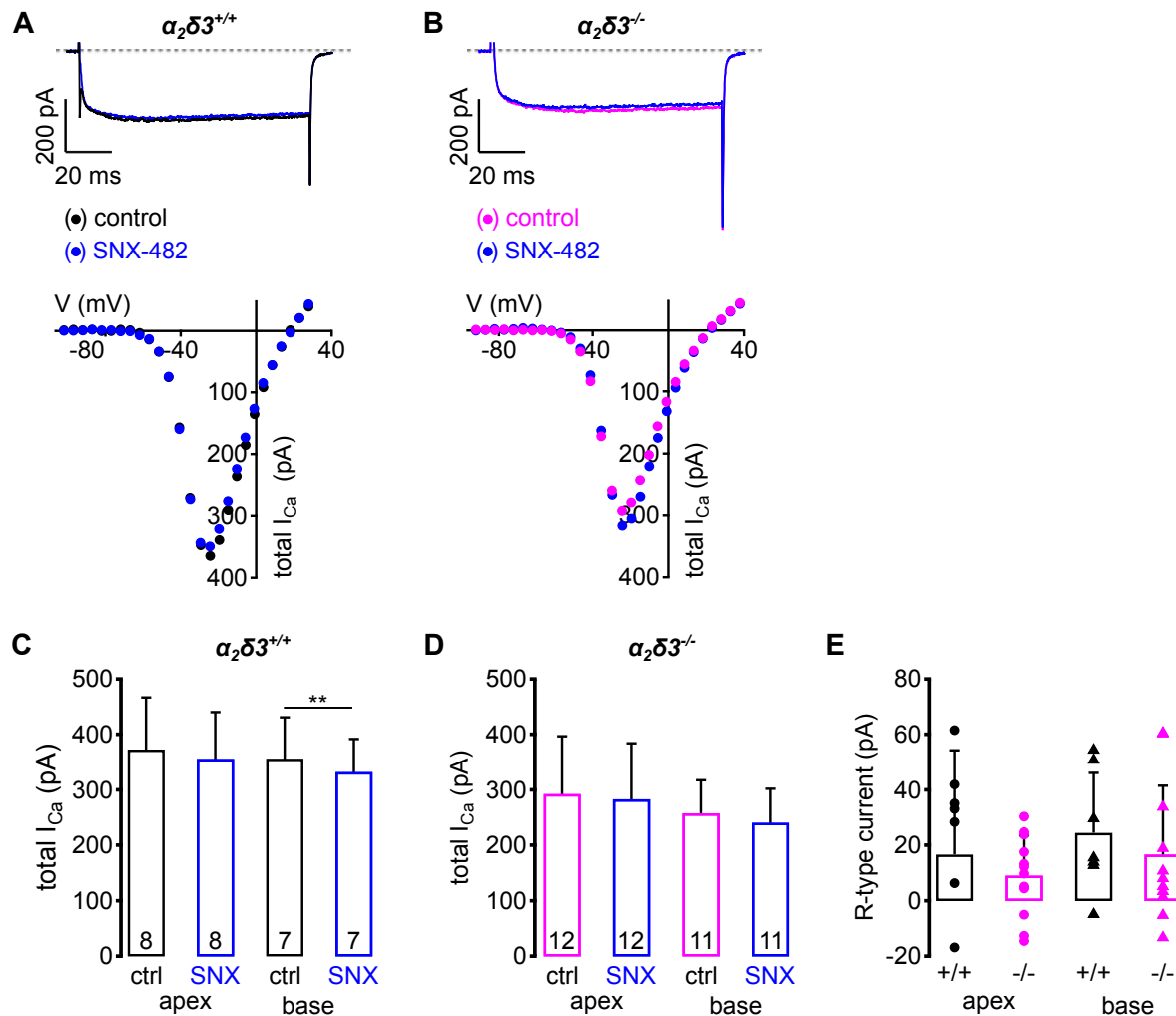
Figure 38. R-type currents in SG neurons of mice aged P20 are not affected by the deletion of α₂δ3

A,B, Whole cell patch clamp recordings of a P20 $\alpha_2\delta3^{+/+}$ (**A**) and $\alpha_2\delta3^{-/-}$ (**B**) SG neurons using 100 ms depolarizing voltage steps. Maximum I_{Ca} traces of a $\alpha_2\delta3^{+/+}$ (**A**) and $\alpha_2\delta3^{-/-}$ (**B**) before ($\alpha_2\delta3^{+/+}$: black; $\alpha_2\delta3^{-/-}$: magenta) and during the application of 1 μM SNX-482 (blue). Corresponding steady-state I-V relations are shown below. In both genotypes, I_{Ca} showed a minimal reduction under the superfusion with 1 μM SNX-482 (**A,B**). **C,D,** Average I_{Ca} (mean ± S.D.) and the effect of 1 μM SNX-482 on SG neurons isolated from P20 $\alpha_2\delta3$ wildtype and knockout mice. The current showed a tendency of reduction in response to the blocker, which is significant for neurons isolated from the base of $\alpha_2\delta3^{+/+}$ mice. As statistical test the Wilcoxon signed test was used. ** $p < 0.01$ **E.** Average contribution of R-type currents (mean ± S.D.) compared between neurons isolated from the apex and base of $\alpha_2\delta3^{+/+}$ and $\alpha_2\delta3^{-/-}$ mice. There was no significant difference between the genotypes for the same cochlear location. As statistical comparison the Wilcoxon rank test was used.

The total I_{Ca} was slightly higher in neurons isolated from $\alpha_2\delta3^{+/+}$ mice compared to the knockout. Nevertheless, the response to the blocker was very weak both in the wildtype (**Fig. 38A,C**) and in the knockout (**Fig. 38B,D**).

In both genotypes and cochlear locations, only tiny R-type currents were found ($\alpha_2\delta3^{+/+}$: apex, 16 ± 37 pA, n = 8; $\alpha_2\delta3^{-/-}$: apex, 9 ± 14 pA, n = 12; $p = 0.11$; $\alpha_2\delta3^{+/+}$: base, 24 ± 12 pA, n = 7; $\alpha_2\delta3^{-/-}$: base, 16 ± 24 pA, n = 11; $p = 0.18$; **Fig. 38E**). No significant difference was found

between both genotypes for the respective cochlear locations. This shows, that R-type currents do not compensate for the loss of P/Q-type currents in $\alpha_2\delta3^{-/-}$ mice.

3.7.5 The composition of Ca²⁺ currents is changed in $\alpha_2\delta3^{-/-}$ mice

Following the pharmacological isolation of HVA Ca²⁺ currents, namely L-, N-, P/Q- and R-type currents, the Ca²⁺ current composition was analyzed in mature SG neurons of $\alpha_2\delta3$ wildtype and knockout mice. Here, the HVA Ca²⁺ channels are of main interest because their α_1 pore is associated with an auxiliary subunit $\alpha_2\delta$, in contrast to LVA (T-type) channels (Dolphin, 2013a). For the comparison of the Ca²⁺ current composition, I_{Ca} values for apex and base were summarized because there was no difference in L-, N-, P/Q- and R-type current components between SG neurons from the apical or the basal cochlea for both genotypes, respectively (**Figs. 35 – 38**). Similarly, in order to determine the average total I_{Ca} the data from neurons isolated from the apex and base were summarized. The results are depicted in Fig. 39 below.
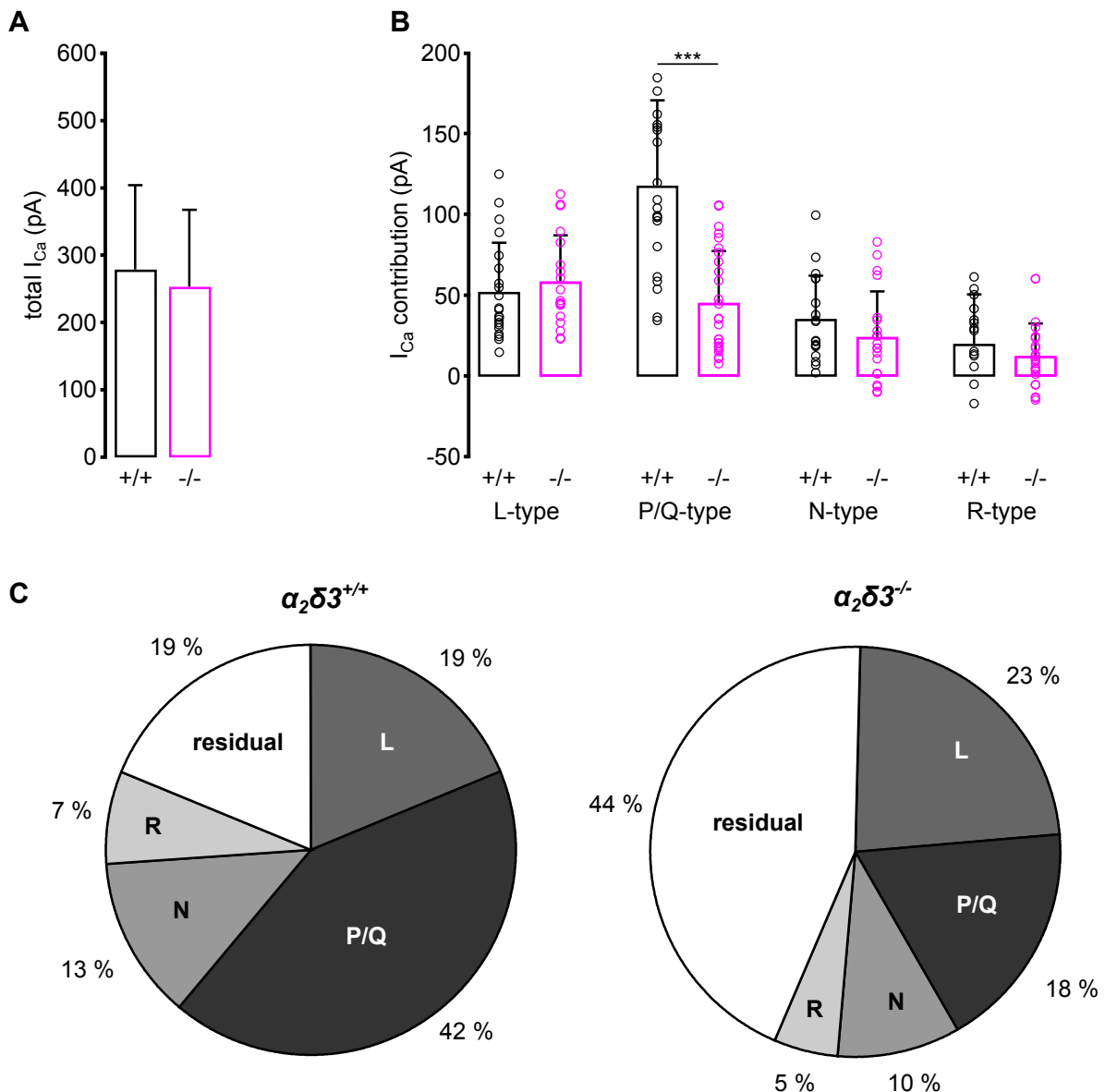
Figure 39. The composition of Ca^{2+} currents rather than the total I_{Ca} is affected by the deletion of α$_2$δ3
A, The total I_{Ca} (mean ± S.D.) was not different between neurons isolated from α$_2$δ3$^{+/+}$ and α$_2$δ3$^{-/-}$ mice. In total 75 wildtype and 89 knockout SG neurons were analyze. As statistical test the Wilcoxon rank test was used. **B,** Sizes of the different Ca^{2+} current types for α$_2$δ3$^{+/+}$ and α$_2$δ3$^{-/-}$ mice. L-, N- and R-type currents showed similar contribution to the total I_{Ca} in both genotypes. Only P/Q-type currents, which make up the majority of the total I_{Ca} current in mature wildtype SG neurons, were significantly reduced in α$_2$δ3$^{-/-}$ mice. Number of cells for L-type currents are: 21 WT and 19 KO, P/Q-type currents are: 21 WT and 27 KO, N-type currents are: 18 WT and 20 KO and for R-type currents are: 15 WT and 23 KO. As statistical test the Wilcoxon rank test was used. *** p < 0.001. **C,** Pie diagram showing the fraction of the different Ca^{2+} currents and a residual current as percentage of the total I_{Ca}. With 42 % P/Q-type currents are the main Ca^{2+} current type in mature SG neurons. A residual current of 19 % remained unblocked. In the knockout, P/Q type currents were significantly reduced and a residual current of 44 % remained.

Average total I_{Ca} of SG neurons isolated from α$_2$δ3$^{+/+}$ and α$_2$δ3$^{-/-}$ mice showed no significant difference (α$_2$δ3$^{+/+}$: 279 ± 125 pA; α$_2$δ3$^{-/-}$: 253 ± 114 pA; *p* = 0.0876; **Fig. 39A**). Even though the total I_{Ca} of SG neurons was unchanged between both genotypes, the composition of the

current mixture was different (**Fig. 39B**). In wildtype SG neurons, P/Q-type currents are the main Ca^{2+} current component amounting to 42 %, whereas in the knockout the deletion of $\alpha_2\delta3$ reduced the P/Q-type current to 18 % ($\alpha_2\delta3^{+/+}$: 118 ± 53 pA; $\alpha_2\delta3^{-/-}$: 46 ± 32 pA; p = 5.3367*10^{-7}; **Fig. 39B**). In $\alpha_2\delta3^{-/-}$ SG neurons, P/Q-type currents were significantly reduced whereas L-type, N-type and R-type currents were not affected by deletion of $\alpha_2\delta3$ (**Fig. 39B, C**). In both genotypes, a residual current remained, which was not blocked by nimoidipine, ω-agatoxin IVA, ω-conotoxin and SNX-482. Because of the large reduction of the P/Q-type current in $\alpha_2\delta3^{-/-}$ mice, the residual current was larger here (**Fig. 39C right**). The compensatory mechanism was not identified and is so far of unknown origin.

3.8 Effect of α₂δ2 and α₂δ3 deletion on the developing endbulb of Held synapse

Axon terminals of SG neurons project onto bushy cells located in the anteroventral cochlear nucleus, where they form the endbulb of Held synapse. The auditory nerve fiber terminals also called boutons grow in size and shape during development of the mice and are fully matured at 9 weeks of age (Limb and Ryugo, 2000). Recently Pirone et al. analyzed the $\alpha_2\delta3^{-/-}$ mouse and found an auditory processing deficit in these mice (Pirone et al., 2014). They found significantly less P/Q-type channels on the soma of SG neurons. Furthermore they could show that the endbulb of Held synapses are malformed in $\alpha_2\delta3^{-/-}$ mice, harboring less post-synaptic densities and less intercellular cisterns. Here the endbulb of Held synapse was analyzed in pre-hearing (P7) and hearing (P20) mice. Therefore I established brain cryosections in our lab that enabled us to investigate the endbulb of Held synapse at both ages. For the analysis of the endbulb of Held synapse, I prepared brain cryosections from the AVCN as described formerly (2.7). From work of Lin et al. it is known that around P9 – 11, more than 70 % of the Ca^{2+} channels are of P/Q-type (Lin et al., 2011). Our motivation was to analyze the effect of α₂δ3 deletion at the endbulb of Held synapse before up-regulation of P/Q-type channels and later when P/Q-type channels are expressed. We aimed to analyze mice at the same age (P5) as we used for the preparation of the SG neurons culture, however isolation of the neonatal mouse brain is very difficult and the cochlear nuclear complex is a very fragile structure, we used mice at the age of P7 where we were able to isolate the whole mouse brain.

The aim of the experiments was to:

1. Analyze the endbulb of Held synapse at P7 and P20 which respect to bouton number and size of VGLUT1-labeled area

2. Figure out if the deletion of α₂δ3 affects synapse development even before the onset of hearing and up-regulation of P/Q-type Ca^{2+} channels

3.8.1 Analysis of the endbulb of Held in pre-hearing and hearing $\alpha_2\delta3^{-/-}$ mice

The endbulb of Held synapse is formed by nerve endings of SG neurons, which form axosomatic contact with bushy cells (BC). Bushy cells are located within the AVCN, which is part of the CNC. Figure 40A shows schematically the connection between hair cells and the BCs in the AVCN. Afferent endings of the SG neurons form in the cochlea, the inner hair cell ribbon-synapse. In the cochlea, nerve fibers bundle to form the 8th cranial nerve, which projects towards the cochlear nucleus. Axon terminal of SG neurons project onto bushy cells located at the AVCN and form the endbulb of Held synapse. Bushy cells were analyzed for

the largest perimeter as described previously. The number of boutons and the VGLUT1-labeled area were analyzed, the results are summarized below (**Fig. 40**).
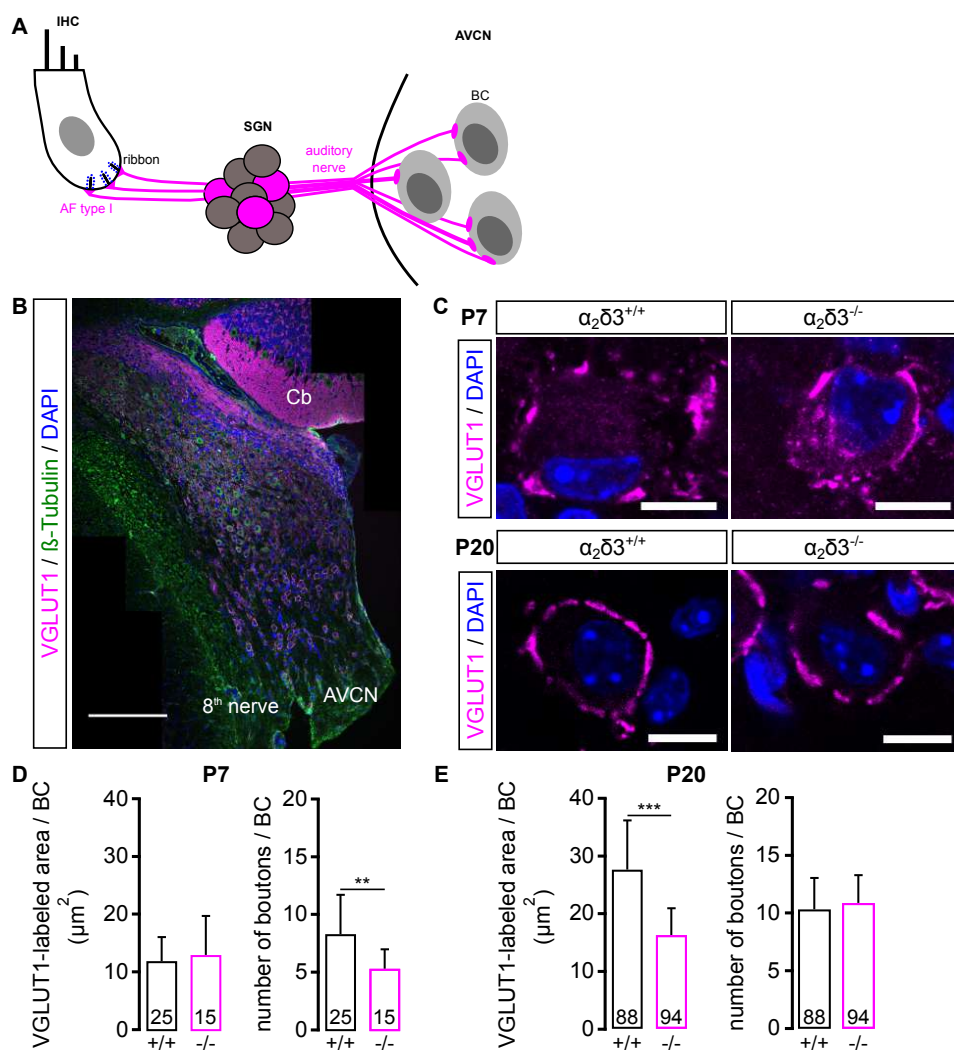
Figure 40. Analysis of the endbulb of Held synapse in $\alpha_2\delta3^{-/-}$ mice at P7 and P20

A, Schematic drawing showing the connections between the cochlea, SG neuron neurons and the AVCN. Type I SG neurons make a precise one to one connection to inner hair cells. In total one inner hair cell receives afferent innervation from 12 - 15 type I neurons. For clearness only 3 SG neurons (red) are shown that contact one inner hair cell. The processes of the SG neurons bundle and form the auditory nerve (8th nerve), which project to the cochlear nuclear complex (CNC), where nerve fibers branche and make synaptic contacts to bushy cells (BC). **B,** Coronal brain slice of the CNC showing the AVCN labeled with VGLUT1, ß-tubulin and DAPI. The slice was labeled using ß-tubulin as neuronal marker, VGLUT1 to label the ANF terminals and DAPI to stain the nuclei. Slice thickness 30 µm, scale bar: 200 µm. Images represent single optical slices, acquired using a 20x/0.8 NA objective. The single optical images were stitched to one overview image using Fiji. **C,** Examples of one bushy cell from P7 and P20 wildtype (C; left) and knockout mice (C; right). The largest perimeter of the cell is shown. From this the VGLUT1-labeled area and the number of boutons per bushy cell (BC) were determined. Scale bar 10 µm. Images were taken using a confocal LSM 710 with a 63x/1.4 NA oil objective **D,** Analysis of the VGLUT1-labeled area and the number of boutons at P7. The average ± S.D. is shown in each graph. At P7 a significant reduction in the number of boutons was found (p < 0.001723 (**)). No significant difference regarding the VGLUT1-labeled area (p > 0.3546 (ns)). **E,** Analysis of the VGLUT1-labeled area and the number of boutons at P20. The average ± S.D. is shown in each graph. At P20, the VGLUT1-labeled area was significantly reduced compared to the wildtype (p < $6.9 * 10^{-10}$ (***)). The

97

number of boutons per bushy cell was unchanged in both genotypes (p > 0.14372 (ns)). Statistical analysis (D and E) was done using the Wilcoxon Rank test *** p < 0.001, ** < 0.01 ± S.D. In total 3 genotypes from each age group were analyzed.

The data show that in $\alpha_2\delta3^{-/-}$ mice aged P7, the number of boutons per bushy cell was significantly reduced compared to their wildtype siblings. An average of 5 boutons was found in the knockout compared to 8 boutons in wildtype. However, the VGLUT1-labeled area was unchanged between both genotypes. This indicates that the single boutons must be bigger in the $\alpha_2\delta3$ knockout compared to the wildtype in order to balance the VGLUT1-labeled area. This indicates that $\alpha_2\delta3$ is important even before the onset of hearing and the massive up-regulation of P/Q-type Ca^{2+} channels. At P20 the number of boutons per bushy cells was unchanged between both genotypes ($\alpha_2\delta3^{+/+}$: 10.33 ± 2.71, $\alpha_2\delta3^{-/-}$: 10.90 ± 2.49; p = 0.14), whereas the VGLUT1 labeled area was significantly reduced in the $\alpha_2\delta3$ knockout ($\alpha_2\delta3^{+/+}$: 27.55 ± 8.51 μm^2 (n = 88), $\alpha_2\delta3^{-/-}$: 16.22 ± 4.6 μm^2; p = 6.07*10^{-11} (n = 94)). These findings are in accordance with the data published by Pirone et al. (2014). The following scheme illustrates the relationship between P/Q-type expression presence or absence of $\alpha_2\delta3$ (**Fig. 41**).
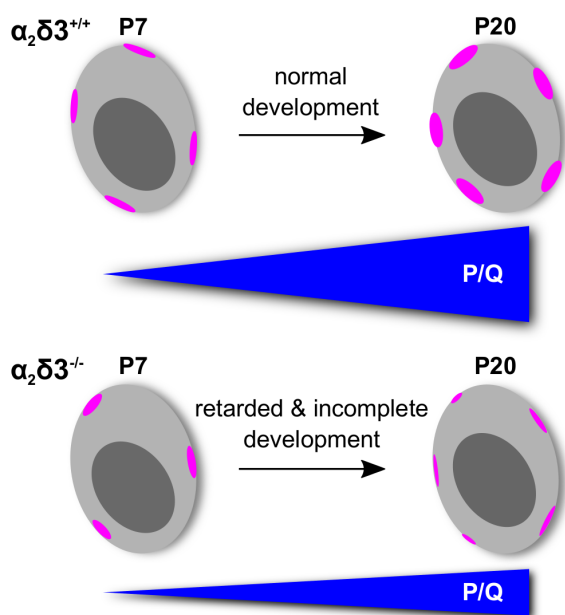
Figure 41. Effect of $\alpha_2\delta3$ deletion on the development of the endbulb of Held synapse
This schematic drawing represents the differences in the development of the auditory nerve fiber terminals in presence or absence of $\alpha_2\delta3$ (WT & KO respectively). The light gray cells represent bushy cells receiving contact by auditory nerve fiber terminals (magenta). The nucleus is shown in dark gray. During the normal development of the endbulb of Held synapse (upper row), the ANF terminals connecting to bushy cells are small in size and in number. During the maturation process these ANF terminals increase in size and also in number until they reach full maturation at approx. 9 weeks of age. At the age of P7, P/Q-type channel expression is lower compared to mature ages, where the channel makes up more than 90 % of the total current at the synapse. In the absence of $\alpha_2\delta3$ at P7 the number of boutons is reduced. Surprisingly the total area is unchanged between both genotypes, showing that single boutons are bigger compared to the wildtype. During

the maturation of the synapse the number of ANF terminals increases but the synapse is not able to fully maturate, resulting in smaller ANF terminals compared to the WT.

The data showed that deletion of $\alpha_2\delta3$ affects the synapse formation even before the onset of hearing. From the literature it is known that beside $\alpha_2\delta3$ also 2 other auxiliary subunits ($\alpha_2\delta1$ and $\alpha_2\delta2$) are expressed. In addition we analyzed the endbulb of Held synapse of mature $\alpha_2\delta2$ mutant mice, to see how the deletion of $\alpha_2\delta2$ affects number of boutons and VGLUT1-labeled area per BC.

3.8.2   Analysis of the endbulb of Held synapse in du/du mice aged P20

Previously different groups showed the importance of $\alpha_2\delta$ for synaptogenesis and that specifically lack of $\alpha_2\delta3$ leads to malformed synapses (Pirone et al., 2014; Procko and Shaham, 2009). Moreover our data indicate an important function for the development of the endbulb of Held synapse even before the onset of hearing. The endbulb of Held synapse of ducky mice (du/du) was analyzed with the aim to figure out if the deletion of $\alpha_2\delta2$ also affects the development of the endbulb of Held synapse. Ducky mice show a severe phenotype including a reduced body size, episodic seizures and mice homozygous for the mutation die after 3 weeks of age. Here only the analysis of mice aged P20 was possible because the genotype cannot be determined using standard PCR techniques. To fulfill this, mouse brains of P20 day old wild type and du/du mice were isolated and stained as described previously. The cells were analyzed at their largest perimeter and the number of boutons and the total VGLUT1 labeled area (μm^2) per cell was analyzed. Three animals from each genotype were analyzed.
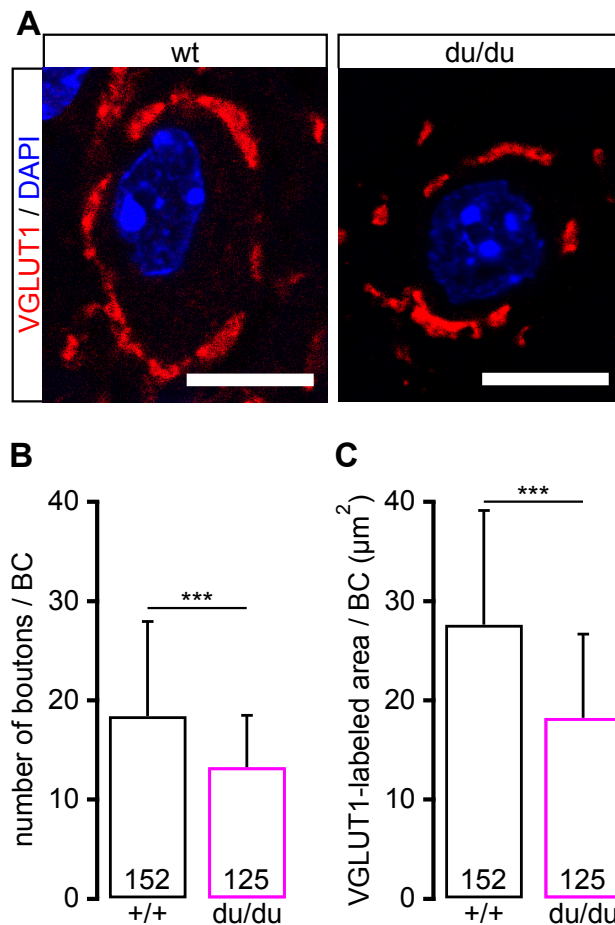
Figure 42. Analysis of auditory nerve fiber terminals at P20 in wildtype and du/du mice
A, Example images of one bushy cell stained for VGLUT1 (red) and DAPI (blue), of a wildtype and a du/du mouse. Scale bar: 5 µm. Images were taken using a confocal LSM 710 63x/1.4 NA oil objective. **B,** Analysis of the VGLUT1 labeled area in wildtype and du/du mice showing the mean ± S.D. At postnatal day 20, du/du mice have a significantly reduced VGLUT1 labeled area compared to their wildtype siblings. **C,** Analysis of the number of boutons indicates a significant reduction in the number of boutons formed at the endbulb of Held synapse in du/du mice. The number of cells analyzed are found in the column of the bar diagrams. Statistic analysis using the Wilcoxon Rank test *** p < 0.001 ± S.D. Data were analyzed with the help of Kerstin Blum. 152 wildtype cells and 125 knockout cells were analyzed.

The analysis showed a significant reduction in the total VGLUT1 labeled area (μm^2) between wildtype and du/du mice (*** $p < 3.33067*10^{-16}$). Also the number of boutons per bushy cell was significantly reduced (*** $p < 6.21734*10^{-8}$) in du/du mice. The data clearly show that also $\alpha_2\delta2$ is important for the synapse development of the endbulb of Held synapse in hearing mice. Combined with the previous findings regarding the $\alpha_2\delta3^{-/-}$ mice it seems that the loss of either $\alpha_2\delta2$ or $\alpha_2\delta3$ cant be fully compensated by the other auxiliary subunits.

4. Discussion

In this work, we analyzed the consequence of $\alpha_2\delta3$ deletion on (i) the composition of the Ca^{2+} current in SG neurons isolated from $\alpha_2\delta3$ wildtype and knockout mice aged P5 and P20 and (ii) on the development of the endbulb of Held synapses before and after the onset of hearing. The main challenge, when recording from these cells, is the presence of the myelin sheath, that surrounds between 90 – 95 % of all type I SG neurons (Rusznák and Szucs, 2009), which is present as early as P0 (Wang et al., 2013) and hampers direct patch clamp recordings from these cells *in vivo*. To overcome the difficulties of recording from acutely isolated tissue, a dissociated SG neuron culture was established. For the analysis of the Ca^{2+} current composition, we focused on L-, P/Q-, N- and R-type currents, because exclusively HVA α_1 subunit channels are associated with the auxiliary $\alpha_2\delta$ subunits (Dolphin 2013; Zamponi, 2005).

Beside an electrophysiological approach, analyzing Ca^{2+} currents in cultured SG neurons, we determined the effect of $\alpha_2\delta3$ deletion on endbulb of Held synapses before (aged P7) and after the onset of hearing (aged P20) by analyzing the size and number of synapses using confocal microscopy. Furthermore, we characterized the endbulb of Held synapses in du/du mice, carrying a functional null mutation of the $\alpha_2\delta2$ subunit to test whether deletion of $\alpha_2\delta2$ affected the structure of the endbulb of Held synapse in the same way as that of $\alpha_2\delta3$ did.

4.1 Deletion of $\alpha_2\delta3$ specifically affects P/Q-type currents in mature SG neurons

The Ca^{2+} current composition of cultured SG neurons was determined using specific Ca^{2+} channel antagonists targeting all members of the HVA Ca^{2+} channel family (Catterall et al., 2005) (Tab. 18). Analysis of the Ca^{2+} current composition in SG neurons isolated from $\alpha_2\delta3$ wildtype mice aged P20 revealed only tiny N- and R-type currents (**Figs. 37 & 38**) as well as a small portion of L-type currents (**Fig. 35**). The findings were similar when analyzing SG neurons isolated from $\alpha_2\delta3^{-/-}$ mice. From these we were able to conclude that the deletion of $\alpha_2\delta3$ did not affect the functionality of neither of these channels. Moreover, we found that P/Q-type currents represent the dominant Ca^{2+} current type (**Fig. 36**) and account for 42 % of the total I_{Ca} (**Fig. 39**).

Lv et al. (2012) had previously analyzed the Ca^{2+} current composition in cultured SG neurons isolated from 3 – 4 month old mice. Their findings are in disagreement with our results, since they found big difference in the expression of the different Ca^{2+} channel types depending also on the tonotopic localization within the cochlea. Our results however showed neither differences in the tonotopic localization of the cells nor a similar Ca^{2+} current composition.

For example, Lv et al. identified L-type currents as the dominant Ca^{2+} current form and described only a small portion of P/Q-type currents. That stands in contradiction to our data, where P/Q-type currents are the dominant Ca^{2+} current with 42 % of the total I_{Ca} and L-type currents making up the second largest component. In addition we also found no significant difference in the expression of either Ca^{2+} channel type between both cochlear localizations (apex vs. base).

The reasons for the different results can have various causes. First of all, on one explanation for the fact that no differences between SG neurons isolated from the apex and base were detected might arise from the treatment with growth factors like NT3 and BDNF. Both growth factors are naturally expressed in the cochlea, where signaling through these receptors are necessary for promoting neuronal survival, stimulating neurite growth and promoting synaptogenesis (Green et al., 2012). In the cochlea both growth factors are present as a gradient with BDNF being predominantly expressed in the base, while NT3 is found mainly in the apex. In our experiments we have treated isolated SG neurons from the apex and base with the same amount of NT3 and BDNF in order to promote growth and to increase the survival rate (personal communication with Prof. Yamoah and Dr. Wang, UC Davis). Because the growth factors have the power to alter the electrophysiological properties of the cells, we might have changed their native electrophysiological properties by making them more uniform (Green et al, 2012).

Secondly, the cochlear region that was analyzed varied between both projects. In our study we have used the whole cochlea and separated the cochlea in the middle, whereas Lv et al. discarded the middle part, which represents the frequency range of best hearing. It has been long postulated that SG neurons represent a heterogeneous cell population, which has recently been confirmed by Sun et al. (2018) and Shrestha et al. (2018) using novel single-RNA sequencing experiments. Both groups were independently able to show, that especially type I SG neurons, which make up the majority of sensory neurons in the cochlea differ in their expression of ion channels, adhesion molecules, transcription factors etc. depending on the tonotopic localization within the cochlea (apex, medial or base). Thus, especially the expression of ion channels can make a big difference when analyzing SG neurons from different cochlear regions, giving an explanation for the high standard deviations and responses the different blockers in our recordings (**Fig. 35 – 38**).

In the past, several groups have studied the Ca^{2+} current composition in cultured SG neurons and have obtained diverse results (Lv et al., 2012, Chen et al., 2011, Shrestha et al., 2018 and Stephani et al., (unpublished)). A study recently published by Shrestha et al (2018) has

categorized type I SG neurons into three sub-populations. Using single-cell RNA sequencing they found several ion channels to be differentially expressed in type I SG neurons and also found P/Q-type channels to be the dominant channel form and L-type channels as the second highest Ca^{2+} channel expressed in SG neurons (mice aged 3 weeks). These findings are in accordance to our patch-clamp recordings. In addition, they found $\alpha_2\delta3$ being the only auxiliary subunit expressed in all three sub-populations of type I SG neurons, while the other auxiliary subunits $\alpha_2\delta1$, $\alpha_2\delta2$ and $\alpha_2\delta4$ are only partially expressed in a small population of cells. This supports our hypothesis, that $\alpha_2\delta3$ preferentially co-assemble with the α_1 subunit of P/Q-type channels.

The Ca^{2+} current composition in SG neurons isolated from $\alpha_2\delta3^{-/-}$ mice revealed that specifically P/Q-type currents are affected by the deletion of $\alpha_2\delta3$. In the $\alpha_2\delta3^{-/-}$ mice we found a reduction of the P/Q-type currents to 18 % of the total I_{Ca} as compared to the wildtype where P/Q-type currents account for 42 % of the total I_{Ca}. All other Ca^{2+} current types (L-, N- and R-type) were not affected by the deletion of $\alpha_2\delta3$ and showed no significant difference when compared to the wildtype.

Our data indicate, that in SG neurons isolated from mice aged P20, P/Q-type channels preferable co-assemble with the auxiliary $\alpha_2\delta3$ subunit. This conclusion is in contrast to the findings reported by Landmann et al. (2018), who discovered two major findings with regard to $\alpha_2\delta3$. First they were able to show, by using double immunolabeling for $\alpha_2\delta3$ in combination with antibodies against either $Ca_v2.1$, $Ca_v2.2$ or $Ca_v2.3$ channels, that the $\alpha_2\delta3$ subunit can co-assemble with all members of the Ca_v2 family in motorneurons (Landmann et al., 2018). Secondly, they reported an up-regulation of $Ca_v2.2$ (N-type) and $Ca_v2.3$ (R-type) channels whereas $Ca_v2.1$ (P/Q-type) channel expression was unchanged and not affected by the deletion of $\alpha_2\delta3$.

When comparing the results of both studies, one should consider that Landmann et al. analyzed the expression of Ca_v channel proteins, while our study focused on the analysis of the currents. Next to the contradictive results of $\alpha_2\delta3$ deletion on P/Q-type protein expression and electrophysiology between the study performed by Landmann et al. and our findings, we similarly could not find a compensatory up-regulation of N-type or R-type protein or channels in cultured SG neurons isolated from mature $\alpha_2\delta3^{-/-}$ mice.

The small response of voltage-gated Ca^{2+} currents to both N- and R-type channel blockers in cultured SG neurons in this study may have different reasons. One explanation can be a heterogeneous response of SG neurons to the blockers (**Figs. 37E & 38E**) visible by their

large standard deviation, resulting on average on relatively small amplitudes to the respective currents. Another reason could be the existence of splice variants responding differently to the respective blockers, as has been reported for different Ca_v channels (Lipscombe et al., 2013; Tottene et al., 2000).

Another important finding of our study is that the total I_{Ca} recorded from SG neurons of $\alpha_2\delta3^{-/-}$ mice was unchanged compared to that of wildtype mice, although a substantial portion of P/Q-type current was missing. This supports the idea that a so far unidentified current compensates for the P/Q-type current loss in the $\alpha_2\delta3^{-/-}$ mice. This is in line with the findings reported by Neely et al. (2010), who recorded similarly sized peak Ca^{2+} inward currents in dorsal root ganglion neurons of $\alpha_2\delta3$ wildtype and knockout mice. The fact that the total I_{Ca} is unaltered between SG neurons isolated from $\alpha_2\delta3$ wildtype and knockout mice indicates that a so far unknown compensatory mechanism must exist.

These could be with great probability T-type channels because (i) we have excluded L-, N- and R-type channels and (ii) T-type channels are functional without co-assembly of any auxiliary subunit (Dolphin, 2018, 2012). Another indication for a possible up-regulation of T-type channels, are findings by Zhang et al. (2002) and Nahm et al. (2005), who showed an up-regulation of T-type channels in P/Q-type deficient mice. This points towards altered T-type channel expression in $\alpha_2\delta3^{-/-}$ mice.

The biggest challenge in analyzing T-type channels is the poor specificity of known T-type channel antagonists. Since T-type channels are referred to as LVA VGCCs and are inactive at voltages above -40 mV, a subtraction protocol of Ca^{2+} currents recorded from two different holding potentials could be used (Zamponi, 2005). Since no specific T-type channel blockers exist that would offer the possibility to differentiate between $Ca_v3.1$, $Ca_v3.2$ and $Ca_v3.3$ channels, non-specific blockers like for example mibefradil or Ni^{2+} could rather be applied to block all expressed T-type channels.

4.2 Small sized P/Q-type currents in neonatal SG neurons

The major component of VGCC currents in SG neurons isolated from mice aged P20 were P/Q-type currents, which were severely affected by the deletion of $\alpha_2\delta3$. In SG neurons isolated from neonatal mice aged P5 only tiny P/Q-type currents were detected in both genotypes (**Fig. 33E**). Although P/Q-type channels are the main Ca^{2+} channels responsible for neurotransmitter release in the mature CNS the composition of VGCCs may switch during development. N-type currents are often expressed at neonatal ages before P/Q-type currents are up-regulated and dominate neurotransmitter release in the mature system (Iwasaki et al.,

2000; Nudler et al., 2003; Rosato Siri and Uchitel, 1999). Double immunolabeling of acutely isolated SG neurons for $Ca_v2.1$ and the Golgi marker GM130 revealed weak expression of $Ca_v2.1$ at the plasma membrane and strikingly intense intracellular expression in the Golgi apparatus at P7 (**Fig. 33F**). Our data suggest that P/Q-type channels are in the process of massive biosynthesis for successive delivery to the plasma membrane towards the end of the first postnatal week. Notably, the sizes of P/Q-type currents in neonatal SG neurons from both wildtype and $\alpha_2\delta3$ knockout mice were not normally distributed. It seems that neurons that do not express P/Q channels exist, while others show a sizeable amount of P/Q currents (up to 90 pA, **Fig. 33E**), suggesting heterogeneity in the development and / or electrophysiological properties of type I SG neurons (Chen et al., 2011; Shrestha et al., 2018; Smith and Davis, 2016). Later, P/Q currents dominate total I_{Ca}, accounting for 42 % in SG neurons isolated at P20. Patch clamp recordings from Lin et al. on acute slices at the endbulb of Held revealed that 85 % of the total I_{Ca} was carried exclusively by P/Q channels around postnatal day 11 (Lin et al., 2011).

Beside P/Q-type currents we also analyzed L-type currents in cultured SG neurons of $\alpha_2\delta3$ wildtype and knockout mice aged P5. In the wildtype we found approx. 80 pA L-type currents in SG neurons isolated from the apex and base. In the knockout we found a significant reduction in the portion of L-type currents in neurons isolated from the apex (**Fig. 32E**), whereas the portion of L-type current in the base was unaltered compared to the wildtype. Here it has to be taken into account, that the total I_{Ca} recorded in SG neurons from the apex of $\alpha_2\delta3^{-/-}$ mice was reduced by more than 40 % compared to recordings from the wildtype. That difference has with great probability a technical origin because later recordings for the portion of P/Q-type currents showed similar total I_{Ca} in SG neurons isolated from the apex of $\alpha_2\delta3$ wildtype and knockout mice. This also means, that the total I_{Ca} (**Fig. 34**) might not be reduced in the $\alpha_2\delta3$ knockout. In order to be able to make a statement on the potential consequence of $\alpha_2\delta3$ deletion on SG neurons isolated from the apex, recordings would need to be repeated. Future experiments will focus on the analysis of N- and R-type Ca^{2+} channels in order to identify the complete Ca^{2+} channel composition in SG neurons isolated from neonatal mice. Furthermore, the analysis of N-type channels would indicate if a developmental switch between N- and P/Q-type channels exist before and after the onset of hearing.

4.3. SG neuron heterogeneity

Several groups have intensively studied SG neurons over the past years with respect to their ion channel composition, protein expression and electrophysiological properties (Adamson et al., 2002; Chen et al., 2001; Lv et al., 2012). Until now, two groups of neurons have been identified, which are referred to as type I and type II SG neurons, based on the presence of the type III intermediate filament protein peripherin. In 1992, Kawase and Liberman were able to classify auditory nerve fibers in mammals into three subclasses based on their spontaneous discharge rate (Kawase and Liberman, 1992).

But statements about the difference between individual SG neurons were not easy to make until recently when Sun et al. (2018) and Shrestha et al. (2018) used single-cell RNA sequencing and identified three subclasses of type I SG neurons based on the expression of specific transcription factors, ion channels, cell adhesion molecules as well as neurotransmitter receptors.

The results of our recording showed a high heterogeneity in the total I_{Ca} and in the response of individual SG neurons to different Ca^{2+} channel antagonists. However, the question remains of how the SG neurons dedifferentiate in culture and whether certain SG neurons are more vulnerable to the isolation process. This shows that electrophysiological measurements alone are not sufficient to fully characterize SG neurons in culture. Experiment combining proteomic tools (e.g. single-cell RNA sequencing), molecular biology (e.g. immunolabeling) together with patch-clamp recordings can be used to extensively characterize the different subtypes and functions of SG neurons, which would help to better understand their functions in auditory processing.

4.4 $\alpha_2\delta3$ affects the endbulb of Held synapse before the onset of hearing

Each axon of an SG neuron branches and innervates various neuron types in the cochlear nuclear complex, such as bushy cells, stellate cells, cartwheel cells, octopus cells and fusiform cells. Each branch of a single auditory nerve fiber branches further at its terminal and contacts the soma of a bushy cell, forming what is called an endbulb of Held synapse, which is the largest synapse of an SG neuron. Previous studies performed by Pirone et al. showed that the absence of $\alpha_2\delta3$ led to malformed synapses at 5 weeks of age, characterized by a smaller size of the synapse and a reduced number of intercellular channel cisterns (Pirone et al., 2014).

Here we imaged endbulb of Held synapses of mice at P7 and P20 at the same ages used for the analysis of the Ca^{2+} current composition in cultured SG neurons. For the morphological

analysis, mice aged P7 rather than P5 were used because the CNC was frequently lost upon dissecting brains at younger ages.

VGLUT1, which is frequently used to label the glutameric boutons of ANF terminals at bushy cells, was used as a maker to label the endbulb of Held synapses. A significant reduction of the VGLUT1-labeled area, corresponding to the size of the presynaptic terminal (Heeringa et al., 2016), yet a normal number of boutons per bushy cells was found in $\alpha_2\delta3^{-/-}$ aged P20 (**Fig. 40E**), which is in accordance with previous findings (Pirone et al., 2014). This phenotype is in place when P/Q currents account for as much as 85 % of the presynaptic Ca^{2+} currents at the endbulb synapse in acute slices between P9 and P11 (Lin et al., 2011) and for 60 % of total I_{Ca} in SG neurons isolated at P20 (this study).

Analysis of the endbulb of Held synapse in $\alpha_2\delta3^{-/-}$ mice aged P7 revealed a reduced number of boutons per bushy cell but a normal total VGLUT1 labeled area (**Fig. 40D**). Consequently, single endbulbs are larger in $\alpha_2\delta3^{-/-}$ mice (aged P7) suggesting that the process of forming complex finger-like endbulb structures is delayed. Notably, the deletion of $\alpha_2\delta3$ affects synapse development before the onset of hearing and before substantial expression of P/Q-type channels, which expression starts around P7. The fact that $\alpha_2\delta3$ can act independently from the VGCC function and from the α_1 subunit has previously been shown by several groups (Dickman et al., 2008; Hoppa et al., 2012; Kurshan et al., 2009; Wang et al., 2016). Using different *Drosophila* mutants, Krushan et al. (2009) showed that the $\alpha_2\delta3$ orthologous straightjacket is essential for the viability of *Drosophila* larvae and indispensable for proper development of the neuromuscular junction, at a time point when Ca_v2 channels are not yet functional (Kurshan et al., 2009). These findings in combination with the data from Pirone et al. and this study data indicate that $\alpha_2\delta3$ is important for the synapse development and morphology. In addition it specifically determines the expression of P/Q-type channels in mature SG neurons. Here, we show for the first time that $\alpha_2\delta3$ controls synapse development and morphology independently of its co-assembly with its preferred α_1 subunit and the Ca^{2+} current flow through the channel in a mammalian system. However, the underlying mechanism remains to be elucidated. Because $\alpha_2\delta$ proteins reside in the extracellular space and have protein-protein-interaction domains, they may functionally interact with many partners in the extracellular matrix filling the synaptic cleft or with proteins at the postsynapse.

We further analyzed the morphology of endbulb of Held synapse in the $\alpha_2\delta2$ du/du mutants at the age of P20 to determine, how the deletion of $\alpha_2\delta2$ affects the development of the endbulb of Held synapses and if the results can be compared to the findings in the $\alpha_2\delta3^{-/-}$ mice. Interestingly, the VGLUT1-labeled area as well as the number of boutons was significantly smaller in du/du mice as compared with their wildtype (**Fig. 42B, C**). This indicates, that deletion of $\alpha_2\delta2$ seems to affect not only synapse development but also their formation by giving a more severe phenotype as compared to the deletion of $\alpha_2\delta3$. It would be interesting to analyze both neonatal endbulb of Held synapses as well as the composition of the Ca^{2+} current in SG neurons in $\alpha_2\delta2$ du/du mutant mice. Our data show that not only $\alpha_2\delta3$ but also $\alpha_2\delta2$ are indispensible for proper synapse development and morphology in the auditory periphery. In this context, also the role of $\alpha_2\delta1$ needs to be determined as well.

The potential that certain $\alpha_2\delta$ subunits can act as receptors involved in synaptogenesis had been shown by Ergulo et al., (2009) and Mendus et al., (2014) but the question remains as to which extent the lack of a particular $\alpha_2\delta$ subunit can be compensated by other $\alpha_2\delta$ isoforms and which compensatory mechanisms exist that balance the total I_{Ca} in the respective knockout animals.

To summarize, we could show that besides the regulation of the expression of the α_1 subunit and hence the amplitude of the Ca^{2+} current, $\alpha_2\delta3$ can also act independently and is required for proper development and morphology of the endbulb of Held synapse. The study of $\alpha_2\delta3$ knockout and $\alpha_2\delta2$ mutant mice showed that the auxiliary $\alpha_2\delta$ subunits are functionally diverse. This makes the analysis of the $\alpha_2\delta$ subunits an interesting research topic in general with regard to the diverse functions and consequences of $\alpha_2\delta$ gene deletion.

4.5   Dissociated cell culture as tool to study SG neurons *in vitro*

Spiral ganglion neurons are indispensable for a proper hearing function and the myelin sheath that enwraps the soma of type I SG neurons enables fast transmission of auditory signals. Even though the myelin sheath is essential for fast transmission, it prevents on the other side direct recording from these cells. Because the myelin sheath is present as early as P0, a dissociated SG neuron culture is essential for the recording of currents. Here, we have established a primary dissociated SG neuron culture using the protocol provided by Prof. Yamoah (Lee et al., 2016) (**Fig. 31**). Especially primary cells often require special treatment during and after the isolation in order to create and maintain an appropriate culture environment mimicking the *in vivo* situations. In our experiments we have isolated cells from

the apical and basal part of the cochlea and cultured them separately. To stimulate growth of the cells, both wells were supplemented with the same of amount of NT3 and BDNF. In native tissue NT3 and BDNF are expressed tonotopically as gradient in the cochlea, with BDNF being more expressed at the base and NT3 being more expressed at the apex (Green et al., 2012). SG neurons display a heterogeneous population of cells, which can be categorized into different groups depending on the expression of for example ion channels or adhesion molecules (Shrestha et al. 2018; Sun et al, 2018). Their properties can be changed by external factors including for example growth factors and coating material (Anand-Apte and Zetter, 1997; Evans et al., 2009; Green et al., 2012). With the identical growth factor treatment of the isolated SG neurons from the apical and basal half, respectively, we might have altered the characteristic properties of the cells making them more uniform (Anand-Apte and Zetter, 1997; Van der Heiden et al., 2001). Because neuron survival and well being strongly depends on proper supplementation with growth factors, we used the same amount of growth factors for both (personal communication with Prof. Yamoah and Dr. Wang, UC Davis). To further analyze the characteristic features of SG neurons it would be interesting to (i) investigate how the application of growth factors and coating material influences SG neuron morphology and behavior and (ii) to culture apical and basal SG neurons with only the more appropriate growth factor.

4.6   Limitations of immunohistochemistry

Immunohistochemistry is a powerful tool used to visualize the localization or co-localization of different proteins within a tissue. However, the validity and accuracy of this method is determined by multiple factors. Here we have tested the specificity of different antibodies (anti- $Ca_v1.3$, anti-$Ca_v2.2$ and anti-$\alpha_2\delta3$) on the tissue of acutely isolated SG neurons from wildtype and the respective knockout mice (**Figs. 22 - 27**).

Immunohistochemical labeling requires proper sample handling, fixation and blocking to obtain a valid reliable labeling. Especially different fixation agents, blocking reagents and times, antibody incubation time and the mounting media can have influences on the outcome of a immunolabeling. Antibodies exist as either monoclonal or polyclonal, with monoclonal antibodies showing higher specificity, as they represent identical immunoglobulins that have been generated from a single clone targeting a single epitope (binding ratio 1:1) at the same time resulting in lower labeling intensity compared to polyclonal antibody formulation that targets different epitopes of the same protein target amplifying the signal (binding ratio > 1:1) (Ramos-Vara, 2017).

The best way to test the antibody specificity in native tissue is using tissue from the respective knockout mouse that should not result in visible staining. This requires however the existence and availability of the knockout line, which is not always available because certain mutations might be lethal early in live (e.g. *Cacna1a* deficient mice or du/du mice). Here we have tested the specificity of antibodies against $Ca_v1.3$, $Ca_v2.2$ and $\alpha_2\delta3$ on SG tissue from *Cacna1b*, *Cacna1d* and *Cacna2d3* knockout mice. Prior to the specificity test, optimum labeling conditions were determined for each antibody. To our dismay, none of the tested antibodies proved to be specific. All tested antibodies showed very similar labeling patterns in the knockout compared with the wildtype tissue (**Figs. 24 - 27**). One reason for the lack of specific anti-$\alpha_2\delta3$ antibodies could be due to the high degree of glycosylation of the $\alpha_2\delta3$ protein close to the epitopes, hampering antibody binding and specificity. Since all tested anti-$\alpha_2\delta3$ antibodies were generated against non-glycosylated polypeptide epitopes we tried to remove the glycosylation using a chemical and an enzymatic reaction. However, these attempts to improve anti-$\alpha_2\delta3$ antibody specificity were also unsuccessful (**Fig. 29**).

The specificity tests for the anti-$Ca_v1.3$ and anti-$Ca_v2.2$ antibodies were performed on acutely isolated SG neuron tissue of the respective knockout mice. Even though the $Ca_v2.2$ antibody had been proven to be specific in the olfactory bulb sections ($Ca_v2.2$, (Weiss et al., 2014)), the antibody labeled SG neurons of the respective knockout mouse. For the $Ca_v1.3$ antibody, the labeling was reduced by more than 90 % in the knockout and only a very weak labeling remained.

These disappointing results indicate that (i) lot-to-lot variability of polyclonal antibodies can be huge, resulting in very different immunolabeling outcomes and (ii) specificity tests with knockout tissue may work for a particular cell or organ type but does not necessarily work in others. The best way to improve labeling would be the generation of monoclonal antibodies, which would raise the chance of more specific labeling. In the case of $Ca_v1.3$, a mouse monoclonal antibody was tested in our lab but did not label the characteristic $Ca_v1.3$ clusters at the presynaptic ribbons in inner hair cells (personal communication with Dr. S. Eckrich and Kerstin Blum) showing that also monoclonal antibody labeling is not always specific.

4.7 Outlook

In this work the consequence of the $\alpha_2\delta3$ deletion was analyzed with respect to effects on the Ca^{2+} current composition in SG neurons on formation of boutons at the endbulb of Held synapse. Previous work by Pirone et al. (2014) showed that (i) deletion of $\alpha_2\delta3$ affects the expression of P/Q-type channels in SG neurons in $\alpha_2\delta3$-/- mice aged 3-weeks and (ii) leads to malformed and retarded synapse development at the endbulb of Held. Because the endbulbs

are too small in the $\alpha_2\delta3$ knockout and whole cell patch clamp recordings are impossible to perform, we analyzed SG neurons before and after the onset of hearing, whose ANF terminals form the endbulb of Held synapse, which projects onto BCs at the CNC.

Analysis of the Ca^{2+} current composition in SG neurons aged P20 revealed that P/Q-type currents account for the main portion of the total I_{Ca}, which is massively down-regulated in $\alpha_2\delta3^{-/-}$ mice. Surprisingly, other HVA Ca^{2+} channels were not up-regulated in the knockout. Here future experiments could include the analysis of T-type channels, which could compensate for the loss of P/Q-type currents in $\alpha_2\delta3^{-/-}$ mice because T-type channels are the only Ca^{2+} channels that are not associated with any auxiliary subunits. Here the poor availability to specific T-type channel blocker might hamper the investigation of the different T-type channel types ($Ca_v3.1$, $Ca_v3.2$ and $Ca_v3.3$).

In context with that, the analysis of the Ca^{2+} current composition in neonatal SG neurons would be very interesting. So far no data (except for our P/Q- and L-type data) are available for neonatal ages, and we have made here a first attempt in analyzing two members of the HVA Ca^{2+} channels. The presences of tiny P/Q-type channels indicate that a different Ca^{2+} channel type dominates in neonatal ages compared to mice aged P20. Therefore it would be very interesting to analyze, N-type, R-type and T-type channels in both genotypes.

Since SG neurons express also $\alpha_2\delta1$ and $\alpha_2\delta2$ it would be interesting to analyze the Ca^{2+} current composition in SG neurons of both mouse lines to identify how their deletion affects the current composition. Furthermore, it would also be interesting to see how the deletion of several $\alpha_2\delta$ subunits affects the current composition, because they seem to be unable to fully compensate for the loss of a specific $\alpha_2\delta$ subunit. Because of the severe phenotype of du/du mice, cross breeding using $\alpha_2\delta2$ mice is not possible. In order to analyze the effect of the deletion of several $\alpha_2\delta$ subunits, I would suggest to isolate SG neurons form $\alpha_2\delta3$ knockout mice and apply siRNA knockdown to silence the other $\alpha_2\delta$ subunits, this would allow electrophysiological analysis of double or triple knockout cells.

With respect to the development of endbulb of Held synapse, it would be interesting to analyze different $\alpha_2\delta$ knockout mice to compare the findings among each other. Using different antibodies, the protein complex at the endbulb of Held synapse could be analyzed in more detail, to identify proteins, that cause the deformation at the synapse or maybe act as receptor for the interaction with different $\alpha_2\delta$ subunits.

5.   References

Adamson, C.L., Reid, M.A., Mo, Z.-L., Bowne-English, J., and Davis, R.L. (2002). Firing features and potassium channel content of murine spiral ganglion neurons vary with cochlear location. J. Comp. Neurol. *447*, 331–350.

Anand-Apte, B., and Zetter, B. (1997). Signaling mechanisms in growth factor-stimulated cell motility. Stem Cells Dayt. Ohio *15*, 259–267.

Antzelevitch, C., Pollevick, G.D., Cordeiro, J.M., Casis, O., Sanguinetti, M.C., Aizawa, Y., Guerchicoff, A., Pfeiffer, R., Oliva, A., Wollnik, B., et al. (2007). Loss-of-Function Mutations in the Cardiac Calcium Channel Underlie a New Clinical Entity Characterized by ST-Segment Elevation, Short QT Intervals, and Sudden Cardiac Death. Circulation *115*, 442–449.

Arikkath, J., and Campbell, K.P. (2003). Auxiliary subunits: essential components of the voltage-gated calcium channel complex. Curr. Opin. Neurobiol. *13*, 298–307.

Baig, S.M., Koschak, A., Lieb, A., Gebhart, M., Dafinger, C., Nürnberg, G., Ali, A., Ahmad, I., Sinnegger-Brauns, M.J., Brandt, N., et al. (2011). Loss of Ca(v)1.3 (CACNA1D) function in a human channelopathy with bradycardia and congenital deafness. Nat. Neurosci. *14*, 77–84.

Barbado, M., Fablet, K., Ronjat, M., and De Waard, M. (2009). Gene regulation by voltage-dependent calcium channels. Biochim. Biophys. Acta BBA - Mol. Cell Res. *1793*, 1096–1104.

Barclay, J., Balaguero, N., Mione, M., Ackerman, S.L., Letts, V.A., Brodbeck, J., Canti, C., Meir, A., Page, K.M., Kusumi, K., et al. (2001). Ducky mouse phenotype of epilepsy and ataxia is associated with mutations in the Cacna2d2 gene and decreased calcium channel current in cerebellar Purkinje cells. J. Neurosci. Off. J. Soc. Neurosci. *21*, 6095–6104.

Bourinet, E., and Zamponi, G.W. (2016). Block of voltage-gated calcium channels by peptide toxins. Neuropharmacology.

Brodbeck, J., Davies, A., Courtney, J.-M., Meir, A., Balaguero, N., Canti, C., Moss, F.J., Page, K.M., Pratt, W.S., Hunt, S.P., et al. (2002). The ducky mutation in Cacna2d2 results in altered Purkinje cell morphology and is associated with the expression of a truncated alpha 2 delta-2 protein with abnormal function. J. Biol. Chem. *277*, 7684–7693.

Bulaj, G., Buczek, O., Goodsell, I., Jimenez, E.C., Jranski, J., Garrett, J.E., Olivera, B.M. (2003). Efficient oxidative folding of conotoxins and the radiation of venomous cone snails. Proc. Natl. Acad. Sci. USA, *100*, 14562-69

Buraei, Z., and Yang, J. (2010). The ß subunit of voltage-gated Ca2+ channels. Physiol. Rev. *90*, 1461–1506.

Cain, S.M., and Snutch, T.P. (2013). T-type calcium channels in burst-firing, network synchrony, and epilepsy. Biochim. Biophys. Acta BBA - Biomembr. *1828*, 1572–1578.

Cao XJ, Oertel D (2010). Auditory nerve fibers excite targets through synapses that vary in convergence, strength, and short-term plasticity. J Neurophysiol. *104*, 2308-20

Carricondo, F., and Romero-Gómez, B. (2018). The Cochlear Spiral Ganglion Neurons: The Auditory Portion of the VIII Nerve. Anat. Rec. *0*.

Catterall, W.A. (2000). Structure and regulation of voltage-gated Ca2+ channels. Annu. Rev. Cell Dev. Biol. *16*, 521–555.

Catterall, W.A., Perez-Reyes, E., Snutch, T.P., and Striessnig, J. (2005). International Union of Pharmacology. XLVIII. Nomenclature and structure-function relationships of voltage-gated calcium channels. Pharmacol. Rev. *57*, 411–425.

Chen, W.C., Xue, H.Z., Hsu, Y. (Lucy), Liu, Q., Patel, S., and Davis, R.L. (2011). Complex distribution patterns of voltage-gated calcium channel α-subunits in the spiral ganglion. Hear. Res. *278*, 52–68.

Chevalier, M., Lory, P., Mironneau, C., Macrez, N., Quignard, J.F., (2006). T-type CaV3.3 calcium channels produce spontaneous low-threshold action potentials and intracellular calcium oscillations. Eur. J. Neurosci. *23*, 2321-9

Curzon P, Zhang M, Radek RJ, Fox GB. (2009). The Behavioral Assessment of Sensorimotor Processes in the Mouse: Acoustic Startle, Sensory Gating, Locomotor Activity, Rotarod, and Beam Walking. Methods of Behavior Analysis in Neuroscience. 2nd edition. Boca Raton (FL): CRC Press/Taylor & Francis; 2009. Chapter 8.

Dabdoub, A., Fritzsch, B., Popper, A.N., and Fay, R.R. (2016). The Primary Auditory Neurons of the Mammalian Cochlea (Springer).

Dallos, P., (2008). Cochlear amplification, outer hair cells and prestin. Curr. Opin. Neurobiol. *18*, 370–376.

Dallos, P., Popper, A.N., and Fay, R.R. (1996). The Cochlea (Springer).

Davies, A., Hendrich, J., Van Minh, A.T., Wratten, J., Douglas, L., and Dolphin, A.C. (2007). Functional biology of the α2δ subunits of voltage-gated calcium channels. Trends Pharmacol. Sci. *28*, 220–228.

Davies, A., Kadurin I., Alvarez-Laviada, A., Douglas, L., Nieto-Rostro. M., Bauer, C.S., Pratt, W.S., Dolphin, A.C. (2010). The $\alpha_2\delta$ subunits of voltage-gated calcium channels form GPI-anchored proteins, a posttranslational modification essential for function. Proc Natl Acad Sci USA *107*, 1654-1659

Defourny, J., Lallemend, F., and Malgrange, B. (2011). Structure and development of cochlear afferent innervation in mammals. Am. J. Physiol. - Cell Physiol. *301,* C750–C761.

Dickman, D.K., Kurshan, P.T., and Schwarz, T.L. (2008). Mutations in a Drosophila alpha2delta voltage-gated calcium channel subunit reveal a crucial synaptic function. J. Neurosci. Off. J. Soc. Neurosci. *28*, 31–38.

Dolphin, A.C. (2009). Calcium channel diversity: multiple roles of calcium channel subunits. Curr. Opin. Neurobiol. *19*, 237–244.

Dolphin, A.C. (2012). Calcium channel auxiliary α2δ and β subunits: trafficking and one step beyond. Nat. Rev. Neurosci. *13*, 542–555.

Dolphin, A.C. (2013). The α2δ subunits of voltage-gated calcium channels. Biochim. Biophys. Acta BBA - Biomembr. *1828*, 1541–1549.

Dolphin, A.C. (2016). Voltage-gated calcium channels and their auxiliary subunits: physiology and pathophysiology and pharmacology. J. Physiol. *594*, 5369–5390.

Edvardson, S., Oz, S., Abulhijaa, F.A., Taher, F.B., Shaag, A., Zenvirt, S., Dascal, N., and Elpeleg, O. (2013). Early infantile epileptic encephalopathy associated with a high voltage gated calcium channelopathy. J. Med. Genet. *50*, 118–123.

Eroglu, Ç., Allen, N.J., Susman, M.W., O'Rourke, N.A., Park, C.Y., Özkan, E., Chakraborty, C., Mulinyawe, S.B., Annis, D.S., Huberman, A.D., et al. (2009a). The Gabapentin Receptor α2δ-1 is the Neuronal Thrombospondin Receptor Responsible for Excitatory CNS Synaptogenesis. Cell *139*, 380–392.

Ertel, E.A., Campbell, K.P., Harpold, M.M., Hofmann, F., Mori, Y., Perez-Reyes, E., Schwartz, A., Snutch, T.P., Tanabe, T., Birnbaumer, L., et al. (2000). Nomenclature of voltage-gated calcium channels. Neuron *25*, 533–535.

Evans, A.J., Thompson, B.C., Wallace, G.G., Millard, R., O'Leary, S.J., Clark, G.M., Shepherd, R.K., and Richardson, R.T. (2009). Promoting neurite outgrowth from spiral ganglion neuron explants using polypyrrole/BDNF-coated electrodes. J. Biomed. Mater. Res. A *91A*, 241–250.

Fekete DM, Campero AM (2007). Axon guidance in the inner ear. Int H Dev Biol. *51* (6-7): 549-56

Fell, B., Eckrich, S., Blum, K., Eckrich, T., Hecker, D., Obermair, G.J., Münkner, S., Flockerzi, V., Schick, B., and Engel, J. (2016). α2δ2 Controls the Function and Trans-Synaptic Coupling of Cav1.3 Channels in Mouse Inner Hair Cells and Is Essential for Normal Hearing. J. Neurosci. Off. J. Soc. Neurosci. *36*, 11024–11036.

Fettiplace, R. (2009). Defining features of the hair cell mechanoelectrical transducer channel. Pflugers Arch. *458*, 1115–1123.

François, A., Laffray, S., Pizzoccaro, A., Eschalier, A., and Bourinet, E. (2014). T-type calcium channels in chronic pain: mouse models and specific blockers. Pflüg. Arch. - Eur. J. Physiol. *466*, 707–717.

Franklin, K.B.J., and Paxinos, G. (2008). The mouse brain in stereotaxic coordinates (Elsevier).

Fuchs PA, Evans MG (1990). Potassium currents in hair cells isolated from the cochlea or the chick. J Physiol. *429,* 529-551

Gavara, N., Manoussaki, D., and Chadwick, R.S. (2011). Auditory Mechanics of the Tectorial Membrane and the Cochlear Spiral. Curr. Opin. Otolaryngol. Head Neck Surg. *19,* 382–387.

Glowatzki E, Fuchs PA (2000). Cholinergic synaptic inhibition of inner hair cells in the neonatal mammalian cochlea. Science. *288,* 2366-8

Green, S.H., Bailey, E., Wang, Q., and Davis, R.L. (2012). The Trk A, B, C's of Neurotrophins in the Cochlea. Anat. Rec. Adv. Integr. Anat. Evol. Biol. *295,* 1877–1895.

Heeringa, A.N., Stefanescu, R.A., Raphael, Y., and Shore, S.E. (2016). Altered vesicular glutamate transporter distributions in the mouse cochlear nucleus following cochlear insult. Neuroscience *315,* 114–124.

Hoppa, M.B., Lana, B., Margas, W., Dolphin, A.C., and Ryan, T.A. (2012). alpha2delta expression sets presynaptic calcium channel abundance and release probability. Nature *486,* 122–125.

Ino, M., Yoshinaga, T., Wakamori, M., Miyamoto, N., Takahashi, E., Sonoda, J., Kagaya, T., Oki, T., Nagasu, T., Nishizawa, Y., et al. (2001). Functional disorders of the sympathetic nervous system in mice lacking the α1B subunit (Cav 2.2) of N-type calcium channels. Proc. Natl. Acad. Sci. *98,* 5323–5328.

Iwasaki, S., Momiyama, A., Uchitel, O.D., and Takahashi, T. (2000). Developmental Changes in Calcium Channel Types Mediating Central Synaptic Transmission. J. Neurosci. *20,* 59–65.

Jun, K., Piedras-Rentería, E.S., Smith, S.M., Wheeler, D.B., Lee, S.B., Lee, T.G., Chin, H., Adams, M.E., Scheller, R.H., Tsien, R.W., et al. (1999). Ablation of P/Q-type Ca2+ channel currents, altered synaptic transmission, and progressive ataxia in mice lacking the α1A-subunit. Proc. Natl. Acad. Sci. U. S. A. *96,* 15245–15250.

Kabir, Z.D., Martínez-Rivera, A., and Rajadhyaksha, A.M. (2017). From Gene to Behavior: L-Type Calcium Channel Mechanisms Underlying Neuropsychiatric Symptoms. Neurother. J. Am. Soc. Exp. Neurother. *14,* 588–613.

Kadurin, I., Ferron, L., Rothwell, S.W., Meyer, J.O., Douglas, L.R., Bauer, C.S., Lana, B., Margas, W., Alexopoulos, O., Nieto-Rostro, M., et al. (2016). Proteolytic maturation of α2δ represents a checkpoint for activation and neuronal trafficking of latent calcium channels. ELife *5.*

Kandler, K., Clause, A., and Noh, J. (2009). Tonotopic reorganization of developing auditory brainstem circuits. Nat. Neurosci. *12,* 711–717.

Kazmierczak P, Müller U. (2012). Sensing sound: molecules that orchestrate mechanotransduction by hair cells. Trends Neurosci. *35,* 220-9

Kawase, T., and Liberman, M.C. (1992). Spatial organization of the auditory nerve according to spontaneous discharge rate. J. Comp. Neurol. *319*, 312–318.

Kim, J.-B. (2014). Channelopathies. Korean J. Pediatr. *57*, 1–18.

Kurbel, S., Borzan, V., Golem, H., and Dinjar, K. (2017). Cochlear potential difference between endolymph fluid and the hair cell's interior: a retold interpretation based on the Goldman equation. Med. Glas. Off. Publ. Med. Assoc. Zenica-Doboj Cant. Bosnia Herzeg. *14*, 8–15.

Kurosaki, T., and Maquat, L.E. (2016). Nonsense-mediated mRNA decay in humans at a glance. J. Cell Sci. *129*, 461–467.

Kurshan, P.T., Oztan, A., and Schwarz, T.L. (2009). Presynaptic α2δ-3 is required for synaptic morphogenesis independent of its Ca2+-channel functions. Nat. Neurosci. *12*, 1415–1423.

Lacinová, L. (2005). Voltage-dependent calcium channels. Gen. Physiol. Biophys. *24 Suppl 1*, 1–78.

Landmann, J., Richter, F., Oros-Peusquens, A.-M., Shah, N.J., Classen, J., Neely, G.G., Richter, A., Penninger, J.M., and Bechmann, I. (2018). Neuroanatomy of pain-deficiency and cross-modal activation in calcium channel subunit (CACN) α2δ3 knockout mice. Brain Struct. Funct. *223*, 111–130.

Lazniewska, J., and Weiss, N. (2017). Glycosylation of voltage-gated calcium channels in health and disease. Biochim. Biophys. Acta *1859*, 662–668.

Li, Y., Meaud, J., and Grosh, K. (2011). Coupling the Subtectorial Fluid with the Tectorial Membrane and Hair Bundles of the Cochlea. AIP Conf. Proc. *1403*, 104–109.

Limb, C.J., and Ryugo, D.K. (2000). Development of Primary Axosomatic Endings in the Anteroventral Cochlear Nucleus of Mice. JARO J. Assoc. Res. Otolaryngol. *1*, 103–119.

Lin, K.-H., Oleskevich, S., and Taschenberger, H. (2011). Presynaptic Ca2+ influx and vesicle exocytosis at the mouse endbulb of Held: a comparison of two auditory nerve terminals. J. Physiol. *589*, 4301–4320.

Lippe W, Rubel EW (1983). Development of the place principle: tonotopic organization. Science. *219*, 514-6

Lipscombe, D., Andrade, A., and Allen, S.E. (2013). Alternative splicing: Functional diversity among voltage-gated calcium channels and behavioral consequences. Biochim. Biophys. Acta *1828*, 1522–1529.

Lv, P., Sihn, C.-R., Wang, W., Shen, H., Kim, H.J., Rocha-Sanchez, S.M., and Yamoah, E.N. (2012). Posthearing Ca(2+) currents and their roles in shaping the different modes of firing of spiral ganglion neurons. J. Neurosci. Off. J. Soc. Neurosci. *32*, 16314–16330.

Lv, P., Kim, H.J., Lee, J.-H., Sihn, C.-R., Fathabad Gharaie, S., Mousavi-Nik, A., Wang, W., Wang, H.-G., Gratton, M.A., Doyle, K.J., et al. (2014). Genetic, Cellular, and Functional Evidence for Ca2+ Inflow through Cav1.2 and Cav1.3 Channels in Murine Spiral Ganglion Neurons. J. Neurosci. *34*, 7383–7393.

Malmierca, M., and Mechán, M. (2004). Auditory System. In In: The Rat Nervous System. Section VI: Systems; Chapter 31, pp. 997–1082.

Mann, Z.F., and Kelley, M.W. (2011). Development of tonotopy in the auditory periphery. Hear. Res. *276*, 2–15.

Mendus, D., Sundaresan, S., Grillet, N., Wangsawihardja, F., Leu, R., Müller, U., Jones, S.M., and Mustapha, M. (2014a). Thrombospondins 1 and 2 are important for afferent synapse formation and function in the inner ear. Eur. J. Neurosci. *39*, 1256–1267.

Nahm, S.-S., Jung, K.-Y., Enger, M.K., Griffith, W.H., and Abbott, L.C. (2005). Differential expression of T-type calcium channels in P/Q-type calcium channel mutant mice with ataxia and absence epilepsy. J. Neurobiol. *62*, 352–360.

Neely, G.G., Hess, A., Costigan, M., Keene, A.C., Goulas, S., Langeslag, M., Griffin, R.S., Belfer, I., Dai, F., Smith, S., et al. (2010). A genome-wide Drosophila screen for heat nociception identifies α2δ3 as an evolutionary-conserved pain gene. Cell *143*, 628–638.

Neher, E. (1992). [6] Correction for liquid junction potentials in patch clamp experiments. Methods Enzymol. *207*, 123–131.

Newcomb, R., Szoke, B., Palma, A., Wang, G., Chen, X. h, Hopkins, W., Cong, R., Miller, J., Urge, L., Tarczy-Hornoch, K., et al. (1998). Selective peptide antagonist of the class E calcium channel from the venom of the tarantula Hysterocrates gigas. Biochemistry *37*, 15353–15362.

Newcomb, R., Chen, X., Dean, R., Dayanithi, G., Cong, R., Szoke, B., Lemos, J., Bowersox, S., and Miljanich, G. (2000). SNX-482: A Novel Class E Calcium Channel Antagonist from Tarantula Venom. CNS Drug Rev. *6*, 153–173.

Nimmrich, V., and Gross, G. (2012). P/Q-type calcium channel modulators. Br. J. Pharmacol. *167*, 741–759.

Nouvian, R., Beutner, D., Parsons, T.D., and Moser, T. (2006). Structure and Function of the Hair Cell Ribbon Synapse. J. Membr. Biol. *209*, 153–165.

Nudler, S., Piriz, J., Urbano, F.J., Rosato-Siri, M.D., Renteria, E.S.P., and Uchitel, O.D. (2003). Ca2+ channels and synaptic transmission at the adult, neonatal, and P/Q-type deficient neuromuscular junction. Ann. N. Y. Acad. Sci. *998*, 11–17.

Nusser, Z. (2000). AMPA amd NMDA receptors: similarities and differences in their synaptic distribution. Curr. Opin. Neurobiol. *10*, 337–341.

Olivera, BM., Cruz, LJ., De Santos, V., LeCheminant, G., Griffin, D., Zeikus, R., McIntosh, MJ., Galyean, R., Varga, J., Gray, WR., Rivier, J., (1987). Neuronal Calcium Channel Antagonists. Discrimination between Calcium Channel Subtypes Using w-Conotoxin from Conus magus Venom. Biochemistry, *26* (8) 2086-2090

Parks, T.N. (2000). The AMPA receptors of auditory neurons. Hear. Res. *147*, 77–91.

Patel, R., and Dickenson, A.H. (2016). Mechanisms of the gabapentinoids and α 2 δ-1 calcium channel subunit in neuropathic pain. Pharmacol. Res. Perspect. *4*.

Pietrobon, D. (2010). CaV2.1 channelopathies. Pflüg. Arch. - Eur. J. Physiol. *460*, 375–393.

Pinggera, A., Mackenroth, L., Rump, A., Schallner, J., Beleggia, F., Wollnik, B., and Striessnig, J. (2017). New gain-of-function mutation shows CACNA1D as recurrently mutated gene in autism spectrum disorders and epilepsy. Hum. Mol. Genet. *26*, 2923–2932.

Pirone, A., Kurt, S., Zuccotti, A., Rüttiger, L., Pilz, P., Brown, D.H., Franz, C., Schweizer, M., Rust, M.B., Rübsamen, R., et al. (2014). α2δ3 Is Essential for Normal Structure and Function of Auditory Nerve Synapses and Is a Novel Candidate for Auditory Processing Disorders. J. Neurosci. *34*, 434–445.

Platzer, J., Engel, J., Schrott-Fischer, A., Stephan, K., Bova, S., Chen, H., Zheng, H., and Striessnig, J. (2000). Congenital Deafness and Sinoatrial Node Dysfunction in Mice Lacking Class D L-Type Ca2+ Channels. Cell *102*, 89–97.

Pringos, E., Vignes, M., Martinez, J., and Rolland, V. (2011). Peptide Neurotoxins that Affect Voltage-Gated Calcium Channels: A Close-Up on ω-Agatoxins. Toxins *3*, 17–42.

Procko, C., and Shaham, S. (2009). Synaptogenesis: New Roles for an Old Player. Curr. Biol. CB *19*, R1114–R1115.

Ramírez, D., Gonzalez, W., Fissore, R.A., and Carvacho, I. (2017). Conotoxins as Tools to Understand the Physiological Function of Voltage-Gated Calcium (CaV) Channels. Mar. Drugs *15*, 313.

Randall, A., and Tsien, R.W. (1995). Pharmacological Dissection of Multiple Types of Ca2+ Channel Currents in Rat Cerebellar Granule Neurons. J. Neurosci. *15*, 2995–3012.

Reijntjes, D.O.J., and Pyott, S.J. (2016). The afferent signaling complex: Regulation of type I spiral ganglion neuron responses in the auditory periphery. Hear. Res. *336*, 1–16.

Roberts, M.T., Seeman, S.C., and Golding, N.L. (2014). The relative contributions of MNTB and LNTB neurons to inhibition in the medial superior olive assessed through single and paired recordings. Front. Neural Circuits *8*.

Roca-Lapirot, O., Radwani, H., Aby, F., Nagy, F., Landry, M., and Fossat, P. (2017). Calcium signalling through L-type calcium channels: role in pathophysiology of spinal nociceptive transmission. Br. J. Pharmacol.

Rosato Siri, M.D., and Uchitel, O.D. (1999). Calcium channels coupled to neurotransmitter release at neonatal rat neuromuscular junctions. J. Physiol. *514*, 533–540.

Rusznák, Z., and Szucs, G. (2009). Spiral ganglion neurones: an overview of morphology, firing behaviour, ionic channels and function. Pflugers Arch. *457*, 1303–1325.

Safieddine, S., El-Amraoui, A., and Petit, C. (2012). The auditory hair cell ribbon synapse: from assembly to function. Annu. Rev. Neurosci. *35*, 509–528.

Santi, C.M., Cayabyab, F.S., Sutton, K.G., McRory, J.E., Mezeyova, J., Hamming, K.S., Parker, D., Stea, A., and Snutch, T.P. (2002). Differential Inhibition of T-Type Calcium Channels by Neuroleptics. J. Neurosci. *22*, 396–403.

Satheesh, S.V., Kunert, K., Rüttiger, L., Zuccotti, A., Schönig, K., Friauf, E., Knipper, M., Bartsch, D., and Nothwang, H.G. (2012). Retrocochlear function of the peripheral deafness gene Cacna1d. Hum. Mol. Genet. *21*, 3896–3909.

Schindelin, J., Arganda-Carreras, I., Frise, E., Kaynig, V., Longair, M., Pietzsch, T., Preibisch, S., Rueden, C., Saalfeld, S., Schmid, B., et al. (2012). Fiji: an open-source platform for biological-image analysis. Nat. Methods *9*, 676–682.

Schroeder, C.I., and Lewis, R.J. (2006). ω-Conotoxins GVIA, MVIIA and CVID: SAR and Clinical Potential. Mar. Drugs *4*, 193–214.

Senatore, A., Zhorov, B.S., and Spafford, J.D. (2012). Cav3 T-type calcium channels. Wiley Interdiscip. Rev. Membr. Transp. Signal. *1*, 467–491.

Sento, S., and Ryugo, D.K. (1989). Endbulbs of held and spherical bushy cells in cats: Morphological correlates with physiological properties. J. Comp. Neurol. *280*, 553–562.

Shrestha BR, Chia C, Wu L, Kujawa SG, Liberman C, Goodrich LV (2018). Sensory Neuron Diversity is in the inner ear shaped by acitivity. Cell *174*, 1-18

Simms, B.A., and Zamponi, G.W. (2014). Neuronal Voltage-Gated Calcium Channels: Structure, Function, and Dysfunction. Neuron *82*, 24–45.

Smith, F.L., and Davis, R.L. (2016). Organ of Corti explants direct tonotopically graded morphology of spiral ganglion neurons in vitro. J. Comp. Neurol. *524*, 2182–2207.

Stefanini, M., Martino, C.D., and Zamboni, L. (1967). Fixation of Ejaculated Spermatozoa for Electron Microscopy. Nature *216*, 216173a0.

Striessnig, J., Pinggera, A., Kaur, G., Bock, G., and Tuluc, P. (2014). L-type Ca2+ channels in heart and brain. Wiley Interdiscip. Rev. Membr. Transp. Signal. *3*, 15–38.

Sun S, Babola T, Pregernig G, So KS, Nguyen M, Su SSM, Palermo AT, Bergles DE, Burns, JC, Mueller U (2018). Hair Cell Mechanotransduction Regulates Spontaneous Activity and Spiral Ganglion Subtype Specification in the Auditory System. Cell *174*, 1247 - 1263

Tottene, A., Volsen, S., and Pietrobon, D. (2000). alpha(1E) subunits form the pore of three cerebellar R-type calcium channels with different pharmacological and permeation properties. J. Neurosci. Off. J. Soc. Neurosci. *20*, 171–178.

Trussell, L.O., Popper, A.N., and Fay, R.R. (2012). Synaptic Mechanisms in the Auditory System (Springer).

Tsunemi, T., Saegusa, H., Ishikawa, K., Nagayama, S., Murakoshi, T., Mizusawa, H., and Tanabe, T. (2002). Novel Cav2.1 Splice Variants Isolated from Purkinje Cells Do Not Generate P-type Ca2+ Current. J. Biol. Chem. *277*, 7214–7221.

Turner, R.W., Anderson, D., and Zamponi, G.W. (2011). Signaling complexes of voltage-gated calcium channels. Channels *5*, 440–448.

Van der Heiden, M.G., Plas, D.R., Rathmell, J.C., Fox, C.J., Harris, M.H., and Thompson, C.B. (2001). Growth Factors Can Influence Cell Growth and Survival through Effects on Glucose Metabolism. Mol. Cell. Biol. *21*, 5899–5912.

Wang, Q., and Green, S.H. (2011). Functional role of NT-3 in synapse regeneration by spiral ganglion neurons on inner hair cells after excitotoxic trauma in vitro. J. Neurosci. Off. J. Soc. Neurosci. *31*, 7938–7949.

Wang J, Zhang B, Jiang H, Zhang L, Liu D, Xiao X, Ma H, Luo X, Bojrab II D, Hu Z. (2013) Myelination of the Postnatal Mouse Cochlear Nerve at the Peripheral-Central Nervous System Transitional Zone. *Front Pediatr* **1**. doi:10.3389/fped.2013.00043

Wang, Y., and Manis, P.B. (2005). Synaptic Transmission at the Cochlear Nucleus Endbulb Synapse during Age-Related Hearing Loss in Mice. J. Neurophysiol. *94*, 1814–1824.

Wang, T., Jones, R.T., Whippen, J.M., and Davis, G.W. (2016). α2δ-3 Is Required for Rapid Transsynaptic Homeostatic Signaling. Cell Rep. *16*, 2875–2888.

Weiss, N., and Zamponi, G.W. (2017). Trafficking of neuronal calcium channels. Neuronal Signal. *1*, NS20160003.

Weiss, J., Pyrski, M., Weissgerber, P., and Zufall, F. (2014). Altered synaptic transmission at olfactory and vomeronasal nerve terminals in mice lacking N-type calcium channel Cav2.2. Eur. J. Neurosci. *40*, 3422–3435.

Wichmann C (2015). Molecularly and structurally distinct synapses mediate reliable encoding and processing of auditory information. Hear Res. *330 PB*, 178-190

Williams, M.E., Marubio, L.M., Deal, C.R., Hans, M., Brust, P.F., Philipson, L.H., Miller, R.J., Johnson, E.C., Harpold, M.M., and Ellis, S.B. (1994). Structure and functional characterization of neuronal alpha 1E calcium channel subtypes. J. Biol. Chem. *269*, 22347–22357.

Yi, L., and David Z, H. (2014). The Cochlear Amplifier: Is it Hair Bundle Motion of Outer Hair Cells? J. Otol. *9*, 64–72.

Yu, W.-M., and Goodrich, L.V. (2014). Morphological and physiological development of auditory synapses. Hear. Res. *0*, 3–16.

Zamponi, G. (2005). Voltage-Gated Calcium Channels (Landes Bioscience).

Zamponi, G.W. (2016). Targeting voltage-gated calcium channels in neurological and psychiatric diseases. Nat. Rev. Drug Discov. *15*, 19.

Zamponi, G.W., Striessnig, J., Koschak, A., and Dolphin, A.C. (2015). The Physiology, Pathology, and Pharmacology of Voltage-Gated Calcium Channels and Their Future Therapeutic Potential. Pharmacol. Rev. *67*, 821–870.

Zhang KD, Coate TM (2017). Recent advances in the development and function of type II spiral ganglion neurons in the mammalian inner ear. Semin Cell Dev Biol. *65*, 80-87

Zheng, J., Madison, L.D., Oliver, D., Fakler, B., and Dallos, P. (2002). Prestin, the Motor Protein of Outer Hair Cells. Audiol. Neurotol. *7*, 9–12.

6.   Acknowledgments